Norwegian University of Life Sciences

Master's Thesis 2020 30 ECTS
Faculty of Science and Technology

Carbon Capture in Molten Salts: An extensive survey of chemical systems with MgO as sorbent

Petter Nygård Lerøen
Environmental Physics and Renewable Energy

Carbon Capture in Molten Salts: An extensive survey of chemical systems with MgO as sorbent

REALTEK

Norwegian University of Life Sciences

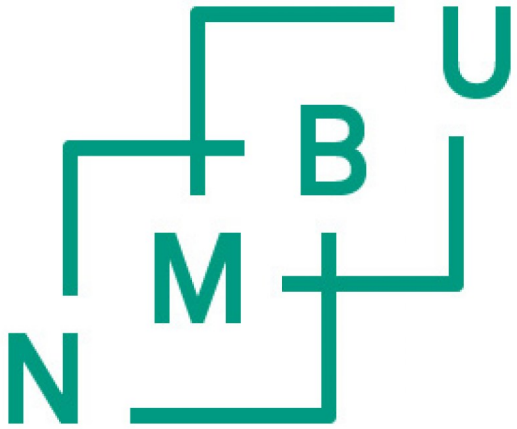

Petter Nygård Lerøen

August 2020

Abstract

Stated in the Paris Agreement, utilization of *Carbon Capture and Storage* (CCS) technologies are an essential part of curbing the increasing trend of carbon dioxide (CO_2) emissions into the atmosphere. CCS is a relatively new set of technologies. However, today's CCS technologies are expensive, and further research and development are needed to lower the cost of this technology.

Through the two last decades, a new technology for capturing CO_2 has emerged, called *Carbon Capture in Molten Salts* (CCMS). The technology of CCMS is a further development of conventional *Calcium Looping* technology (CaL). Instead of using solid calcium oxide (CaO) as CO_2-sorbent such as CaL, CCMS uses an *alkaline earth metal oxide* (MO) dissolved or partially dissolved in inorganic molten salts as a CO_2-sorbent. CCMS takes advantage of the reversible reaction between the sorbent (MO) and CO_2 to form a *carbonate* (MCO_3). By having the sorbent dissolved in molten salts, the reaction kinetics between the sorbent and CO_2 can be improved. The carbonate can release the captured CO_2 and regenerate the sorbent through endothermic decomposition. Unlike CaL, by having a dissolved or partially dissolved CO_2-sorbent in molten salts, CCMS avoids the obstacle of degrading the CO_2-sorbent after a few cycles of CO_2 capture and release, which is a costly problem for CaL.

Today the CCMS technology has mostly been tested with CaO as CO_2-sorbent. CaO has shown promising results during CO_2 capture in CCMS.

However, the reversible reaction between CaO and CO_2 has a relative high reaction enthalpy, thus large amounts of energy is required to maintain the reaction. This energy requirement is the main cost driver for CCMS with CaO. By using magnesium oxide (MgO) as CO_2-sorbent instead of CaO in the CCMS process, much of the energy needs could be avoided. Since the reversible reaction between MgO and CO_2 has a lower reaction enthalpy than

CaO, thus, less energy is required to maintain the reversible reaction. MgO also has higher theoretical CO_2 absorption capacity than CaO. For these reasons, finding chemical systems suitable for CCMS with MgO as sorbent is the focus of this thesis.

Twenty-seven salt mixtures have been screened, all salt mixtures possess a lower eutectic melting point than 305 °C. The largest group of salt mixtures screened is the nitrate salts, due to their low eutectic melting points of 117-237 °C. The two other salt mixture groups are considerably smaller, one group consisting of halide salts, and the other group consists of both halide and nitrate salts. The halide salt mixtures have relatively high eutectic melting points, 217-301 °C, and the salt mixtures consisting of both halide and nitrate salt have molar ratios heavily skewed towards the nitrate salt, >87.7 mol%.

None of the nitrate salt mixtures possess a component that reacts with MgO and CO_2, meaning the MgO is inert in a nitrate melt. All of the halide salt mixtures screened had a component would have an exchange reaction with MgO and CO_2. The halides-nitrate salt mixtures do not have a component that reacts with MgO and CO_2. Most of the salt mixtures screened possess Lewis base characteristics.

Two successful experiments were conducted with LiF-NaF-KF or FLiNaK salt and MgO as CO_2-sorbent. Both experiments used 450 g with salt and 50 g MgO. The first experiment was conducted with 500 °C for 550 minutes, where the total CO_2 absorbed was 16.6 g. The second experiment was conducted with 650 °C; the experiment lasted for 1200 minutes; the total CO_2 absorbed was 44.5 g; this shows that MgO has a high CO_2 absorption capacity, but the CO_2 capture rate is inefficient.

A third experiment was attempted, with 450 g of molten CuCl-KCl salt and 50 g of MgO. The experiment was initially successful for 10 minutes before technical complications appeared, and the experiment had to be canceled. However, a useful insight into the behavior CuCl-KCl was observed in the first 10 minutes, where almost no CO_2 was absorbed.

Sammendrag

Utalt i Parisavtalen, vil utnyttelse av *Karbonfangst og lagrings* (Carbon Capture and Storage - CCS) teknologier være en essensiell del av reduksjonen av karbondioksid (CO_2) utslippene. CCS er en relativt ny gruppe av teknologier, men disse teknologiene er i dag dyre. Dermed er det nødvendig med videre forsking og utvikling av disse teknologiene, for å senke denne kostnaden.

Gjennom de to siste tiårene, har en ny teknologi for karbonfangst blitt utviklet. Denne teknologien kalles *Karbonfangst i saltsmelter* (Carbon Capture in Molten Salts - CCMS). CCMS teknologien er en videreutvikling av konvensjonell *Kalsiumlooping* (Calcium Looping - CaL) teknologi. I motsetning av CaL som bruker kalsiumoksid (CaO) i fast fase som CO_2-sorbent, bruker CCMS et jordalkalisk metalloksid (MO) som er oppløst eller delvis oppløst i smeltet uorganiske salter som CO_2-sorbent. CCMS utnytter den reversible reaksjonen mellom CO_2-sorbent (MO) og CO_2, og den reversible reaksjonen skaper et karbonat (MCO_3). Når CO_2-sorbenten er oppløst i en salt smelte, kan reaksjons kinetikken mellom CO_2-sorbent (MO) og CO_2 bli forbedret. Karbonatet kan løslate det fangede karbondioksidet og regenerere CO_2-sorbenten gjennom endoterm dekomposisjon. Ulikt som CaL, når CO_2-sorbenten er oppløst i smeltet salt, unngår CCMS degradering av CO_2-sorbenten etter noen runder med karbonfangst og løslatelse. Degraderingen av CO_2-sorbenten er et dyrt problem for CaL.

I dag har testingen av CCMS teknologien blitt gjort i hovedsak med CaO som CO_2-sorbent, og CaO har gitt lovende resultater som CO_2-sorbent i en CCMS prosess. CCMS med CaO krever store mengder med energi siden prosessentalpien av den reversible reaksjonen er høy, og dette er den største kostnadsdriveren for CCMS med CaO.

Ved bruk av magnesiumoksid (MgO) som CO_2-sorbent istedenfor CaO i CCMS, kan de store energi kostnadene bli redusert. Prosessentalpien for CCMS med MgO er betraktelig lavere en med CaO. MgO har også høyere teo-

retisk CO_2-bærevene enn CaO. På grunn av disse fordelene er hovedfokuset av denne oppgaven å finne kjemiske systemer som passer til MgO i CCMS.

Tjuesyv saltblandinger har blitt screenet, alle saltblandingene har eutektisk smeltepunkt lavere enn 305 °C. Den største gruppen av de screenede saltblandingene er nitratsaltblandingene, denne gruppen har relativt lave eutektiske smeltepunkter (117-237 °C). De to andre gruppene er en betydeligere mindre. Den ene gruppen består av halogensaltblandinger og den andre gruppen er både halogen og nitratsaltblandinger. Halogensaltblandingene har en relativt høye eutektiske smeltepunkter, (217-301 °C). Den siste gruppen, halogen-nitrat gruppen, der alle saltblandingene har som kjennetegn at det molare blandeforholdet er veldig forskjøvet mot nitratsaltene, >87.7 mol%. Ingen av komponentene i nitratsaltblandingene reagerer med MgO and CO_2, som betyr at MgO vil være inert i smeltet nitrat salt. Alle de screenede halogensaltblandingene har komponenter som reagerer med MgO and CO_2. Likt som nitratsaltblandingene, har halogen-nitratsaltblanding gruppen ikke noen komponenter som reagerer med MgO og CO_2. Nesten alle saltblandingene har en Lewis-base-karakteristikk. To vellykkede eksperimenter med LiF-NaF-KF eller FLiNaK salt, der MgO var CO_2-sorbent ble gjennomført. Begge eksperimentene brukte 450 g med salt og 50 MgO. Det første eksperimentet ble gjennomført på 500 °C over 550 minutter, der 16.6 g CO_2 ble absorbert. Det andre eksperimentet ble gjennomført på 650 °C over 1200 minutter, der totale absorberte CO_2 var 44.5 g. Dette viser at MgO har stor CO_2-absorbsjonskapasitet, men fangstraten er veldig treg og lite effektivt.

Ett tredje eksperiment ble forsøkt, med 450 g med smeltet CuCl-KCl salt, med 50 g MgO. I starten var eksperimentet vellykket, men etter 10 minutter dukket det opp tekniske problemer, og eksperimentet måtte bli avbrutt. De 10 første minuttene ga interessant innsikt, der MgO absorberte nesten ingen CO_2 i de 10 første minuttene.

Acknowledgements

The completion of this thesis marks the end of my Master's degree in Environmental Physics and Renewable Energy at the Norwegian University of Life Sciences, NMBU. This thesis accounted for 30 credits and was conducted through the spring and summer of 2020.

First and foremost, I wish to thank my primary advisor, Heidi S. Nygård, for your excellent counsel, support, ideas, and encouragement. I am very grateful that you have helped and trained me in the laboratory, as well as being available at all hours of the day for my questions. My thanks go to the secondary advisor, Espen Olsen, for your great knowledge of this subject has been a crucial part of helping me with the work through this thesis. I am very grateful for you both for taking much time to help me with this thesis; without you, this thesis would never have seen the light of day. I also want to thank Sepideh Niazi for your help with the laboratory equipment.

I want to thank my parents for encouraging me to pursue science and technology; without them, I would not have been here writing this. I want to thank my partner, Linn Egeland, for the encouragement you gave me when I worked with this thesis.

Contents

List of Figures

List of Tables

Abbreviations

ASU	Air Separation Unit
CaL	Calcium Looping
CCS	Carbon Capture and Storage
CCMS	Carbon Capture in Molten Salts
CCUS	Carbon Capture, Utilization and Storage
CDR	Carbon Dioxide Removal
CSP	Concentrated Solar Power
DAC	Direct Air Capture
EOR	Enhanced Oil Recovery
FTIR	Fourier Transform Infrared spectrometry
GCCSI	Global CCS Institute
GHG	Greenhouse Gas
IEA	The International Energy Agency
IGCC	Integrated Gasification Combined Cycle
IPCC	Intergovernmental Panel on Climate Change
ITRI	Industrial Technology Research Institute
NGCC	Natural Gas Combined Cycle
MFC	Mass Flow Controller
ppm	Parts Per Million

Chapter 1

Introduction

1.1 Introduction

The global average surface temperature has increased with 0.85 °C between 1880 and 2012. The dominant influence on the climate is the increased anthropogenic activities[1] since the mid-20th century. Global warming to this very day has caused profound alterations in the natural systems of the world. Alterations such as extreme droughts, storms, and floods have become ever more present in weather patterns of the world. The consequences of these changes affect millions of people in areas most impacted by the changing climate. Some low and middle-income countries have experienced a decline in food security mainly caused by a changing climate. People living in large cities, coastal areas, small islands, and high mountain ranges are likely to be the most affected by the changing climate[1]. A probable cause of the changing climate might be linked to the use of fossil fuel and the consequent emissions of carbon dioxide (CO_2).

The first systematic observations of the atmospheric concentration of CO_2 in the atmosphere were made in 1958 in Hawaii, at the Mauna Loa Observatory by Charles David Keeling. During his observations, Keeling observed that the CO_2 concentrations in the atmosphere increased steadily, with an average of 0.7 ppm yearly. Figure 1.1 depicts the atmospheric concentration of CO_2 measured at the Mauna Loa Observatory in the period 1958-1972. He concluded that the increased concentration of CO_2 is due to the use of fossil fuels[2][3].

[1] Anthopogenic activities: Human activities.

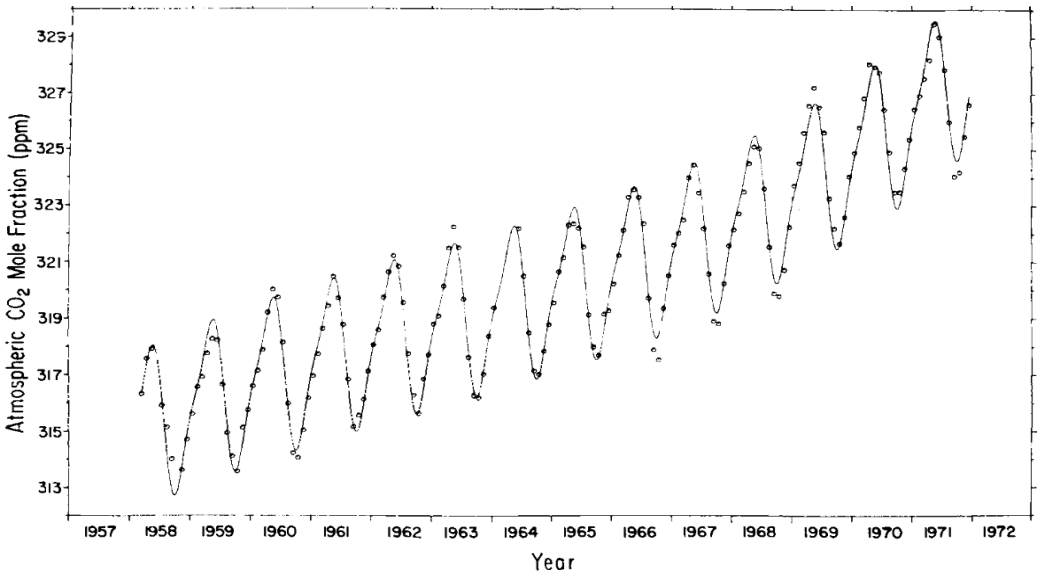

Figure 1.1: The figure depicts the Keeling curve. The plot illustrates the atmospheric CO_2 mole fraction (ppm) vs. time in years, measured at the Mouna Loa Observatory from 1957 to 1976. The circles in the plot are the monthly average CO_2 concentrations, while the oscillating curve is the least square estimate based on the monthly CO_2 concentrations. This figure is reproduced with permission from Keeling *et al.*(1976)[2].

During the period between 1970 and 2010 the CO_2 emissions from fossil fuel combustion and industrial processes were responsible for 78% of the total increased greenhouse gas emissions. Between the years 2000 and 2010, the total annual anthropogenic CO_2 emissions have increased by 10 giga tonnes. The energy, industry, transport, and construction sectors are responsible for this growth. The increase of CO_2 emissions is the result of the global growth of economies and populations. The consensus between scientists and politicians is that the increased CO_2 emissions in the latter decades are the leading cause of global warming[4].

For this reason, 195 countries signed *The Paris Agreement* in 2015. The Paris Agreement is a legally binding agreement between the participating countries to restrict global warming. The goal is to make the average global temperature well below 2 °C, preferable 1.5 °C by 2100, compared to the pre-industrial[2] average temperature. The Paris Agreement also demands that each of the participant countries increase their ability to adapt to climate change and encourages the reduction of emissions[5].

[2]Pre-industrial is referred to before 1750 by IPPC.

In 2018 The Intergovernmental Panel on Climate Change (IPCC) published a report on how to reach the 1.5 °C goal. The report summarizes several pathways on how to reach this goal. One of the objectives mentioned in the report is to reach net-zero CO_2 emissions globally by 2050. This goal can be attained by deploying *Carbon Dioxide Removal* (CDR) measures. These are measures aimed at reducing the concentration of CO_2 in the atmosphere, as well as reducing the CO_2 emissions. The report mentions that the implementation of *Carbon Capture and Storage* (CCS) technologies are needed to reach the goal within the limited time frame[1].

Carbon Capture and Storage (CCS) is an umbrella term for technologies and methods that enables the capture and storage of CO_2. The process of CCS usually starts with the separation of CO_2 from flue gas. Then the CO_2 is processed and transported to the storing site.

Carbon Capture in Molten Salts (CCMS) is a new technology developed at *the Norwegian University of Life Sciences* (NMBU). CCMS builds on the same principles as *Calcium-Looping* (CaL). The difference between CCMS and CaL is the CO_2 sorption particles are completely or partially dissolved in molten salt, whereas in CaL, the sorption particles are in a solid phase.

The melt consists of inorganic salt and alkali earth metal oxide. When testing this technology, promising results were revealed. Using *calcium oxide* (CaO) as sorbent dissolved in a few select mixtures of salt yielded a high CO_2 capturing rate from a gas mixture with 14 vol% CO_2[6]. Unlike technologies using similar capture techniques, the sorbent in CCMS does not deteriorate after a few cycles of CO_2 capture[7].

Today the CCMS technology has mostly been tested with CaO as CO_2-sorbent. CaO has shown promising results during CO_2 capture in CCMS; however, CaO needs large amounts of energy to be regenerated, 885 °C, after capturing CO_2. This is due to the high reaction enthalpy of the decarbonation reaction. The high energy requirements are the main cost driver of CCMS with CaO.

By using MgO as CO_2-sorbent instead of CaO, some of the problems of CaO can be avoided. The regeneration temperature of MgO is much lower than CaO, 305 °C. MgO also has a lower reaction enthalpy than CaO; thus, MgO has the potential to be less energy demanding than CaO.

MgO also has a higher theoretical CO_2-carrying capacity than CaO, 1.092 g CO_2 per 1 g MgO, while CaO has 0.7847 g CO_2 per 1 g CaO. Thus MgO as a sorbent is less energy demanding than CaO. For this reason, finding chemical systems suitable for CCMS with MgO as sorbent is the focus of

this thesis.

1.2 The Purpose of the Thesis

This thesis will focus on finding potential chemical systems for CCMS where MgO is the CO_2-sorbent. The systems must potentially lower the energy cost of the CCMS and/or be able to capture CO_2 from gas mixtures with low CO_2 content. The analysis of the potential chemical systems will be through looking at the theoretical properties of the system, simulating and making models of how the system is acting in different conditions, and looking at the system behavior in practical applications in research papers.

The aim is of this thesis is to provide a basis for further research and development into CCMS, by highlighting the data gathered and analyzed in this thesis.

1.3 The Contents of the Thesis

This thesis contains a theoretical background-, method-, results-, discussion-, and conclusion chapter. A bibliography of the references also included.

The theoretical background chapter begins with the description of the greenhouse gasses and the importance of reducing the emission of these gases, which is the core basis of CCS. The chapter continues with the description of CCS, its strategies, technologies, and application with other technologies.

This thesis was initially experimentally based, where testing of MgO as a CO_2 sorbent in different salt mixtures. However, due to the university shutting down from the SARS-CoV-2 (also known as the coronavirus) outbreak in spring 2020, it was decided that the thesis should be redirected as a literary research thesis. Still, two successful experiments were conducted before the shutdown. The method chapter consists of two parts, the first part consists a description of the method for the screening. The second part consists of describing the experimental part of the thesis.

The thesis continues with the discussion chapter, where the potential chemical systems with MgO as the sorbent for CCMS will be reviewed. The last chapter is where the thesis will be concluded, and giving remarks on where further research should be directed.

Chapter 2

Theory

2.1 The Greenhouse Effect and Greenhouse Gases

The greenhouse effect is a process where certain gases in the earth's atmosphere absorb thermal radiation. The gases then emit the absorbed energy in every direction, including towards the earth's surface. This causes the temperature of the earth's surface to rise. The mean temperature of the earth's surface would be at -18 °C instead of 15 °C if these gases would not be present in the atmosphere.

These gases are referred to as *greenhouse gases*. The most important greenhouse gases are water vapor (H_2O), carbon dioxide (CO_2), methane (CH_4), nitrous oxide (N_2O), and ozone (O_3). Water vapor is responsible for 50% of the greenhouse effect, while clouds and CO_2 are responsible for 25% and 20%, respectively[8].

The concentration of CO_2 in the atmosphere has increased by 30% since the industrial revolution. The concentration of other greenhouse gases such as CH_4 and N_2O has increased as well, 150% and 15%, respectively. Gases such as hydrofluorocarbons (HFC), chlorofluorocarbons (CFC), hydrochlorofluorocarbons (HCFC), and perfluorocarbons (PFC) has been added in the atmosphere by human activity. These gases, also referred to as fluorocarbons, they do not occur naturally in the atmosphere, and they cause an amplified greenhouse effect[9][10].

2.1.1 Carbon Dioxide

Carbon dioxide is a chemical compound or a molecule that consists of one carbon atom and two oxygen atoms. The carbon dioxide molecule is a linear type molecule, and the chemical formula is CO_2. At room temperature, 25 °C, and at a pressure of 1 atm, CO_2 is in gaseous form. During these conditions, CO_2 is invisible, and it possesses a weak acidic taste and smell. At temperatures below -57 °C, CO_2 condenses into a liquid, CO_2 becomes a solid at -78 °C. Figure 2.1 depicts the phase diagram of CO_2, The y-axis represents the pressure (atm), and x-axis represents the temperature (°C). The phase diagram is divided into four sections, the section of CO_2(s) describes the conditions where CO_2 is a solid, CO_2(l) describes when CO_2 is a liquid, and CO_2(g) describes when CO_2 are in gaseous state. The last section describes when CO_2 is a super-critical fluid. The red dot represents the triple point, when CO_2 is in a solidus, liquidus and gaseous state at the same time[11].

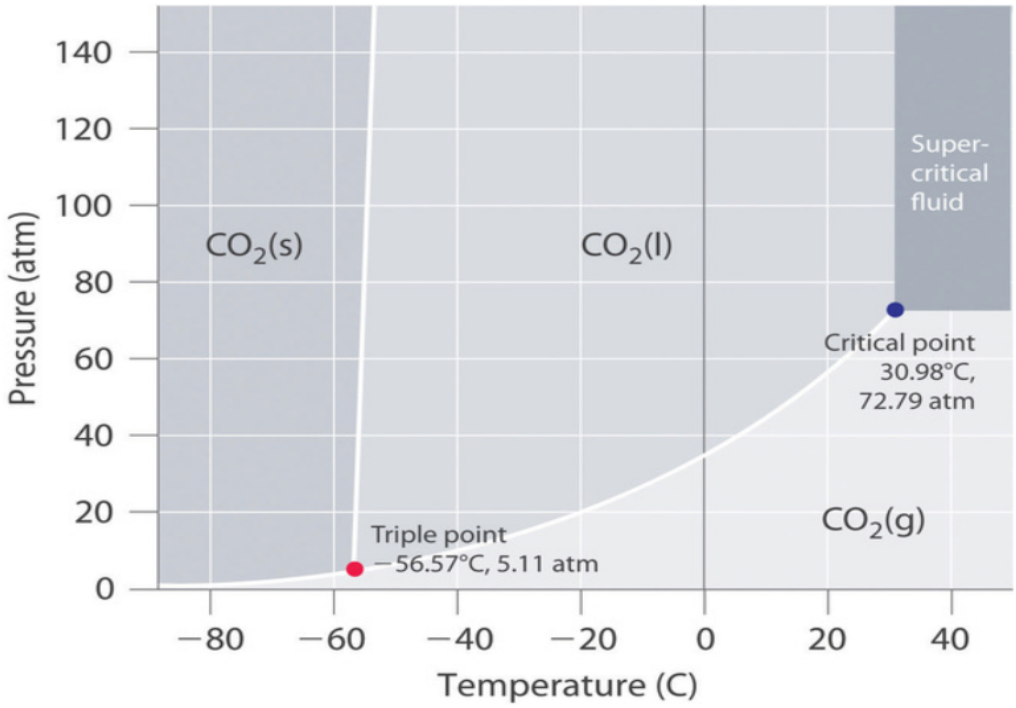

Figure 2.1: A phase diagram of CO_2. The y-axis represents the pressure (atm), and x-axis represents the temperature (°C). The figure is reproduced by permission of LibreTexts[11].

The molecule of CO_2 is very stable; it has to be heated to 2000 °C before it breaks up into carbon monoxide (CO) and oxygen gas (O_2). CO_2 easily dissolves in water.

Organisms such as humans and other animals can create carbon dioxide thought the respiratory system. CO_2 can also be created during a combustion process between hydrocarbons and O_2, where CO_2 is an end product. Unlike animals, plants consume CO_2 gas. During photosynthesis, plants consume CO_2 along with water and sunlight to create carbohydrates and O_2. Thus the plant life is reducing the CO_2 concentration in the atmosphere[12].

Greenhouse gas emissions from anthropogenic sources fueled by hydrocarbons such as power plants, industry, transport, are the main culprit of the rise of CO_2 concentration in the atmosphere. The cumulative anthropogenic CO_2 emissions to the atmosphere between 1750 and 2011 were 2040 $\pm$ 310 billion tonnes CO_2. Approximately 40% of the emitted CO_2 has remained in the atmosphere. The remaining 60% has been stored on land, in plants, and in the soil. The ocean has absorbed 30% of the emissions, thus making the ocean more acidic.

Half of the accumulated CO_2 emissions (1750-2011) have occurred during the last 40 years. The most important driver of increased CO_2 emissions can be traced to the global economic and population growth from 1970 to 2010[4]. In June of 2020, the atmospheric concentration of CO_2 was measured to be 416 ppm. The concentration of CO_2 is estimated to grow by 2 ppm every year[4][13]. See Figure 2.2 for a visual representation of the atmospheric concentration of CO_2 at the Mauna Loa Observatory.

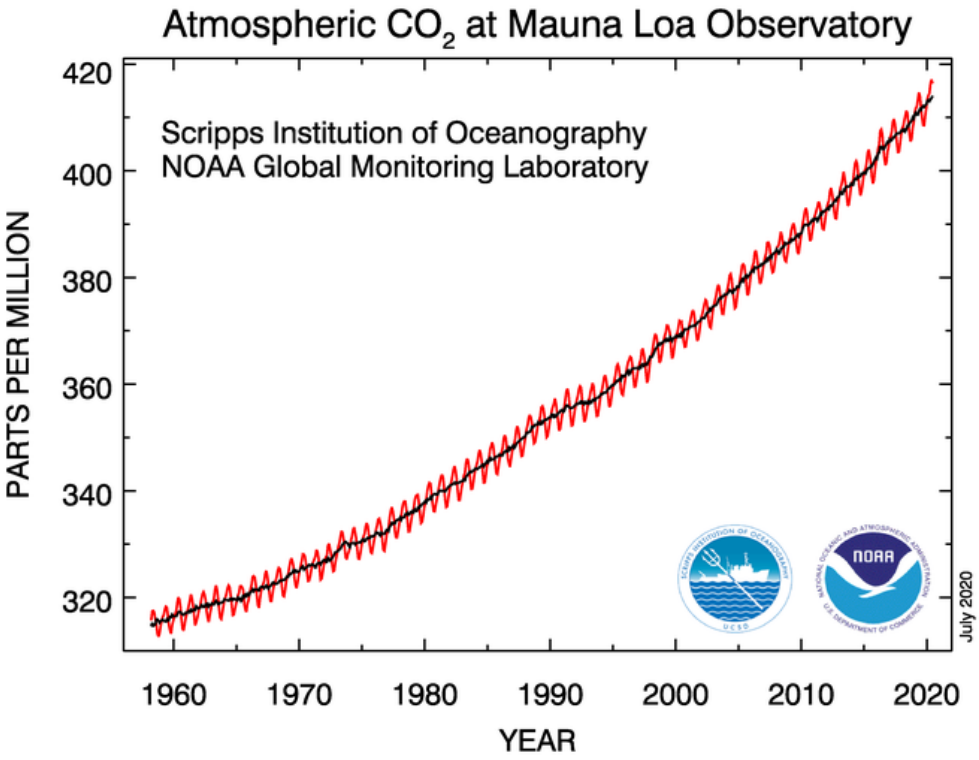

Figure 2.2: The figure illustrates the atmospheric concentration in parts per million of CO_2 at the Mauna Loa Observatory in Hawaii, USA. The figure illustrates the concentration of CO_2 in the atmosphere in the period from 1958 to 2020. The figure is reproduced by permission of *National Oceanic and Atmospheric Administration* (NOAA)[13].

The number of large CO_2 emission sources, over 0.1 million tonnes CO_2 yearly, has been estimated to be over 7500. Although these sources are distributed around the world, but four emissions clusters have been observed. The location of these clusters are: North America, Northwest Europe, Southeast Asia, and South Asia (the Indian-subcontinent). Future projections, up to 2050, show a likely increase in emission sources of CO_2. This is mainly due to increased activity by the power and industrial sectors in regions such as South Asia and Southeast Asia.

The power and industrial sectors together hold a dominant position in the total global CO_2 emissions, where 60% of all CO_2 emissions are sourced from these sectors, see Table 2.1[14][15].

These sectors have boilers and furnaces as their primary sources of CO_2

emissions. Since these are often considered as large stationary sources of CO_2, they present an opportunity for the addition of a CO_2 capturing plant[14].

Table 2.1: Worldwide profile of large stationary CO_2 sources, the vol% of CO_2 in the exhaust gas stream of the sources, and the total % of CO_2 by each source[14].

Source	vol% CO_2 in gas stream	% of total CO_2 emission
Coal	12-15	59.69
Natural gas (Turbine)	3	5.68
Natural gas (Boiler)	7-10	5.62
Fuel oil	8	4.89
Cement production	20	6.97
Refineries	3-13	5.97
Steel mills	15	4.71
Ethylene production	12	1.93
Other	-	4.54

2.1.2 Other Greenhouse Gases

The greenhouse gas that contributes the most to global warming after CO_2 is methane, CH_4. The cattle industry, along with rice production, combustion of biomass, waste, and fossil fuels, are the primary sources of CH_4 increase in the atmosphere. The concentration of CH_4 is more than double today than it was before the industrial revolution. In 2008 the atmospheric concentration of CH_4 was 1775 ppb, compared with 750 ppb before the industrial revolution. The lifetime of CH_4 in the atmosphere is relatively short, 12 years, compared to CO_2, which can stay in the atmosphere for up to 200 years[8][16].

After CH_4, nitrous oxide, or N_2O, is the third most important greenhouse gas. The primary anthropogenic sources of N_2O are the use of nitrogen fertilizers and biomass burning. The pre-industrial concentration of N_2O in the atmosphere was about 285 ppb, compared to 320 ppb in 2008. A major N_2O sink is found in the stratosphere, where N_2O is oxidized into NO_x.

Next comes CFC and HCFC, these are important greenhouse gases. Although the concentration of these gases in the atmosphere is relatively small, <1 bbp, they have a large potential of contributing to the greenhouse effect[16].

Figure 2.3 illustrates he total amount of the most important greenhouse gases (GHG), in Gigatonne CO_2-equivalent per year, emitted into the atmo-

sphere in the period 1970 to 2010. The area beneath the graph is divided into sections where each section is representing a specific type of greenhouse gas[1].

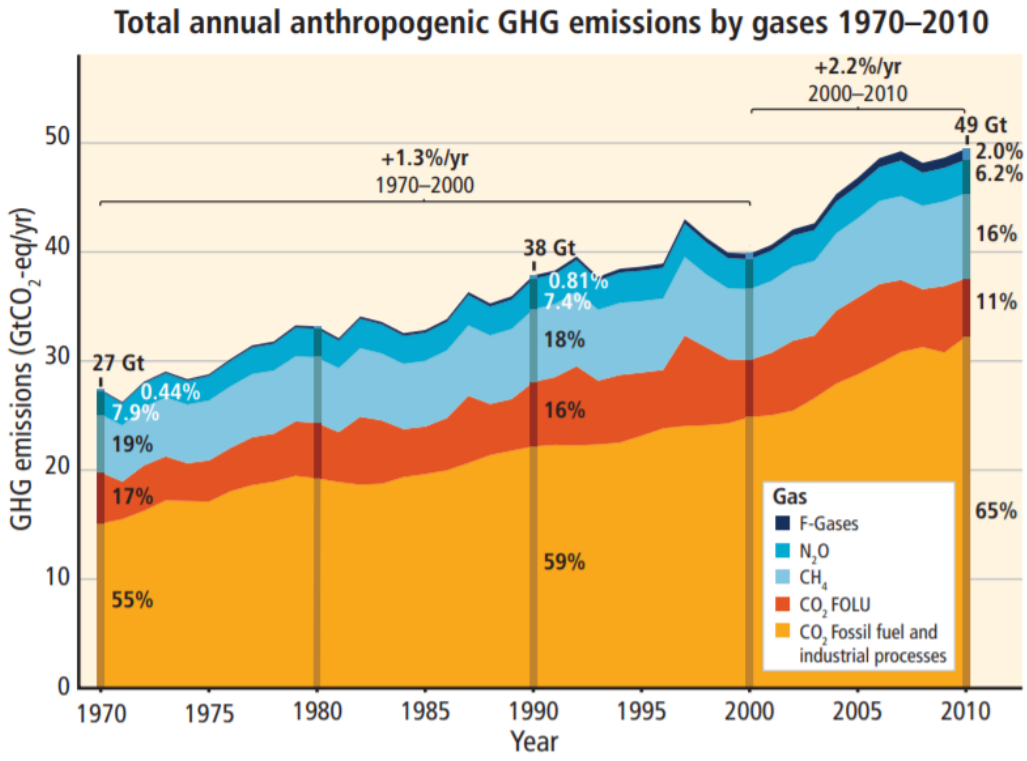

Figure 2.3: The figure illustrates the total amount of the most important greenhouse gases (GHG) emitted into the atmosphere, in Gigatonne CO_2-equivalent per year. This figure is reproduced with permission from V. Masson-Delmotte mfl. IPPC (2018)[1].

2.1.3 Climate Change

The change of weather patterns over an extended period in a specified location, or globally, can be defined as climate change. This definition covers the change of mean temperatures, rainfall, and wind currents. The change in how frequent extreme weather occurs belongs to this definition as well. The first temperature measurement with a thermometer started in the late 19^{th} century. Since then, the mean temperature of the earth's surface increased by approximately 0.8 °C. The global mean temperature increased at a higher

rate after 1950 due to the increased emissions of greenhouse gases into the atmosphere by human activities[17].

The impact of climate change until now has been significant, especially for natural systems. The change of rainfall patterns and increased snow and ice melt are changing hydrological systems in the nature and thus affecting water resources in terms of quality and quantity in different locations in the world. The wildlife, who are dependent on these systems, have changed their behaviors as a response to the changes. Human systems have been affected by climate change, as well. Negative impacts on crop yields in different locations have shown to be more numerous than the positive impacts brought by climate change. The increased frequency of extreme climate-related events such as heatwaves, droughts, floods, cyclones, and wildfires in the last few decades has shown the vulnerability of human and ecological systems.

The future impact of climate change might cause the likelihood of extreme weather occurring more frequently and will last longer. Climate events such as heatwaves will last longer, and precipitation events will be more intense in many regions of the world. The polar ice caps will continue to melt, making the global mean sea level rise. The acidification and warming of the ocean will continue, putting the organisms and people dependent on the ocean at risk. The systems the modern world is dependent on, such as infrastructure, agriculture, and water resources, are increasingly at risk due to increased frequency of extreme weather, rising sea levels, and change in the ecological systems[4].

2.2 Carbon Capture and Storage (CCS)

Carbon Capture and Storage (CCS) is the process of separating CO_2 from a gas mixture, such as flue gas, and then store it permanently. The primary purpose of CCS is to reduce the anthropogenic CO_2 emissions in the atmosphere, in order to slow down or stop climate change caused by the increasing CO_2 concentrations. CCS consists of applying a varied set of strategies and technologies. There are three primary strategies for capturing CO_2: *pre-combustion*, *post-combustion*, and *oxy-fuel combustion* CO_2-separation. All of these strategies apply different types of technologies to capture, process, and store CO_2. The different strategies will be discussed in the next subsections[14][18].

2.2.1 CCS Strategies

Pre-combustion

Pre-combustion carbon capture is a process where CO_2 is extracted from the fuel before the combustion takes place. The first step of the process is to produce *synthesis gas* or "syngas" from the fuel. Syngas is a mixture of hydrogen gas (H_2) and CO. Since the fuel mainly consists of hydrocarbons, the fuel must react with either steam or oxygen/air. These processes are called *steam reformation* and *partial oxidation*, respectively. Equation (2.1) describes the steam reformation reaction, Equation (2.2) describes the partial oxidation reaction.

$$C_xH_y + xH_2O \rightleftharpoons xCO + (x + y/2)H_2 \tag{2.1}$$

$$C_xH_y + x/2O_2 \rightleftharpoons xCO + (y/2)H_2 \tag{2.2}$$

If the process of producing syngas uses both steam and oxygen, the process is called *auto-thermal reforming*, where the endothermic reaction of the steam reforming is balanced by the exothermic reaction of the partial oxidation process. The second step consists of reacting the CO gas from the syngas with steam to create CO_2 and H_2. This process is called *water-gas shift* (WGS), Equation (2.3) describes the WGS reaction.

$$CO + H_2O \rightleftharpoons CO_2 + H_2 \tag{2.3}$$

The CO_2 is then separated from the H_2 gas by either a physical or chemical absorption process, which gives hydrogen-rich fuel as a result. The applications of hydrogen-rich fuel are many, such as fueling gas turbines, engines, and fuel cells[19][20].

A pre-combustion CCS system can be retrofitted into a *natural gas combined cycle* (NGCC) power generation system, as well as an *integrated gasification combined cycle* (IGCC) system. The efficiency loss of an NGCC system with carbon capture ranges from 8% to 16%-points. Syngas production, the shift reaction, the CO_2 separation from the H_2 gas, and the compression and drying of the CO_2 is the main culprit of the efficiency loss. However, the most significant efficiency loss of IGCC with carbon capture is happening in the WGS section of the system. The WGS section is responsible for 44% of the entire efficiency loss, where the total efficiency loss of the IGCC with

carbon capture ranges between 8% and 11%-points. The CO_2 capture rate ranges between 84-94% for both NGCC and IGCC[19].

Problems arise when using pure H_2 gas in gas turbines designed to use syngas as fuel. Some of these problems include different combustion properties of hydrogen, a significant difference of higher and lower heating values of hydrogen, approximately 18%, the need to dilute the hydrogen gas with nitrogen or steam to lower the flame temperature, as well as lowering the NO_x emissions[20][21]

Post-combustion

Post-combustion carbon capture is the second strategy. This strategy consists of removing the CO_2 from the flue gas after the combustion of the fuel has taken place. This means that during a post-combustion carbon capture process, the hydrocarbon fuel can be combusted as normal, without the carbon capture process interfering with the combustion-process. The post-combustion method also allows for easy retrofitting existing power plants with CCS, which is the reason it is the most studied of all the carbon capture strategies[22].

A key obstacle for post-combustion carbon capture is the low concentration of CO_2, between 3 and 20%, and low pressure of approximately 1 atm, of the given flue gas[23].

Oxy-fuel

Oxy-fuel combustion is the third strategy, where fuel combusts with pure oxygen and recycled flue gas. The resulting flue gas consists mostly of CO_2, water, particulates, and sulfur dioxide (SO_2). The water can be condensed and removed from the flue gas. The gas then can be purified of SO_2 by flue gas desulfuration methods. A conventional electrostatic precipitator can remove the particulates in the gas. The remaining flue gas consists of a high concentration of CO_2, between 80 and 98% CO_2 depending on the fuel used[24]. The CO_2-rich flue gas can then be compressed, transported, and stored. This process consumes large amounts of oxygen.

One of the drawbacks of oxy-fuel combustion is the energy-intensive process of separating oxygen from air. The process is carried out by an *Air Separation Unit* (ASU). The ASU and the compression of the CO_2 are reducing the overall efficiency of the plant by 8 to 12%[25].

2.2.2 CCS Technologies

The previous section summarized the strategies of CCS. The following section will focus on the technologies applied by the beforementioned strategies. Most of the following examples are technologies used by post-combustion CCS.

Amines

Currently, the most advanced and cost-effective technologies of post-combustion carbon capture are technologies based on *amines*[22]. Amines consist of alkaline nitrogenous compounds, where alkyl or aryl groups have replaced one, two, or three hydrogen atoms in an ammonia molecule[26].

The process of separating CO_2 from flue gas is be carried out by an amine scrubbing unit. The first step contains sending flue gas into an absorber. Inside the absorber, the flue gas reacts with an aqueous amine solution. The aqueous amine solution absorbs the CO_2 from the flue gas. The amine solution, which contains the captured CO_2, is transferred to a desorber. Inside the desorber, the CO_2 is released by heating the amine solution. The released CO_2 is compressed and sent to storage[22].

Since the carbon absorption process by the amine solution is effective, it makes this process well-suited for capturing CO_2 from dilute and low-pressure flue gas streams. This allows relatively easy retrofitting of existing powerplants and other large-scale fixed-point sources of CO_2[27].

Calcium Looping

Calcium Looping, CaL, is a method for capturing carbon that takes advantage of the reversible reaction between calcium oxide (CaO) and calcium carbonate ($CaCO_3$) to capture and release CO_2. First, the CaO enters *the carbonator* with flue gas; the CO_2 in the flue gas reacts with the CaO sorbent and forms $CaCO_3$ at 600 to 850 °C[25]. The reaction is an *exothermic reaction*[1]. Second, the $CaCO_3$ exits the first vessel and enters the second vessel, *the calciner*. In the calciner, the temperature is around 900 °C[25]. This temperature causes an *endothermic reaction* of the $CaCO_3$, and thus CO_2 and CaO are formed, see Equation (2.4). The pure CO_2 leaves the calciner

[1]For a description of *exothermic* and *endothermic reactions* see Subsection 2.3.4.

to be processed and stored. The CaO sorbent is sent back to the carbonator for a new carbon capture cycle, see Figure 2.4[28][29][30].

$$\begin{aligned} &CaO(s) + CO_2(g) \rightleftharpoons CaCO_3(s) \\ &\Delta H_{T=885^\circ C} = -165\ kJ/mol \end{aligned} \tag{2.4}$$

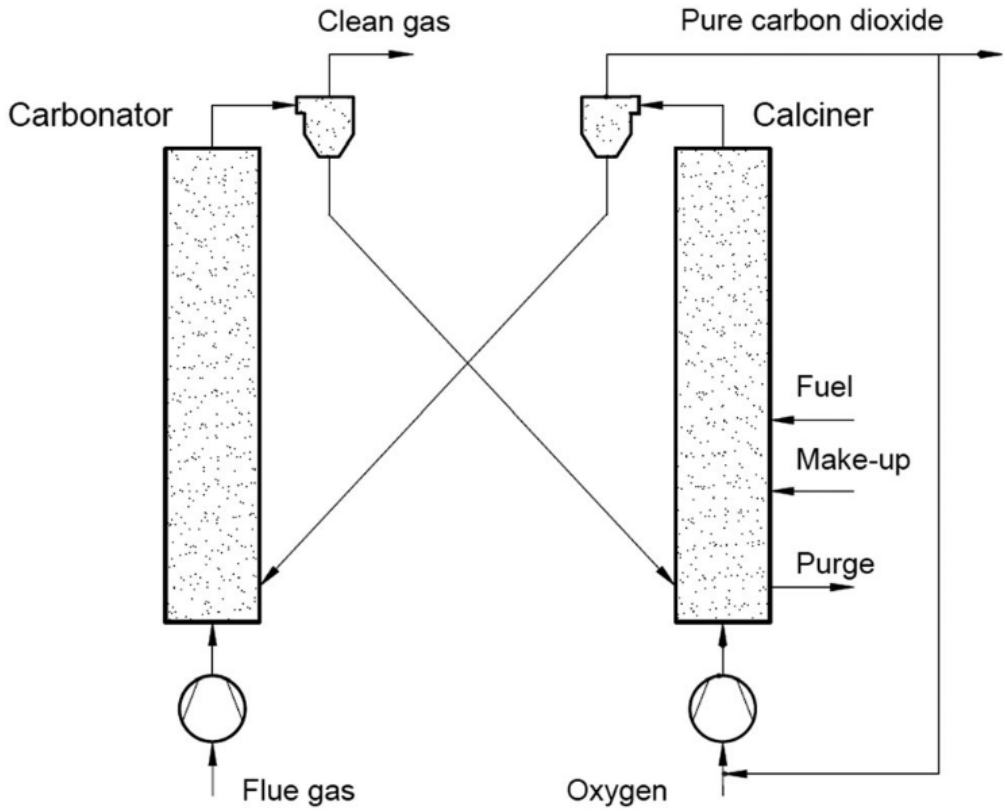

Figure 2.4: The figure shows a flowchart of a CaL system. The flue gas containing CO_2 enters the carbonator, where the CO_2 reacts with the CaO and forms $CaCO_3$. The purified flue gas exits the system while the $CaCO_3$ is sent to the calciner. In the calciner, $CaCO_3$ is then heated up and forms CO_2 and CaO. The pure CO_2 is then sent to storage while the CaO is sent back to the carbonator for a new cycle. This figure is reproduced with permission from Hanak *et al.*(2015)[30].

The advantages of this technology, compared to other promising carbon capture technologies, such as amines, is the use of *fluidized bed technology*

in the calciner and carbonator. Fluidized bed technology allows for smaller structures, unlike the large towers used for amine scrubbing[28]. The efficiency penalty is between 6 and 8% for a power plant that has a CaL system installed, compared with a power plant without CaL[25]. The excess heat generated in the high-temperature CaL process can be supplied to a steam cycle, thus increasing the overall efficiency of the process [25][29][31]. The raw material needed for CaL is limestone, which is cheap to source and is environmentally friendly and abundant in nature. The waste product of the CaL process, the spent CaO, has potential usage in other industries, most notably in the cement industry. The recent example highlights the possible synergic relationship between the cement industry and CaL[25][31].

A big challenge with CaL is the degradation of the CaO sorbent. The high temperature and the duration of calcination increase the sintering of the CaO. The higher partial pressures of steam, CO_2, and other impurities also increase the sintering of the sorbent. Sintering is the change of pore shape, pore shrinkage, and grain growth of the sorbent particles[28][29]. Figure 2.5 illustrates the carrying capacity of CaO during 50 CO_2 absorption-desorption cycles in a CaL process. After a few cycles the carrying capacity of CaO has been significantly diminished[28].

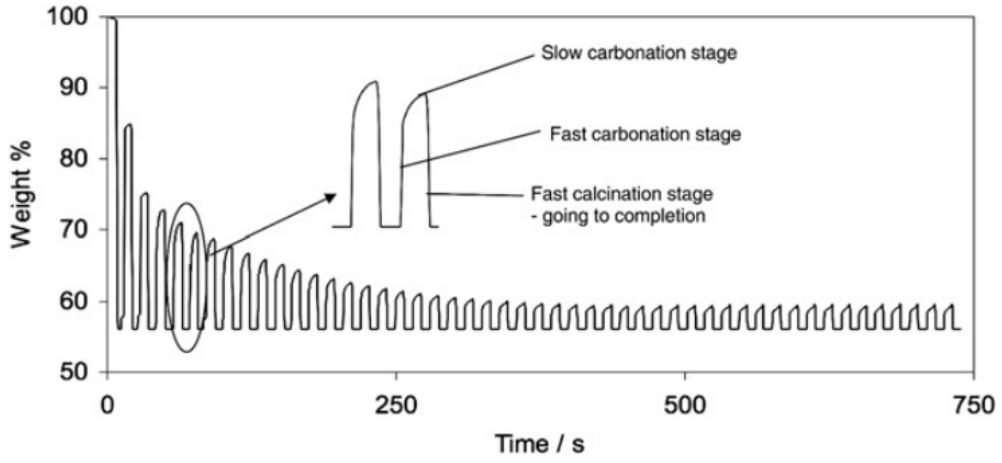

Figure 2.5: The figure represents the carrying capacity of CO_2 by CaO after 50 cycles of absorption-desorption in a CaL process. The figure is a graph depicting the change of carrying capacity by weight vs. time. Figure is reproduced with permission from Blamey *et al.* (2010)[28].

The current development of this technology has progressed to pilot-scale operations. In Germany and Spain, at the University of Darmstadt and La Pereda, respectively, major demonstration projects of CaL have been carried out. The project has been extensively testing circulating fluidized bed technology. In Taiwan, a 1.9 MW_{th} pilot plant uses a bubbling fluidized bed carbonator and a rotary kiln calciner, which has been running for a year. Based on these test projects, the Industrial Technology Research Institute (ITRI) has estimated that the cost of carbon capture with CaL could be less than 30 USD per tonne of CO_2[31].

Membranes

Unlike the different technologies of capturing carbon mentioned before, which uses a solvent to capture carbon, the *membrane technology* uses physical separation of CO_2 from flue gas. Membranes use a semipermeable barrier to sort a gas stream consisting of two or more components into a retentate and a permeable stream, see Figure 2.6.

The potential advantage of membrane technology compared to other technologies is the compactness of membranes. Membranes are modular and are easy to install. Low capital cost and energy consumption, and low maintenance. Membranes have high flexibility in operations, and compared with other methods of carbon capture membranes require a minimal amount of chemicals[32][33].

The disadvantage of this technology is the increased mass transfer resistance, especially when the membranes are wetted. Since the advantages are numerous, they can in this case outweigh the disadvantages, which makes membranes a potential competitor to conventional CO_2 capture technologies[33].

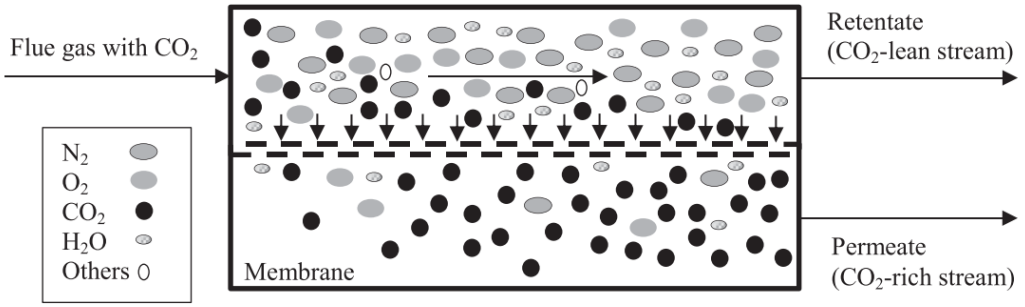

Figure 2.6: The figure depicts a CO_2 separation process by a membrane. CO_2-rich flue gas enters the membrane. The flue gas is purified of CO_2 when the CO_2 diffuses through the semipermeable barrier. The pure CO2 gas stream is sent to processing and storage. Figure reproduced with permission from Khalilpour *et al.* (2015)[32]

Cryogen Separation

Cryogen separation, or *cryogen distillation* is a method of separating CO_2 gas from flue gas by distillation. The distillation process happens at very low temperatures and high pressures. The process contains cooling down the flue gas to the desublimation temperature of CO_2, -100 °C to -135 °C. The solidified CO_2 is separated from the other gases in the flue gas mixture and compressed at a high pressure of 100-200 atm. Up to 90-95% of the amount of CO_2 in the flue gas can be separated and stored[24]. Since cryogen separation is conducted at low temperatures and high pressures, energy consumption is rather high. Estimates place the energy consumption at 600-660 kWh tonne captured CO_2 in liquid form[24].

2.2.3 Transport

The transport of CO_2 can occur by pipeline, ship, rail, and road. The quantity and the destination of the CO_2 determine the method of transportation. The transportation of CO_2 will occur mainly in pressurized pipelines since it is the most cost-effective method where transport by ships will prove more cost-effective over long distances, >1000 km, at smaller quantities. CO_2 transport by rail and road will be feasible for moving CO_2 on a small scale to specialized applications[25][31]. The technology of moving CO_2 streams through pipelines is well known; there are approximately 6000 km of pipeline,

which serves to transport CO_2[31][34]. Most of these pipelines serve the *Enhanced Oil Recovery* (EOR) industry[2].

2.2.4 Storage

When the CO_2 has been separated, it needs to be permanently stored. It can be achieved by storing CO_2 in geological formations; these formations range from deep saline aquifers and oil- and gas reservoirs. These geological formations or storage sites could potentially hold up to tens of million tonnes of CO_2, where physical and chemical mechanisms keep the CO_2 trapped[24].

Much of the technology needed to be able to store CO_2 in geological formations could be based on extraction methods used in the oil industry. Enhanced Oli Recovery (EOR) is a method of oil extraction where CO_2 is injected in a depleted oil reservoir to recover more oil, see Figure 2.7. Enhanced oil recovery has been practiced since the 1970s; thus, the technology and expertise are at a mature level[25][31][34].

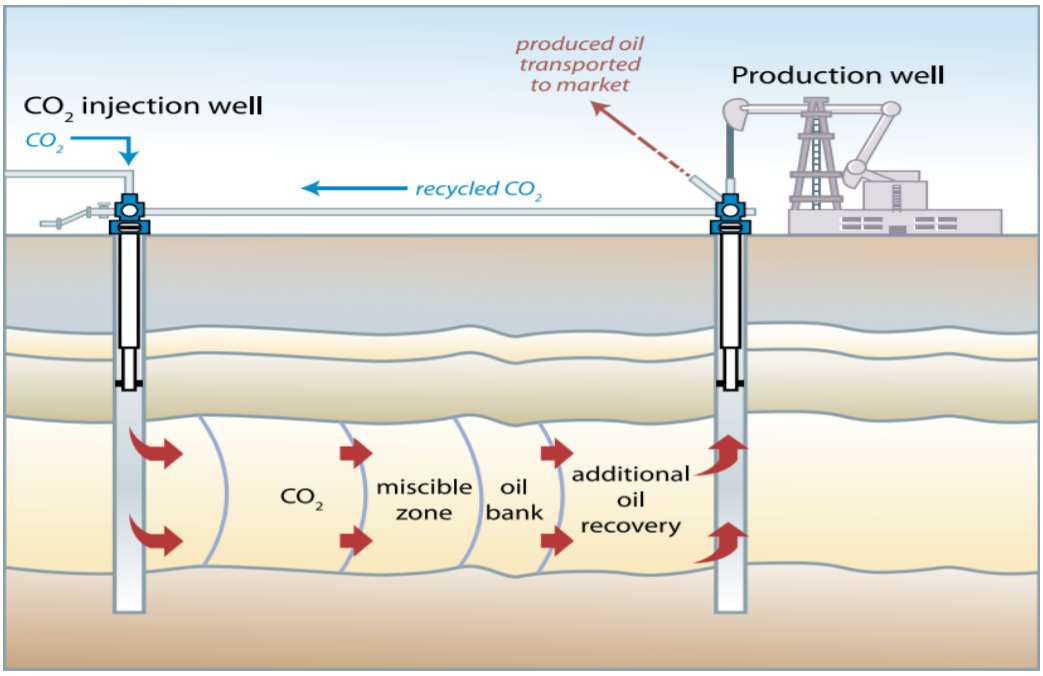

Figure 2.7: The figure depicts an EOR scheme. The figure reproduced with permission by B. Metz mfl. IPCC [14].

[2]See Subsection 2.2.4 for description of EOR.

2.2.5 Carbon Capture, Utilization and Storage (CCUS)

Carbon Capture, Utilization, and Storage (CCUS) are an expansion of the concept CCS, where the carbon is not permanently stored but utilized for other purposes. There are industrial processes that use CO_2. These are mainly in food and beverage production, but also used in chemical, plastic, or fuel production[25][31][35]. The CO_2 could also be supplied as a nutrient to grow houses and micro algae ponds for biomass production[27][36].

The advantage of CCUS over CCS is the value added to the CO_2 by utilizing it for industrial purposes. Adding value to CO_2 might increase the incentive of companies and governments to invest in CCS/CCUS technologies. The disadvantage of the CCUS concept is that it does not remove CO_2 from the atmosphere as CCS does; it only circulates it[25].

2.2.6 Direct Air Capture (DAC)

Direct Air Capture is what the name implies; it is the process of capturing carbon directly from the air. Compared with conventional carbon capture technologies, which use concentrated point sources of carbon, direct air capture presents several advantages.

First, direct air capture can provide a means to adjust the concentration of CO_2 in the atmosphere. Second, direct air capture technology can be an option of mitigating greenhouse emissions from mobile and distributed sources, such as automobile transport and the agricultural industry. Third, by installing direct air capture technology at the CO_2 storing site, any leakage from the site could be recaptured by direct air capture technology. This technology could potentially be placed anywhere as long it has a sufficient energy source and adequate sequestering sites to store the CO_2, which leads to the disadvantages of this technology. The air is a source of carbon 100-300 times more diluted than concentrated sources such as gas and coal power plants[25]. This leads to higher energy input, and treatment of much larger volumes of gas by direct air capture technology, compared to carbon capture technologies using concentrated point sources[31].

One DAC technology to take note of is Climework's DAC design, which uses the alkaline-functionalized adsorbents to capture CO_2 directly from the air. The CO_2 capturing process goes as follows; an untreated air stream enters the "Collector." Within the Collector, a filter is placed. The CO_2 in the airstream is chemically bound to the filter. The process continues until the

filter is saturated with CO_2. Once the filter is saturated, the desorption starts by heating the filter from 80 to 120 °C and reducing the Collector's pressure; this technique is called *temperature-vacuum-swing* (TVS). The desorbed CO_2 is then funneled into a storage unit. After cooling of the Collector, the process starts over again, see Figure 2.8 for a visual description of the technology[37].

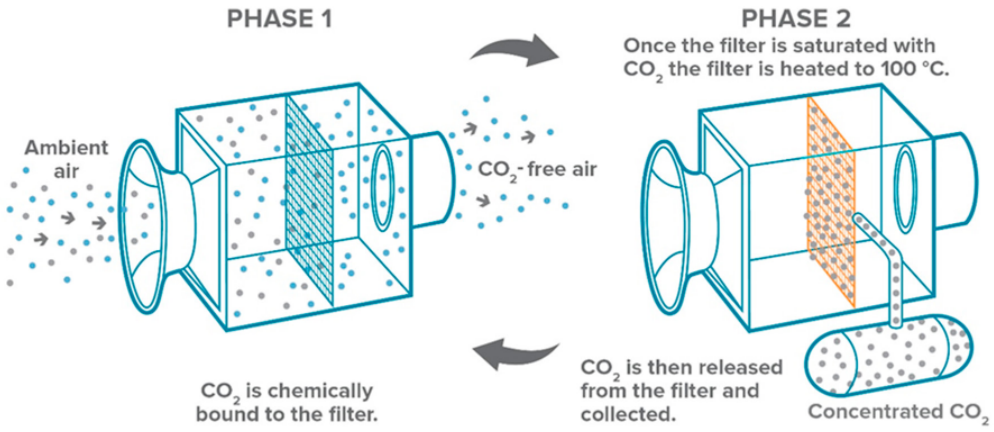

Figure 2.8: The figure depicts the Climatework's CO_2-Collector scheme. The figure reproduced pressure with with permission by V. Gutknecht *et al.*[37].

2.2.7 Present Status of CCS

According to the Global Carbon Capture and Storage Institute's (GCCSI) report, *Global Status of CCS 2019*, there are presently 51 large-scale CCS facilities in operation, under construction, or in development. This is an increase from 37 facilities in 2017. 19 of these facilities are operating, and where 4 are under construction. 28 of the facilities are under development, where 10 of these are in advanced stages of development, while 18 are still in early development stages.

The operational facilities today have a combined storage capacity to capture and store approximately 40 million tonnes of CO_2 per year—the capacity for storing CO_2 is expected to increase with around one million tonnes within the next 12-18 months after November 2019.

More than 25 million tonnes of CO_2 were permanently stored in 2019, where the source of CO_2 came from the power and industry sectors. Two new CO_2 capture and storage facilities started operations while other facilities

reached new CO_2 storage milestones. Some of these facilities are the Gorgon Natural Gas Processing Plant, where CO_2 injection into geological formations started in 2019. It the largest dedicated geological CO_2 storage facility in the world, where the facility will store up to 4 million tonnes of CO_2 per year.

The Alberta Carbon Trunk Line (ACTL) is a CO_2 transport project in Alberta, Canada. A pipeline of 240 km will transport CO_2 to either be stored or used in industries that require CO_2, such as the oil industry (EOR) and fertilizer production. The transport capacity is around 1.6 million tonnes of CO_2 per year.

Shute Creek Gas Processing Plant in Wyoming, US, Great Plains Synfuels Plant in North Dakota, US, Sleipner, and Snøhvit CO_2 Storage Facilities in Norway and Petrobas Santos Basin CO_2-EOR Facility in Brazil has cumulatively captured 100 million, 38 million, 22 million, 10 million tonnes of CO_2 respectively. All of the facilities use the captured CO_2 for EOR, except for Sleipner and Snøhvit, who permanently store the captured CO_2 in geological formations in the Norwegian continental shelf.

Based on the most recent studies of CCS, the cost of capturing CO_2 could cluster around 43 USD per tonne CO_2 captured for facilities planning to be operational in the period 2024-2028. Pilot-scale plants, which apply new carbon capture technologies, promise a capture cost of 33 USD[3][38] per tonne CO_2.

2.3 Carbon Capture in Molten Salts (CCMS)

In this section, the chemistry behind of *Carbon capture in molten salts* (CCMS) will be explained. However, it is necessary to explain the concept of *molten salts* before the chemical background of CCMS.

2.3.1 Molten Salts

As the name implies, molten salts are salt or a mixture of salts in a fluid phase. Usually, these molten salts or melts are in the solid phase at STP[4] and then become fluid at elevated temperatures. In industrial applications,

[3]The USD exchange rate of November 2019.

[4]STP: Standard Temperature and Pressure, meaning the temperature and pressure conditions are 25 °C and 1 atm, respectively.

molten salts have many desired traits, such as high heat capacity and high-temperature range, >1000 °C, as well as high ionic and electrical conductivity[39][40]. Molten salts are used in the production and treatment of metals, notably aluminum production, where the melt is used as an electrolyte in *the Hall-Heroult process*. Batteries and fuel cells that operate at high temperatures use molten salts due to its heat carrying capacity and high ionic conductivity[40]. Molten salts can also be used to store energy harvested from *Concentrated Solar Power* (CSP) facilities[41][42]. Molten salts do not only have applications in renewable energy but in nuclear energy as well. Molten salt can be used as a coolant for nuclear fuel, where the nuclear material is dissolved in the melt[43].

Even though molten salts have many benefits in certain applications, there are still many challenges with molten salts. The high temperatures required of molten salts make it harder and often more expensive to choose materials for the equipment used in a process where molten salts are required. Another challenge is the high corrosion rate of the equipment, which is mainly due to the high operating temperature and the corrosive nature of salt. More precaution is required when operating with molten salts since many potential incidents could happen, such as fire, explosions, exposure to toxic substances[39][40].

2.3.2 Chemical Background of CCMS

Carbon capture in molten salts (CCMS) is a method that uses the same principle as CaL to capture CO_2. Like CaL, CCMS uses the reversible carbonation reaction between an alkaline earth metal oxide such as CaO and CO_2. The main difference between CCMS and CaL is that the sorbent in a CCMS process is either dissolved or partially dissolved in the molten salt while CaL operates with a solid sorbent. The advantage of CCMS compared to CaL is that the sorbent does not degrade under operation. CCMS also has a faster kinetics between the sorbent and CO_2 compared to CaL. The CO_2 capturing process by the sorbent, in this case, CaO is described in Equation (2.5)[44].

$$CaO(s, diss) + CO_2(g) \rightleftharpoons CaCO_3(s, diss) \tag{2.5}$$

This process could be performed with any alkaline earth metal oxide (MO), in this thesis the main focus is by using MgO in the melt instead of

CaO, see Equation (2.6).

$$\begin{aligned} &MO(s, diss) + CO_2(g) \rightleftharpoons MCO_3(s, diss) \\ &M = Be, Mg, Ca, Sr, Ba \end{aligned} \tag{2.6}$$

The extraction of CO_2 by CCMS from a flue gas uses the same procedure as CaL, where CO_2 is separated from the flue gas by absorption and then desorbed as pure CO_2 by using *thermal swing*. Thermal swing is a term used when raising the operating temperature of the CCMS process so that the carbonization reaction of the sorbent reverses and starts decarbonizing instead.

Figure 2.9 illustrates the *Gibbs free energy*[5] (ΔG) vs. the temperature of the reaction between CO_2 and a alkaline earth metal oxide such as MgO or CaO, Equation (2.6). The reactions shown in the upper left corner of the figure will go rightwards as long as the Gibbs free energy is less than 0. The Gibbs free energy of the reactions are dependent on the temperature of the reactions. If the temperature of the reactions is raised to where the Gibbs free energy is above 0, the reactions will reverse leftwards, this method is called "thermal swing".

[5]Gibbs free energy will be explained in detail in Subsection 2.3.3.

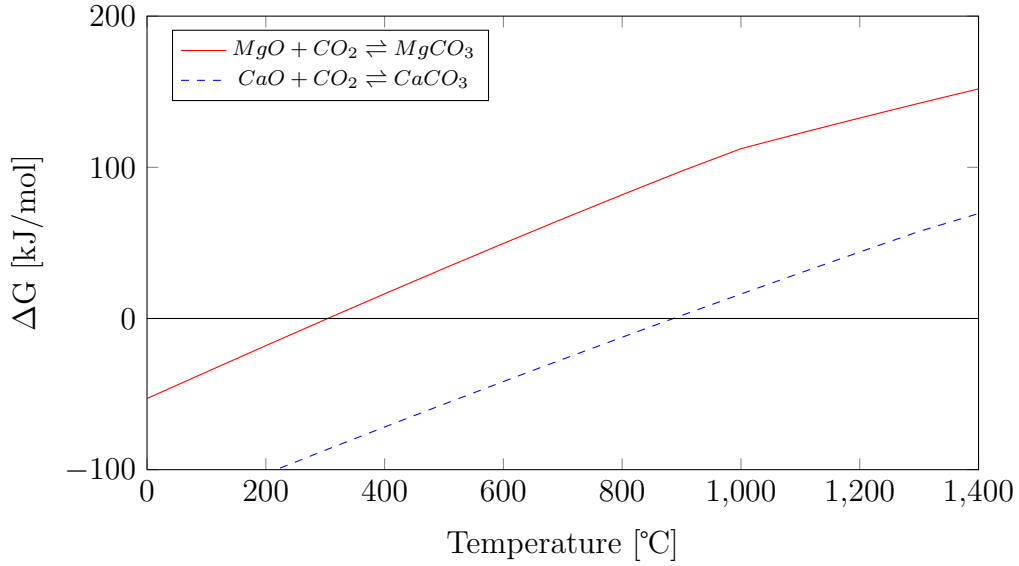

Figure 2.9: The figure depicts the Gibbs free energy (ΔG) vs. temperature (°C) for the carbonation reaction $MO + CO_2 \rightleftharpoons MCO_3$ (2.6) with $M = Mg$ and Ca, at 1 atm. The reactions shown in the upper left corner will go rightwards as long as the Gibbs free energy is below 0. The figure is made from simulations from HSC Chemistry 6.12[45].

In a CCMS process, the sorbent will either be dissolved or partially dissolved in the melt. Depending on the molten salts system, the melt will be chemically inert for both the sorbent and CO_2. That is unless if a specific salt, often a metal halide salt, is a component in the molten salts system used. The reactivity between the salt and the sorbent depends on what type of sorbent is used, and what type of salts are present in the melt.

When the sorbent reacts with CO_2 and creates a carbonate, the alkali metal halide, in this case, will then react with the carbonate, see Equation (2.7).

$$\begin{aligned} &MCO_3(s, diss) + 2AH(l) \rightleftharpoons MH_2 + A_2CO_3(s, diss) \\ &M = Be, Mg, Ca, Sr, Ba, Ra \\ &A = Li, Na, K, Rb, Cs \\ &H = F, Cl \end{aligned} \tag{2.7}$$

This reaction is called an *exchange reaction*. The reaction is causing the concentration of carbonates in the melt to decrease. The decrease of

carbonates causes the equilibrium point of the reaction between the sorbent and CO_2 to go rightwards. When the equilibrium point is farther to the right, it causes the sorbent to carbonate at a higher rate, in turn making the CO_2 capturing process more effective.

The total reaction equation of a CCMS process could be described as Equation (2.8).

$$MO + CO_2 + 2AH \rightleftharpoons MH_2 + A_2CO_3 \tag{2.8}$$

The reaction between the sorbent, CO_2 and the alkali metal halide also allows for higher operating temperatures for CCMS. This could be useful for some salt mixtures that possess a higher eutectic melting point than the decarbonation temperature of the carbonated sorbent used in the melt. For example, FLiNaK-salt possesses an eutectic melting point of 454 °C, while $MgCO_3$ starts decarbonzing at 305 °C. However, since the MgO and CO_2 do react with the components of the FLiNaK-salt (LiF-NaF-KF), it allows the usage of MgO with FLiNaK-salt at higher temperatures than 305 °C. Figure 2.10[6] shows that the highest temperature before the FLiNaK melt along with MgO start decarbonizing is 675 °C.

2.3.3 Gibbs Free Energy

Gibbs free energy (ΔG) is a value that describes where a reversible reaction will go, left or right. As well as in what rate the reaction will go in either direction. Gibbs free energy is described as a function of the enthalpy (ΔH), the temperature (T), and the entropy (ΔS) of the reaction, see Equation (2.9).

$$\Delta G^\circ = \Delta H^\circ + T\Delta S^\circ \tag{2.9}$$

G is the Gibbs free energy, H is the enthalpy, T is the absolute temperature, and S is the entropy. The value of ΔG determines which direction the reaction goes. If a reversible reaction has a value of $\Delta G < 0$, it means that the reaction will move to the right. In other words that the MgO is carbonated in a CCMS process. If $\Delta G > 0$, the reversible reaction will go to the left, which means that in a CCMS process, the $MgCO_3$ decarbonates and

[6]Figure 2.10 is illustrated in Subsection 2.3.3.

turns into MgO and CO_2. If a reaction takes place under a specific temperature where the reactants and products occur at the same rate, the reaction has reached its equilibrium point, or $\Delta G = 0$. The temperature where the reaction has $\Delta G = 0$ is called the *equilibrium temperature*[46][47].

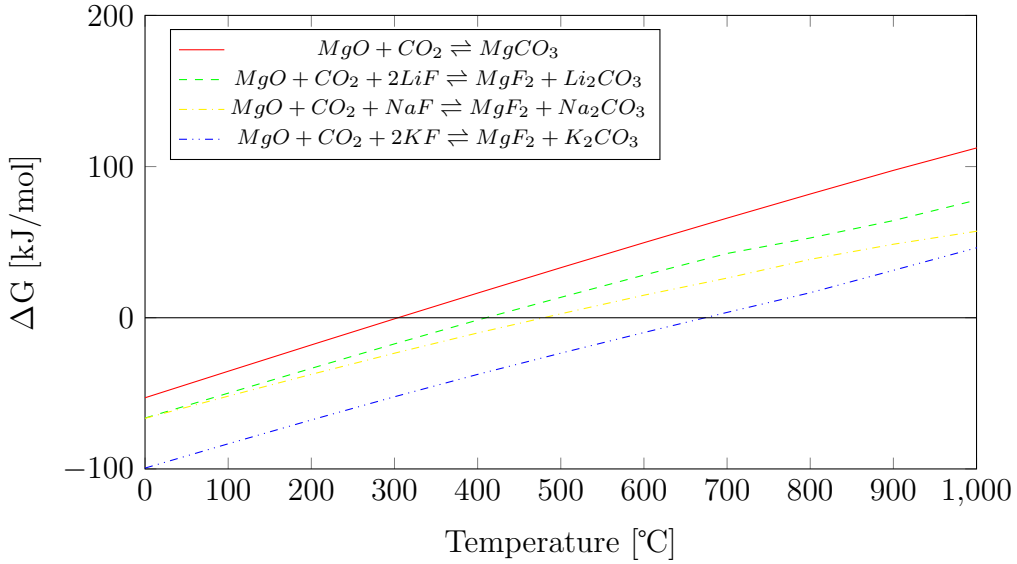

Figure 2.10: The figure depicts the Gibbs free energy (ΔG) vs. temperature (°C) for the carbonation reaction $MO + CO_2 \rightleftharpoons MCO_3$ (2.6) with $M = Mg$, and the total reaction $MgO + CO_2 + 2AF \rightleftharpoons MgF_2 + A_2CO_3$ (2.8) with $A = Li, Na, K$, and where F is fluoride. The reaction will go to the right if the temperature gives a negative ΔG value. If the temperature gives a positive ΔG value, the reaction will go to the right. The figure is made from simulations from HSC Chemistry 6.12[45].

Figure 2.10 depicts the Gibbs free energy against the temperature (°C) for the carbonation reaction, Equation (2.6), and the total reaction, Equation (2.8). As the figure illustrates $MgCO_3$ start decarbonizing at 305 °C, since $\Delta G = 0$ for the carbonation reaction. This means that any CCMS operation where the MgO sorbent is inert in the melt, it must have a operating temperature below 305 °C. By comparison, when MgO and CO_2 reacts with alkali metal fluorides, it allows for higher operating temperatures for MgO in CCMS. The figure illustrates the temperatures where $\Delta G = 0$ of the three total reactions $MgO + CO_2 + 2AF \rightleftharpoons MgF_2 + A_2CO_3$(2.8) with $A = Li, Na$, and K.

When choosing a chemical system, it is essential to know what the equi-

librium temperature of that system is. The operating temperature will swing over and under the equilibrium temperature during the CCMS process. Raising technical, economic, and safety measures might be necessary if the equilibrium temperature is high.

2.3.4 Heat of Reaction

The amount of energy that must be added or removed during a chemical reaction to keep all of the substances in the reaction at the same temperature is called *the heat of reaction*. If the chemical reaction is happening during constant pressure, the heat of reaction represents the change in the thermodynamic quantity called enthalpy. In other words, the change of thermodynamic quantity defined by the difference of the enthalpy value of substances after the reaction and the enthalpy value of the substances before the reaction. The symbol ΔH usually represents the heat of reaction. If ΔH of a reaction is positive, the reaction is said to be endothermic, meaning that the reaction needs heat energy to maintain the reaction. If ΔH is negative, the reaction is said to be exothermic, meaning the reaction releases energy in the form of heat[48].

In CCMS, the ΔH is important, since during decarbonization of the sorbent, the carbonated sorbent needs heat energy to release the CO_2. The heat required during the decarbonization process depends on the sorbent, see Equation (2.10) and (2.11).

$$\begin{aligned} &CaCO_3 \rightleftharpoons CaO + CO_2 \\ &\Delta H_{T=885^\circ C} = 165.8 kJ/mol \end{aligned} \tag{2.10}$$

$$\begin{aligned} &MgCO_3 \rightleftharpoons MgO + CO_2 \\ &\Delta H_{T=305^\circ C} = 98.8 kJ/mol \end{aligned} \tag{2.11}$$

The Equation (2.10), the reaction has a ΔH of 165.8 kJ/mol compared to Equation (2.11), where the reaction has ΔH of 98.8 kJ/mol, meaning less energy is needed to maintain the decarbonization reaction of $MgCO_3$ than $CaCO_3$. By using MgO as a sorbent in a CCMS process, the energy costs have the potential be substantially lower than by using CaO.

Equation (2.12) and Table 2.2 and 2.3 show the reaction enthalpy and the equilibrium temperature of the reactions between the MgO sorbent, CO_2,

and a metal salt. The salts listed on Table 2.2 and 2.3 are components of the salt mixtures screened in this thesis.

$$\begin{aligned} &MgO + CO_2 \rightleftharpoons MgCO_3 \\ &\Delta H_{T=305^\circ C} = -98.8 kJ/mol \end{aligned} \tag{2.12}$$

Table 2.2: The table show the equilibrium temperature ($T_{\Delta G = 0}$) and the reaction enthalpy of the carbonation reaction between MgO, CO_2, and an alkali metal salt (AH), $MgO + CO_2 + 2AH \rightleftharpoons MgH_2 + A_2CO_3$ (Total reaction), along with the reaction $MgCO_3 + 2AH \rightleftharpoons MgH_2 + A_2CO_3$ (Exchange reaction). The reaction will go rightwards: when $\Delta G > 0$ beneath the temperature, and $\Delta G < 0$ above the temperature. Note, (H) has usually been denoted as a halide, in this case (H) also includes the nitrates (NO_3). The data is gathered from HSC Chemistry 6.12[45].

	Total reaction		Exchange reaction	
Salt (AH)	$T_{\Delta G = 0}$	ΔH	$T_{\Delta G = 0}$	ΔH
LiF	410	-103	$\Delta G < 0$	
NaF	475	-93	$\Delta G < 0$	
KF	675	-125	$\Delta G < 0$	
LiCl	-2	-49	4168	149
NaCl	$\Delta G > 0$		$\Delta G > 0$	
KCl	$\Delta G > 0$		$\Delta G > 0$	
$LiNO_3$	3771	1588	2804	809
$NaNO_3$	3371	1382	2457	679
KNO_3	3478	1506	2635	862

Table 2.3: The table show the equilibrium temperature ($T_{\Delta G = 0}$) and the reaction enthalpy of the carbonation reaction between MgO, CO_2, and a non-alkali metal salt (AH_2), $MgO + CO_2 + AH_2 \rightleftharpoons MgH_2 + ACO_3$ (Total reaction), along with the reaction $MgCO_3 + AH_2 \rightleftharpoons MgH_2 + ACO_3$ (Exchange reaction). Note, (H) has usually been denoted as a halide, in this case (H) also includes the nitrates (NO_3). This table was made due to one of the non-alkali metal salts ($BeCl_2$) screened in this thesis did react with MgO and CO_2 with in the specified operating temperature range for CCMS with MgO as sorbent. The data is gathered from HSC Chemistry 6.12[45].

	Total Reaction		Exchange Reaction	
Salt	$T_{\Delta G = 0}$	ΔH	$T_{\Delta G = 0}$	ΔH
$CdCl_2$	5309	1334	3047	406
$BeCl_2$	849	-176	2360	-182
$Ca(NO_3)_2$	3563	773	1754	169

2.3.5 Hydrolysis in CCMS

Hydrolysis is a word derived from the two Greek words, *hydro*, meaning "water" and *lysis*, meaning "to split apart." The hydrolysis reaction is the reaction of splitting apart a water molecule (H_2O) to H^+-ions and OH^--ions[49].

Some salts can start a hydrolysis reaction if in contact with water. Salts are strong electrolytes that usually dissolve completely in water; however, some salts react with water. The reaction between water and an anion or a cation of a salt is called *salt hydrolysis*[46]. The salt hydrolysis reaction generally be described as:

$$AB(s) + H_2O(l) \rightleftharpoons AH(aq) + BOH(aq) \tag{2.13}$$

Hydrolysis of water in molten salts is not equivalent to the hydrolysis reaction of salt in an aqueous solution. That is not to say the hydrolysis of water in a molten salt mixture is not essential. Water vapor/gas mixed with flue gas could hydrolyze with some of the components in the molten salt mixture and create undesirable compounds.

A salt consisting of an alkaline earth metal (A) ion and two halide ions (X) hydrolyzing with water can be expressed as:

$$AX_2(l) + H_2O(l) \rightleftharpoons AO(s, diss) + 2HX(g) \tag{2.14}$$

Some halide salts give way to a different reaction than Equation (2.14), where hydrogen gas and chloride gas are created, shown in Equation (2.15).

$$MX_2(l) + H_2O(l) \rightleftharpoons MO(s, diss) + X_2(g) + H_2(g) \tag{2.15}$$

Where M is a non-alkaline earth metal. If the salt is an nitrate salt instead of a hailde salt the Equation (2.16) will be used.

$$MN(l) + H_2O(l) \rightleftharpoons MOH(s, diss) + 2HN(g) \tag{2.16}$$

Where N represents the nitrate salt in the reaction. If either reactions occur during a CCMS-process, measures have to be taken due to the undesirable compounds that could occur during the CCMS process[50].

2.3.6 The Lewis Acid-Base Properties of Molten Salts

To determine if a molten salt mixture is potentially able to dissolve the MgO sorbent sufficiently, the Lewis acid-base characteristics of the components in the molten salt mixture must be known. The American chemist G. N. Lewis defined an acid as a substance that can accept a pair of electrons from a donor substance, and a base to be a substance that can donate a pair of electrons to another substance[46].

Generally a molten salt mixture is a *Lewis base* if the melt contains an abundance of available uncomplexed anions that can stabilize certain metal ions. The anions and the metal ions form coordination complexes[7] that exhibit reduced volatility. A Lewis base melts also tends to contain an abundance of monovalent cations such as alkali metals ions. In other words, these molten salt mixtures are Lewis bases because of the abundance of uncomplexed anions, X^-, that act as electron-donating components.

However, molten salt mixtures that are *Lewis acids* are the opposite of the Lewis bases. Most of the anions already attached to the coordination complexes in the melt. Meaning there are no "free" anions that stabilizes the metal ions present in the molten salt mixture, which means that Lewis acidic melts contain metal ions that possess higher thermodynamic activity coefficients. Since the metal ions in the melt have higher thermodynamic activity coefficients means that they have increased reactivity and volatility. A molten salt mixture that is a Lewis acid contains an abundance of cations

[7] Coordination complexes or coordination compounds are substances that have a chemical structure where a central metal atom is surrounded by nonmetal atoms or group of atoms called ligands.

with a coordination number that exceeds the oxidation state, meaning ions from the transition metals, rare earth, and lanthanides[51].

An example of a basic molten salt mixture is eutectic FLiNaK salt. As explained above, molten eutectic FLiNaK fits the description of a Lewis base. The abundance of uncomplexed anions, in this case F^--ions, and the monovalent cations such as Li^+, Na^+, and K^+, in the melt. If MgO is present in this FLiNaK melt, it will probably not be able to dissolve sufficiently, since MgO is also a Lewis base.

As the example shows, to potentially dissolve the MgO sorbent sufficiently, the molten salt mixture probably must be a Lewis acid.

2.3.7 Magnesium

In this subsection the element magnesium (Mg), and the CO_2-sorbent central in this thesis, MgO, will be explained.

Mg is the seventh most common element in the earth's crust; it occurs in nature as dolomite ($CaCO_2{\cdot}MgCO_3$) and carnallite ($KCl{\cdot}MgCl_2{\cdot}6H_2O$). Mg usually extracted from seawater through electrolysis[52]. It is worth mentioning that 1 km^3 of seawater contains 1.3 million kg of Mg. The abundance of Mg and the fact that the extraction of Mg is a relatively easy process make Mg a cheap resource[53].

The oxidized form of Mg is magnesium oxide (MgO), also known as magnesia. MgO is the second most common compound found in the earth's crust, which makes it a cheap and available candidate for CO_2 sorption. Along with the abundance of MgO, MgO possesses suitable basicity, which increases the chemical reactivity with the acidic CO_2. The theoretical CO_2 uptake capacity by MgO is 1.09 g CO_2 per 1 g MgO, or 109 wt%. This theoretical uptake capacity is high compared to the other metal oxide-based sorbents, such as CaO, which possesses a theoretical CO_2 uptake capacity of 0.78 g per 1 g CaO, or 78 wt%. MgO requires lower energy input compared to CaO-based sorbents due to the relatively low temperature needed to regenerate MgO, see Figure 2.9. Lastly, MgO is non-corrosive, which lowers the maintenance expenses of the CO_2 capture equipment, and MgO is eco-friendly to extract from nature.

The reactivity between CO_2 and commercially available pure MgO in solid phase have typically shown to be far from satisfactory, 0.02 g per 1 g MgO, or 2.0 wt%. The unsatisfactory performance is due to slow kinetics between the MgO sorbent and the CO_2. As well as the low sorbent surface area which the

CO_2 can react with to create $MgCO_3$. This, in turn, leads to the impermeable $MgCO_3$ layer that covers the sorbent surface, hindering further CO_2 sorption. However, studies show that by adding certain compounds with the MgO gives an increased reaction kinetics between the MgO and CO_2. Lastly, the deterioration of the MgO sorbent due to sintering after a few sorption-desorption cycles reduces MgO as a viable sorbent even further[54][55].

The examples above refer to that MgO is a sorbent in solid phase. By having MgO sorbent dissolved in molten salt, all of these problems mentioned above could be evaded.

2.3.8 Earlier Studies of CCMS

In 2013, Olsen *et al.* conducted a study to examine what molten salt system would be most effective for capturing CO_2, using CaO as sorbent. Two systems gave significant results, CaO-LiF-CaF_2 and CaO-NaF-CaF_2. Both systems had a total conversion rate of 92% from CaO to $CaCO_3$. This rate of conversion led to very efficient absorption of CO_2 by the sorbent. The recorded CO_2 concentration of the gas exiting the reactor was below the detection limit of the analyzer, 0 ppm recorded, or less than 400 ppm. These results show that the sorbent was able to perform approximately complete absorption of CO_2 until the sorbent was saturated. The following desorption stage was less effective than the absorption stage, where the conversion of CaCO°3 to CaO was 47.5% and 83.8% for CaO-NaF-CaF_2 and CaO-LiF-CaF_2, respectively[6].

The year after, 2014, Tomkute *et al.* carried out a study to find the optimal operating temperature of a cyclic CO_2 capture process with a CaF_2-$CaCl_2$ molten salt system with CaO as sorbent. The most efficient system had 15 wt% of CaO in CaF_2-$CaCl_2$ (11.7-73.3 wt%). The absorption process was conducted at 705 °C, while a complete desorption process was conducted at 945 °C. The carrying capacity of this system was 0.667 g per 1 g sorbent. This system went through 12 absorption/desorption cycles and did not show any sign of degrading, see Figure 2.11. A CaO-$CaCl_2$ (5.32-94.68 wt%) system was tried as well, where the system was cycled ten times. There was no sign of a degrading sorbent. This system achieved a carrying capacity of 0.504 g CO_2 per 1 g sorbent[56].

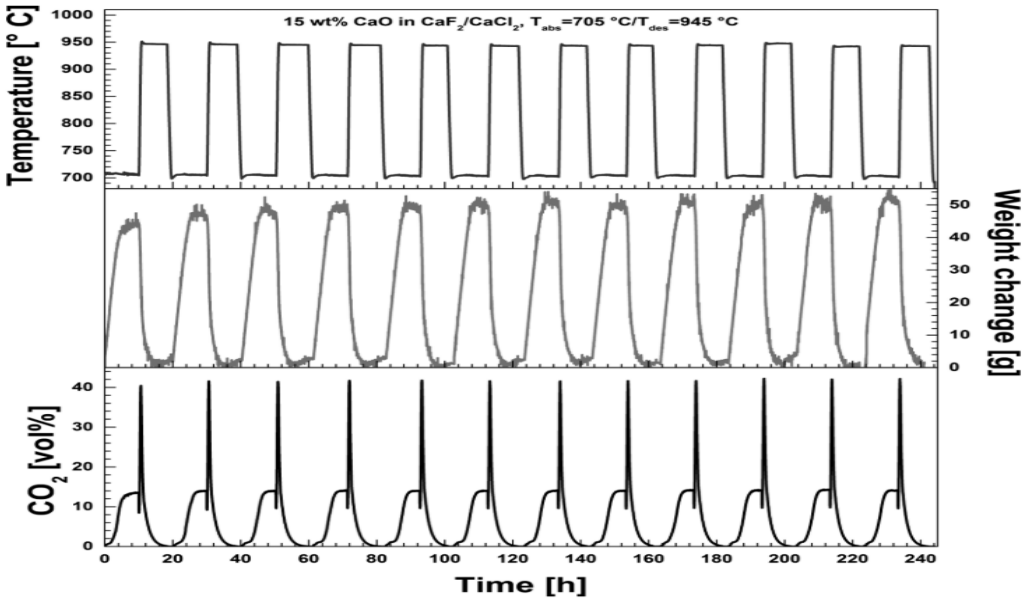

Figure 2.11: The figure show 12 cycles of CO_2 capture with 15% CaO in eutectic CaF_2-$CaCl_2$. The CaO sorbent maintains its CO_2 carrying capacity through the 12 cycles. The figure is reproduced with permission from Tomkute *et al.* (2014)[56].

In 2017, a study carried out by Nygård *et al.* found by having the CaO sorbent dissolved in molten salt had significant benefits. In CaL where the CaO sorbent is in a solid-state, the reaction between the CaO and CO_2 takes place on the surface of the sorbent; this causes carbonate to accumulate on the sorbent surface. The CO_2 has to diffuse through the carbonate to reach the unreacted CaO. This challenge is absent in CCMS, where the thought is that the carbonate dissolves in the molten salt immediately after the reaction—thus freeing the surface CaO to react with the incoming CO_2—making fast kinetics between CaO and CO_2 through the carbon capture process. The molten salt systems used in this study were CaO-$CaCl_2$ and Ca-CaF_2-CaCl. The systems tested for cyclic CO_2 capture. The performance of both molten salt systems showed that the CO_2 capture capacity increased in the first cyles and then stabilized. The systems did not show any deterioration of the reaction kinetics. The sorbents captured over 80% of the CO_2 before they were saturated. The best performing molten salt system achieved a capture fraction of 93.5%, and the system had 15 wt% CaO in CaF_2-$CaCl_2$ at 730 °C. While the system with the highest sorption capacity at 0.109 g CO_2 per 1 g sorbent was 20 wt% CaO in CaF_2-$CaCl_2$ at 700 °C, these results show

that CCMS with these molten salt systems performs better than CaL[44].

The CCMS experiments before 2017 were mainly conducted with a gas consisting of only CO_2 and N_2 gas. However, since real flue gas exiting a power plant will consist of CO_2 and N_2 gas, as well as water vapor, SO_2, NO, trace gases, and particles, it was necessary to test the effects of using one of these additional gases in the CCMS process. In the spring of 2017, master's degree student Maria Hansen conducted experiments to investigate if hydrolysis occurred in the melt when water vapor was added to the flue gas entering the molten salt reactor. Hydrolysis did occur when water vapor came in contact with molten CaF_2-$CaCl_2$. The hydrolysis reaction between the CaF_2-$CaCl_2$ and the water vapor created HF and HCl acids. Since HF and HCl can cause adverse effects on the human body when exposed, it is preferable to reduce the hydrolyzing effects of water in the molten salt. Hansen found that having a higher concentration of CaO sorbent in the melt reduces the hydrolysis reaction, and by lowering the operating temperature. The results found in Hansen's master thesis were publicized in an article in 2017[57].

In the spring of 2018, the master student Nils Amund Rusås Ruud investigated the sulfation of the CaO and $CaCO_3$ in a eutectic mix of molten CaF_2-$CaCl_2$ salt. Ruud wanted to see how SO_2 would affect the carbon capture process. Since the reaction between CaO/$CaCO_3$ and SO_2 is thermodynamically favorized over the carbonation of CaO. The gas entering the molten salt reactor consisted of up to 0.5% SO_2 and 3% O_2 gas. Ruud's experiments show that the CO_2-capture rate was reduced inverse proportionally to the amount of SO_2 in the gas entering the reactor. Meaning indirect sulfation of the CaO and direct sulfation $CaCO_3$ did occur[58].

In 2019, master student Åshild Grøtan conducted several experiments with different types of sorbent and salt mixtures. Grøtan tried to find alternative chemical systems that could reduce the high energy costs of the CCMS process. Grøtan tested MgO, CaO, and SrO in different types of molten salt mixtures. Grøtan found that MgO had stable CO_2 absorption, 73% of the MgO converted to $MgCO_3$, but a low CO_2 capture rate. The SrO sorbent had a higher conversion to $SrCO_3$, 90%, than MgO. However, SrO were more unstable absorption than MgO. LiF-CaF_2 with CaO as sorbent was shown to have the most effective carbon capture of any chemical system tested. The CaO-LiF-CaF_2 system was able to obtain complete absorption form a gas with 4 vol% CO_2, which is a very low concentration[59].

2.4 FTIR Spectroscopy

During the experiments, a *Fourier Transform InfraRed* (FTIR) spectrometer was used to measure the CO_2 concentration of the gas exiting the molten salt reactor.

Infrared spectrometry is a method to identify chemical compounds, usually organic compounds. When a chemical compound sample is analyzed, an *infrared light* (IR) beam strikes the sample. The sample absorbs some of the energy of the IR beam. The energy of the IR beam that is not absorbed is analyzed. The wavelengths of the IR beam can describe the contents of the sample. IR spectrometers utilize the vibrations of the non-linear molecules. Molecules with N atoms vibrate at a frequency of 3N-6. When IR radiation strikes a molecule, the molecule will absorb some of the radiation. The absorbed radiation has the same frequency as the vibrations of the molecule. Because of these absorptions, a unique absorption band is created. The absorption band works as a "fingerprint" so that the molecule can be identified[60].

The first generation of infrared spectrometers emerged in the 1940s by the need for a simple, reliable technique to analyze organic materials. The first generation infrared spectrometers were based on dispersive technology. Even though the infrared spectrometers were a powerful tool, it had its shortcomings, such as slow scanning speed, low throughput, and need for manual operations. In the 1960s, the Fourier Transform Infrared (FTIR) spectrometer was developed for commercial use. The usage of FTIR spectrometers was primary for advanced research due to the high costs and the requirement of large computers to run the FTIR. The technological advancements since the 1960s reduced the cost of running the FTIR spectrometer, as well, enhanced the capabilities of the FTIR. Today FTIR is widely used for organic compounds identification[61].

An FTIR spectrometer consists of several parts, such as an IR light source, beamsplitter, a laser, a detector, and two mirrors. One of the mirrors is fixed while the other mirror is moving. The mirror and the beamsplitter are collectively referred to as the interferometer. Infrared light from the IR source hits the beamsplitter. The beamsplitter divides the IR light in two. The split light beams hit the mirrors, and the mirrors reflect the light beams to the beamsplitter, where they recombine. When the IR beams recombine, their wavelength might or might not be the same. If the wavelength is the same, they have traveled the same distance and recombine constructively. If

the distance between the moving mirror and the stationary mirror from the beamsplitter is not equal, the two recombining IR beams will have different wavelengths and create a destructive interference pattern. The recombined IR beam then passes through a sample. The sample absorbs some of the energy of the beam while the rest of the energy is transmitted. The transmitted energy hits the detector, and the detector records the total intensity of the energy into a signal. The signal sent to a computer where it is digitized and processed. The computer uses a Fourier transform algorithm to produce a spectrum of signals from the detector. Which, in turn, creates a "single beam" spectrum. The "single beam" spectrum is then analyzed by comparison with a reference or "background." A "background" is a collected single beam spectrum without a sample, see Figure 2.12[61].

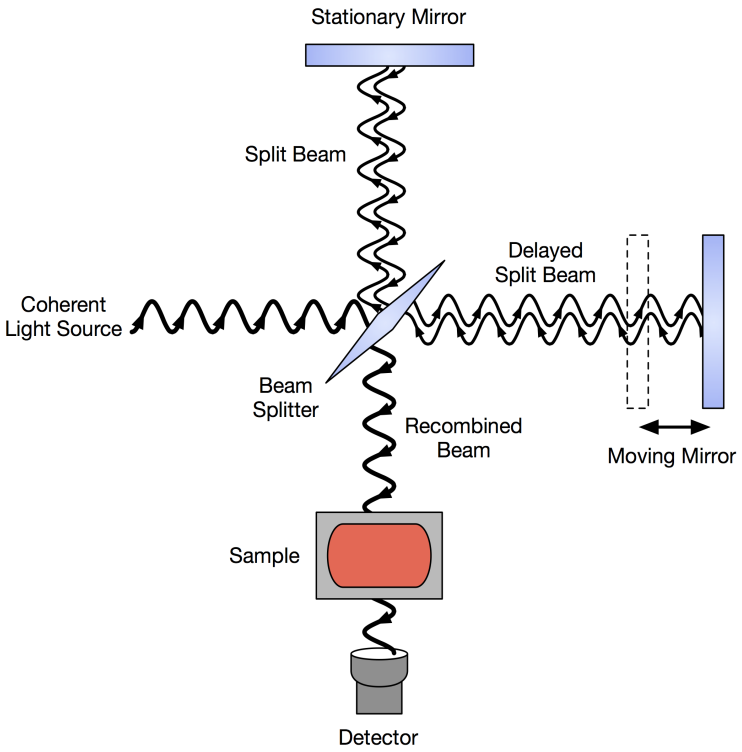

Figure 2.12: The figure illustrates how FTIR-devices function. An IR-beam is split in two, where the beams reflected by one stationary mirror and one moving mirror. The reflected beams are then recombined; this creates an interference pattern. The recombined beam is then beamed through a sample. The energy that was not absorbed by the sample is analyzed. The figure is sourced from Wikimedia Commons[62].

Chapter 3

Method

3.1 Screening

In this section, the screening method of the salt mixtures that could potentially be used in the CCMS process with MgO as a CO_2-sorbent will be explained. The screened salt mixtures are initially chosen by their eutectic melting points. The eutectic melting points of the salt mixtures screened must be below 305 °C, due to the $MgCO_3$ starts decarbonizing over 305 °C, see Equation (2.6) and Figure 2.10. The identification of the salt mixtures with the criteria mentioned, a database of phase diagrams named ACerS-NIST *Phase Equilibria Diagram Database* 3.1.0 were used[63].

After finding salt mixtures that fulfill the requirement mentioned above, the next step is determining if any of the screened salt mixtures have components that would interact with the MgO sorbent and CO_2, through Reaction[1] (2.7) and (2.8). If any of the screened salt mixture's components react with MgO and CO_2 through Reaction (2.7) and (2.8) the reaction enthalpy must be taken into consideration, a low reaction enthalpy is desired. Thermal stability of all the screened salts will be determined and if any hydrolysis reaction would happen when operating any of the screened salt mixtures. The thermal stability, the reactivity with MgO and CO_2, reaction enthalpy, and hydrolysis of a salt mixture are determined by simulating Reaction (2.7), (2.8), and (2.14) with HSC Chemistry[45]. If any of the salt mixtures' components do not react with MgO, the CO_2 capturing process could be less effective and higher operating temperatures cannot be achieved during the CCMS process.

[1]Equation will be referred to as "Reaction" through Chapter 3 and 4.

If the salt mixtures components are not thermally stable within the specified temperature range, they are also not suitable for CCMS. If any of the salt mixtures components hydrolyze under the specified operating temperature range, measures have to be taken to deal with the hydrolysis.

The next step is to determine if the salt mixture is a Lewis acid or a base. The content laid out in Subsection 2.3.6 have been used during the screening of the salt mixtures. If a salt mixture will act as a Lewis acid towards the sorbent, it might be able to dissolve the MgO sorbent sufficiently. Since there is very little literature on the solubility of MgO in molten salts, only one article is found on the matter[64]. The article discusses the solubility of MgO in molten $MgCl_2$-$CaCl_2$ salt. Thus the approach explained in the Subsection 2.3.6 is the only way to determine if a molten salt mixture might dissolve the MgO sorbent sufficiently based on the Lewis acidity or basicity of the molten salt mixture.

Lastly, the practicality of operating any of the screened salt mixtures in a CCMS process must be determined.

3.2 Experimental

3.2.1 Purpose

This section will describe the method of the CCMS experiments with molten FLiNaK and Copper(I)chloride-potassium chloride (CuCl-KCl) salt mixture with MgO as sorbent.

This thesis's first task was to test one of the hypotheses laid forth in Åshild Grøtan's master thesis, and then find and test other salt mixtures that have the necessary characteristics to be used in a CCMS process. Since the thesis focus was redirected rather early, any method of finding suitable salt mixtures was not conducted. This thesis' advisor suggested both salt mixtures used in the experiments. It was meant that the thesis' author was to find suitable salt mixtures independently; as explained above, this did not happen.

3.2.2 Experimental Equipment

The Layout of the Equipment

The molten salt reactor, with its components, is illustrated in Figure 3.1. The reactor consists of an electric tube furnace that can reach temperatures of up to 1250 °C. Within a ceramic tube is placed within the electric tube furnace. This ceramic tube is protecting the heating components of the tube furnace from wear and tear. A radiation shield is mounted at the bottom of the tube furnace. This shield has a circular shape, and its purpose is to reduce the energy loss. A suspension crane mounted over the tube furnace. The molten salt reactor is hung from this suspension crane and lowered inside the ceramic tube within the tube furnace.

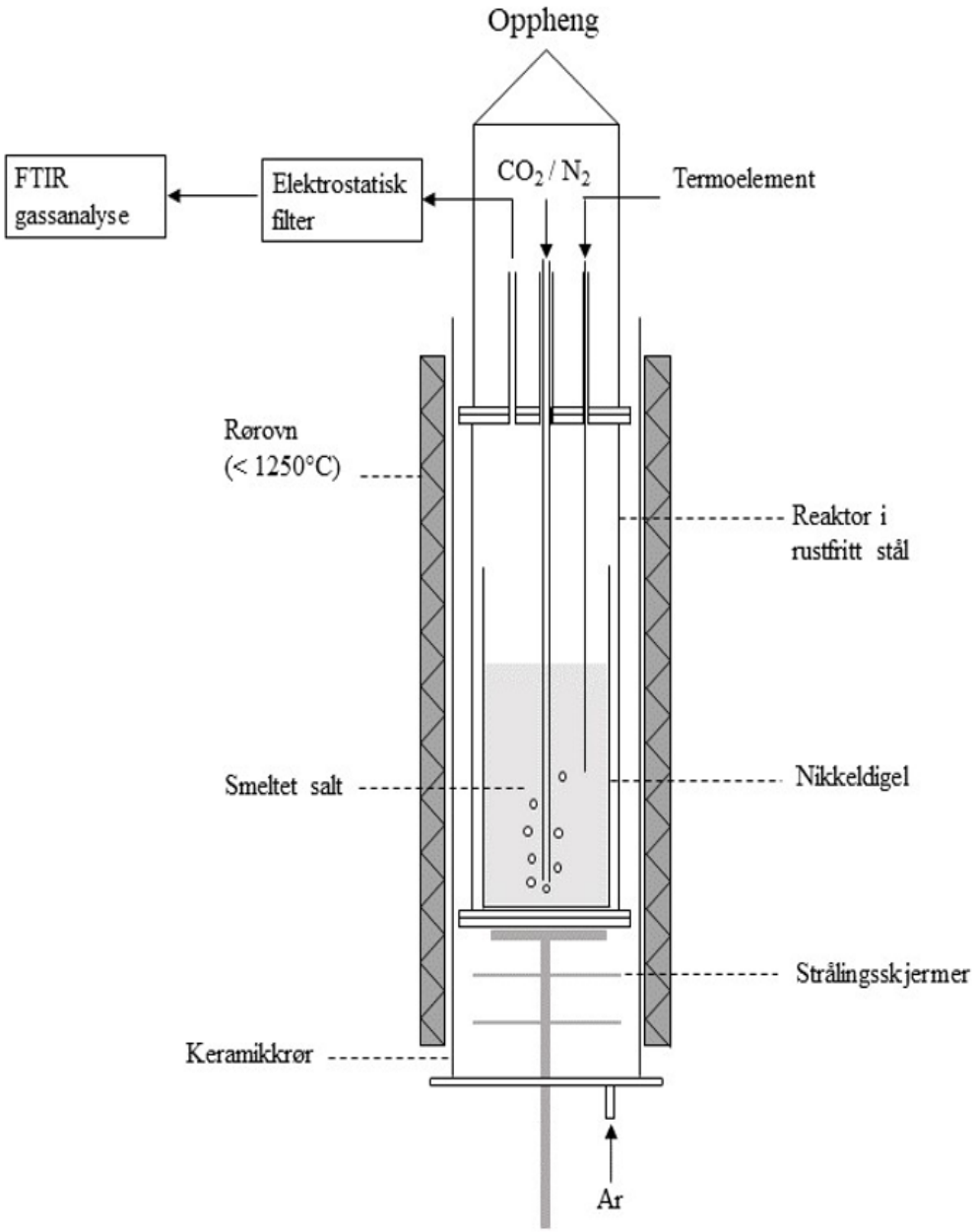

Figure 3.1: The components of the experimental equipment. The components names are in Norwegian. "Rørovn" - Pipe oven, "Smeltet salt" - Molten salt, "Keramikkrør" - Ceramic tube, "Reaktor i rustfritt stål" - Reactor of stainless steel, "Nikkeldigel" - Nickel crucible, "Strålingsskjermer" - Radiation shield, "Termoelement" - Thermostat, "Oppheng" - Suspension crane, "Elektorstatisk filter" - Electrostatic filter, "FTIR gassanalyse" FTIR gas-analysis. The figure is a modified version made by Heidi S. Nygård.

The reactor consists of stainless steel; a nickel crucible is placed within the reactor. The crucible has the purpose of holding the salt and the CO_2-sorbent. The top-lid of the reactor has two inlets and one outlet. In Figure 3.1, the rightmost inlet is where the thermostat put through into the molten salt. The thermostat used is a *K-type (NiCr-NaAl) thermostat*. The inlet in the middle shown in Figure 3.1, is the gas inlet. A nickel pipe connected to the gas source via a plastic pipe is put through the reactor's gas inlet and into the molten salt. The nickel pipe is placed 1 cm over the bottom of the nickel crucible. The nickel pipe's diameter is 11 mm, and the inner diameter of the pipe is 7.5 mm. The gas from the source is led into the molten salt through the nickel pipe. The gas "bubbles" through the molten salt and arrives at the gas outlet at the reactor's top-lid. The outlet is connected to an electrostatic filter that removes most impurities from the gas. After going through the electrostatic filter, the gas is led into the FTIR to be analyzed. Mineral wool is placed between the top-lid and the main body of the reactor. The mineral wool serves to seal the reactor making it airtight, save for the gas entering, and exiting the reactor from the gas source. The bottom lid of the reactor also has the same arrangement as the top lid.

The gas source consists of two gas tanks, CO_2, and N_2-gas, connected to a *Mass Flow Controller* (MASS-STREAM, M+W Instruments GmbH, EL-FLOW Prestige), this controller will be referred to as MFC form now on. The gas entering the reactor is a combination of CO_2 and N_2-gas; the MFC controls these two gas components' concentrations. The MFC logs the concentrations of CO_2 and N_2-gases with the software *Lab-view 8.2* (National Instruments).

Whenever the reactor is hot, before, during, and after an experiment, N_2-gas must flow through the reactor. The N_2-gas stream through the reactor is primarily to create an inert atmosphere within the reactor and to stop any molten salt sealing shut the nickel pipe by solidifying inside the nickel pipe. From the bottom of the electrical tube furnace, a small stream of Ar-gas enters the space between the suspended reactor and the ceramic tube. This stream of Ar-gas has the purpose of reducing the corrosion of the reactor. At the top of the tube furnace, heat isolation in mineral wool (*Superwool 607 Blanket*) is placed.

The electrostatic filter consists of a metal thread, that served to clean the gas passed through the electrostatic filter. The metal thread has a voltage of 6-8 kV between its ends, almost no current passing through it. The high voltage creates an electrical field along the thread; when salt particles enter

this field, the particles ionize and become dust attached to the inner wall of the stainless steel cylinder. This high voltage metal thread is placed within a grounded stainless steel cylinder—the stainless steel cylinder covered by a larger cylinder made of polyoxymethylene (POM). The electrostatic filter has the purpose of protecting the FTIR from contamination and wear and tear by salt particles.

Gases and Chemicals

All gases and chemicals used in the experiments are listed in Table 3.1 and 3.2.

Table 3.1: The gases used for the experiments, the gases are supplied by AGA AS.

Gas	Prod.Nr	Quality	Purity
Ar	100324	4.0	99.99%
N_2	100776	5.0	99.999%
CO_2	100764	4.5	99.995%

Table 3.2: Specification for the chemicals used in the experiments. The suppliers are Sigma Aldrich (SA), Alfa Aesar (AA), and VWR.

Compound	CAS-No. EC-No.	Prod.No. Lot.No.	Quality Purity (%)	g/mol	Supplier
MgO	1309-48-4 2215-171-9	83540.290 18G024135	 99.3	40.31	VWR
LiF	7789-24-4 MKBH4522V	237965	 98.5	25.94	SA
NaF	7681-49-4 232-151-5	27859.293 18K124119	 100	41.99	VWR
KF	7789-23-3 232-151-5	26820.293 18K124120	Normapur 99	58.1	VWR
KCl	7447-40-7	31248 SZBD0670V	puriss, 99.5-100.5	74.55	SA
CuCl	7758-89-6 231-842-9	11871	 97.0	98.99	AA

3.2.3 Approach

Preparations

The salts used in the experiment were dried a storage oven at around 200 °C in 24 hours. For the salts used in the experiments, this approach was sufficient. The MgO sorbent had to be calcinated at higher temperatures before it was used in the experiments.

Calcination of the Sorbent

The MgO sorbent was calcinated in a muffle oven (Thermconcept, Furnace KC 128/13 NB). MgO is heated up to 1000 °C at 4 hour period when the temperature has reached 1000 °C; it stays at that temperature for 10 hours. After 10 hours of calcination of the MgO, the MgO is cooled down to 200 °C. The MgO is then moved to the storage oven. Figure 3.2 describes the calcination regime.

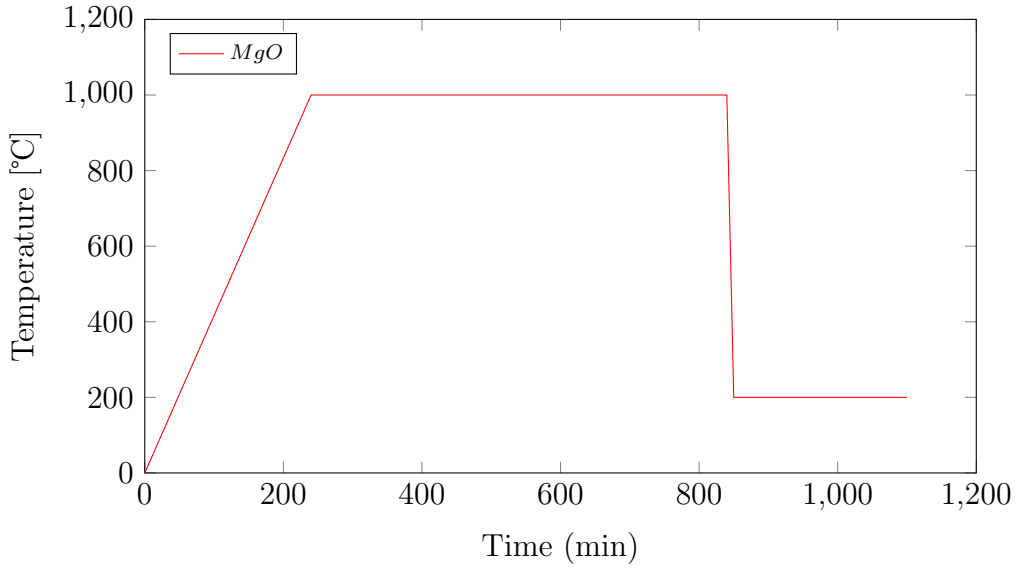

Figure 3.2: The calcintaion regime of the MgO sorbent. The cooling segment of the graph is not accurate.

Filling the Crucible Before the Experiment

Salt in powdered form is more voluminous than solidified salt after being melted. Meaning then filling the crucible, only a part of the salt and sorbent's total amount could fit the crucible; thus, the salt and sorbent in the crucible must be melted and cooled before rest of the salt and sorbent entered the crucible. The melting and then filling salt and sorbent would continue to 500 g of it is placed in the crucible. The crucible is approximately 16 cm from its inner bottom to the top; depending on the salt mixture, 500 g of salt and sorbent would fill around 10 cm. The salt mixture is melted in the muffle oven at around 50-100 °C above the specific salt mixture's eutectic melting point in the crucible. The salt is heated to a rate of 250-300 °C per hour. When the desired temperature was reached, it stayed at that temperature for 2-3 hours to ensure the salt was adequately melted.

Conducting the Experiment

The preparations explained above are done a day or a few hours before the experiment. The nickel crucible is filled with salt and sorbent and then weighted to see if the desired amount of salt and sorbent is in the crucible. The crucible is placed in the reactor. The nickel pipe that leads the gas and the thermostat is placed a few centimetres above unmelted salt. See Figure 3.1, to see where the reactor is placed in the tube oven.

The tube oven is turned on to heat the salt. During the heating of the salt, a stream of 0.2 l/min N_2 gas flows through the reactor and an Ar gas stream entering from the bottom of the tube oven.

When the salt is melted, the nickel tube and the thermostat are lowered to 1 cm above the crucible's bottom. N_2 gas is bubbling the molten salt; this is done for an hour to ensure the salt mixture and sorbent are adequately mixed. During this period of mixing, the FTIR is prepared for the experiment. The FTIR must be flushed to remove trace particles from earlier experiments. The flushing process consists of flowing a stream of N_2 gas straight from the MFC through the FTIR for 30 minutes. After the flushing, a background specter of the N_2 gas is made. Then the calibration of the CO_2 concentration between the FTIR and the MFC is done. The calibration process is done when the CO_2 concentrations from the MFC to the FTIR are stable in 30 minutes. The electrostatic filter is disassembled, and the components are cleaned of ionized salt particles.

When everything is prepared, and the salt's temperature has reached its desired value, the CO_2 absorption experiment can start. The stream of N_2 gas is increased to 0.6 l/min, and a 0.1 l/min CO_2 stream is added to the N_2 stream. The combined gas stream is flowing through the molten salt and out of the reactor to the FTIR. The FTIR measures the CO_2 concentration of the gas exiting the reactor. The absorption experiment ends when the concentration of CO_2 entering the FTIR is around the same as the concentration exiting the MFC.

When the experiment is over, the tube oven is turned off, and the nickel tube and the thermostat are elevated over the molten salt to make sure they are not stuck in the salt when it is solidified. The stream of CO_2 gas is turned off, and the N_2 gas stream is reduced to 0.2 l/min. The stream of N_2 gas into the reactor serves to make an inert atmosphere and make sure that no salt climbs into the nickel tube.

After the Experiment

When the reactor has cooled to a safe temperature, the nickel crucible is removed from the tube oven. The salt has solidified as a slab at the bottom of the crucible. Removing this salt from crucible requires reheating the salt to a liquid state. The nickel crucible is placed in the muffle oven. Depending on the salt mixture used, the temperature is set at 150 °C over the given salt mixture's eutectic melting point in the crucible. The salt-containing crucible is heated at the given temperature for 2-3 hours to ensure the salt is properly melted. After 2-3 hours inside the muffle oven, the crucible with molten salt is removed from the oven with iron tongs. The molten salt is poured into a square iron crucible, where the salt quickly solidifies. The iron crucible lays in a bed of sand within a wooden box. The sand bed is to protect the floor from heat damage and capture droplets of molten salt that might splash out of the iron crucible. The quick cooling of the molten salt in the iron crucible makes the salt very brittle; thus, it is easy to remove the salt from the crucible. The salt that is not easily removed usually sticks to the edges of the square iron crucible. This salt must be either washed with water, brushed, or picked with a chisel to remove it from the iron crucible.

3.2.4 Calculations

Calibrations

Before every experiment is conducted, it is necessary to conduct a calibration between the MFC and FTIR. The FTIR does not register the correct concentrations of CO_2 exiting the reactor; thus, a calibration is needed. N_2 and CO_2 gas with the same concentrations meant for the experiment flow directly from the MFC to the FTIR for 30 minutes. The data gathered by the concentration logging software of the MFC and the FTIR are used to calculate the calibration constant k, see Equation (3.1). This constant is multiplied into the data series gathered by the FTIR.

$$k = \frac{\frac{1}{n}\sum_{i=1}^{n} x_i}{\frac{1}{m}\sum_{j=1}^{m} x_j} \tag{3.1}$$

k is the calibration constant, n and m are total numbers of data samples gathered by the FTIR and MFC, respectively. x_i and x_j represent the data samples gathered by FTIR and MFC, respectively.

$\mathbf{PPM_m}$ to vol%

The data samples gathered by the MFC are given in l/min, at the pressure of 1 atm, and the temperature of 20 °C. However, the FTIR gives its measurements of the concentration at ppm_m[2]. Comparing the data set from the MFC and FTIR, ppm_m is converted to vol%; this is done by Equation (3.2)-(3.5).

$$\dot{m}_{N_2} = \dot{v}_{N_2}\frac{M_{N_2}P}{RT} \tag{3.2}$$

$$\dot{m}_{CO_2} = \frac{\dot{m}_{N_2}}{\frac{1}{[CO_2]_{ppm_m}\cdot 10^{-6}} - 1} \tag{3.3}$$

$$\dot{v}_{CO_2} = \dot{m}_{CO_2}\frac{RT}{M_{CO_2}P} \tag{3.4}$$

[2] ppm_m: parts per million by mass.

$$[CO_2]_{vol\%} = \frac{\dot{v}_{CO_2}}{\dot{v}_{CO_2} - \dot{v}_{N_2}} \tag{3.5}$$

$\dot{m}_{N_2}$ and $\dot{m}_{CO_2}$ are the mass flow of N_2 and CO_2, respectively. $\dot{v}_{N_2}$ and $\dot{v}_{CO_2}$ are the volume flow of N_2 and CO_2, respectively. M_{N_2} and M_{CO_2} are the molar masses of N_2 and CO_2, respectively. $[CO_2]_{ppm_m}$ is the concentration CO_2 measured by the FTIR. Lastly, R is the ideal gas constant, T is the temperature, 20 °C, and P are pressure, 1 atm.

3.2.5 Absorption

Theoretical Maximal Absorption

As shown in the Equation (3.6) one mole of CO_2 is absorbed by one mole of MgO sorbent.

$$MgO + CO_2 \rightleftharpoons MgCO_3 \tag{3.6}$$

The equation is explained further in the Section 2.3. The total mass of CO_2 reacted with the sorbent is given by dividing the molar mass of CO_2 by the molar mass of the metal oxide sorbent, MO, and multiplying the molar mass ratio with the total mass of the metal sorbent reacted with CO_2. Equation (3.7) describes the relationship of the absorbed CO_2 and carbonated metal oxide.

$$m_{CO_2} = m_{MO}\frac{M_{CO_2}}{M_{MO}} \tag{3.7}$$

m_{CO_2} and m_{MO} are masses of reacted CO_2 and the metal oxide sorbent, respectively. M_{CO_2} and M_{MO} are the molar masses of CO_2 and the metal oxide sorbent, respectively. Table 3.3 shows the molar masses of CO_2 and MgO and the molar mass ratio between the two substances.

Table 3.3: The table presents the molar masses of CO_2, and the sorbents MgO, CaO, SrO, and the molar mass ratio between CO_2 and the sorbents. NOTE, CO_2 is not a sorbent, event if it is labeled as such in the table.

Sorbent	Molar mass (g/mol)	M_{CO_2}/M_{MO}
CO_2	44.01	-
MgO	40.30	1.092
CaO	56.08	0.7847
SrO	103.6	0.4248

Experimental Absorption Calculations and Plotting

The calculation and plotting of the CO_2 absorption in the experiments are calculated and modeled in Python. The calculation of CO_2 absorption during the experiment is based on the trapezoid method, see Equation (3.8).

$$\int_a^b f(x)dx \approx \sum_{i=1}^{N} \frac{f(x_{i-1}) + f(x_i))}{2} \Delta x \tag{3.8}$$

The absorption of CO_2 is calculated by subtracting the total mass entering the reactor with the total mass of CO_2 exiting the reactor during the experiment's period.

Chapter 4

Results and Discussion

4.1 Introduction

The screened salt mixtures are organized into three groups; first, the nitrate salts will be discussed, secondly, the halide salts, and lastly, halide-nitrate salt mixtures. The salt mixtures in each group possess similar characteristics; these include eutectic melting point, Lewis acidity or basicity, molar ratio, and reactivity with MgO and CO_2.

The halides salt mixtures are the most numerous of the screened salt mixtures, mainly due to the low eutectic melting points of the nitrate salt mixtures. The halide salt group is considerably smaller than the nitrate salt group. To reduce the number of salt mixtures screened in this thesis, it was decided that the halide salt mixtures must have a component that reacted with MgO and CO_2 to be screened in this thesis. The halide-nitrate group is considerably smaller than the nitrate group as well. The salt mixtures in this group possess relatively high eutectic melting points, and they all have very similar eutectic molar ratios. The results of the experiments conducted for the initial thesis will be discussed in halide section, since all of the salts used in the experiments are halides.

4.2 Nitrate Salt

There is a wide range of studies conducted on molten nitrate salts, where the solar thermal energy community has conducted many of these studies. Mainly due to the high heat capacity, good thermal conductivity, and the

relatively low eutectic melting points of binary and tertiary nitrate salt mixtures[65]. In recent years more studies have been conducted by the CCS community on promoting MgO by molten nitrate salts. In these studies, researchers try to prepare and modify the MgO sorbent by treating it in molten nitrate salts. The idea is; by modifying the MgO sorbent with nitrates increases the reaction kinetics between CO_2 and MgO[66]. Unlike this thesis, where we study the suitability of MgO being a CO_2-absorber, while the studies use the MgO sorbent as a CO_2-adsorber[66][67][68].

Alkali- and alkaline-earth metal nitrate salts have the following benefits that it is cheap, less corrosive than other salts, easily accessible, the eutectic melting point is relatively low, and have high thermal stability[69].

Alkali metal nitrates such as lithium nitrate ($LiNO_3$), sodium nitrate ($NaNO_3$), and potassium nitrate (KNO_3) possess high thermal stability. They can handle temperatures up to 435 °C without any of the alkaline metal nitrate salts decomposing to their oxide forms[70]. The high thermal stability of $LiNO_3$, $NaNO_3$, and KNO_3 means that they can withstand the operating temperatures during a carbon capture process with MgO as sorbent.

4.2.1 Pure Alkali Metal Nitrates

The molten salt mixtures consisting only of alkali metal nitrates show a similar quality and behavior. The mixtures of alkali metal nitrate salts screened in this thesis have relatively low eutectic melting points, a range between 120 °C and 230 °C.

Table 4.1: List of the pure alkali metal nitrate salt mixtures, their eutectic compositions and melting points.

Salt mixture	Eutectic composition (mol%)	Eutectic (℃)
$LiNO_3$ - $NaNO_3$	53.8 - 46.2	195
$LiNO_3$ - KNO_3	42.2 - 57.8	125
$LiNO_3$ - $CsNO_3$	56.0 - 44.0	160
$NaNO_3$ - KNO_3	50.0 - 50.0	221
KNO_3 - $CsNO_3$	60.0 - 40.0	230
$LiNO_3$ - $NaNO_3$ - KNO_3	37.64 - 17.48 - 44.87	120
$LiNO_3$ - $NaNO_3$ - $RbNO_3$	28.53 - 20.16 - 51.31	130
$LiNO_3$ - $NaNO_3$ - $CsNO_3$	40.15 - 13.15 - 46.58	132
$NaNO_3$ - KNO_3 - $RbNO_3$	36.30 - 26.10 - 37.60	148
$NaNO_3$ - KNO_3 - $CsNO_3$	31.21 - 36.70 - 32.09	154

The phase diagrams of the binary salt mixtures from Table 4.1 seem to possess somewhat different curves in their phase diagrams. The salt mixtures containing $LiNO_3$ on Table 4.1 tend have similar eutectic molar ratios.

The Figure 4.1 show the curve of $LiNO_3$-$NaNO_3$ has a wide V-shaped "valley," meaning that there are more room for error when mixing the $LiNO_3$-$NaNO_3$ salts.

Figure 4.2 illustrates the phase diagram of $NaNO_3$-KNO_3. This phase diagram possesses a wide "valley" at its eutectic melting point. The curve of this diagram show a U-shaped "valley", making slight mixing errors less consequential for the eutectic melting point the salt mixture. The area above the upper line describes where the salt mixture is in liquids phase, the area below the upper line describes where the salt mixture is in a solidus state.

The phase diagram of $LiNO_3$-$CsNO_3$ is illustrated in Figure 4.3. This salt mixture possesses an interesting characteristic that it has two eutectic melting points, the lowest of these two points are listed on Table 4.1. However, both these points have steep V-shaped "valleys", making mixing errors more consequential, and thus making this salt mixture a less practical to use in CCMS.

The phase diagrams of the tertiary salt mixtures on Table 4.1, do not seem to possess any interesting characteristics.

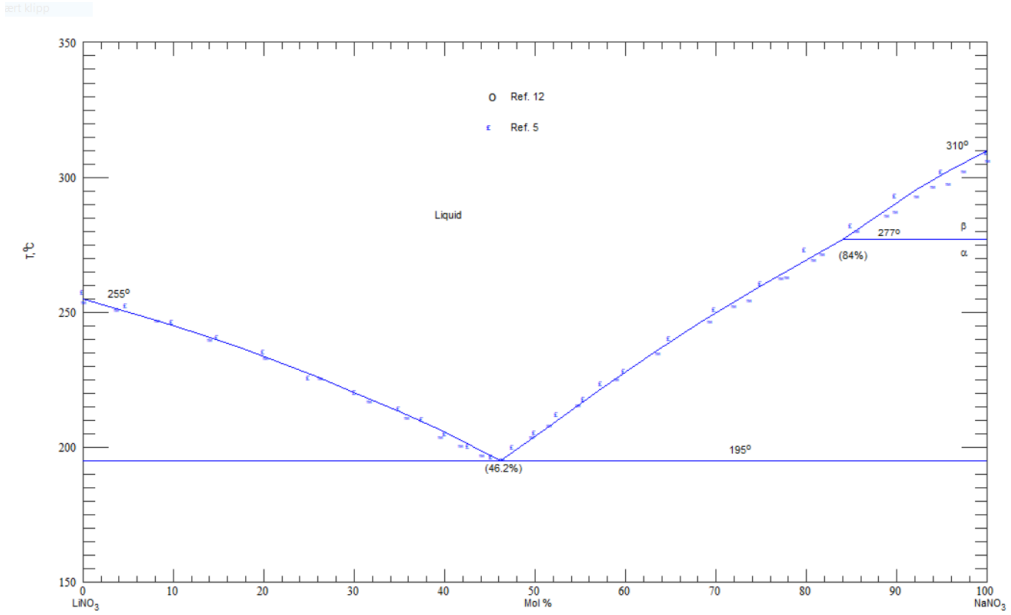

Figure 4.1: A phase diagram of the binary salt mixture $LiNO_3$-$NaNO_3$. The y-axis represents the temperature in (°C), while the x-axis represents the molar ratio (mol%) between $LiNO_3$ and $NaNO_3$. The phase diagram is sourced from the ACerS-NIST *Phase Equilibria Diagram Database* 3.1.0[63].

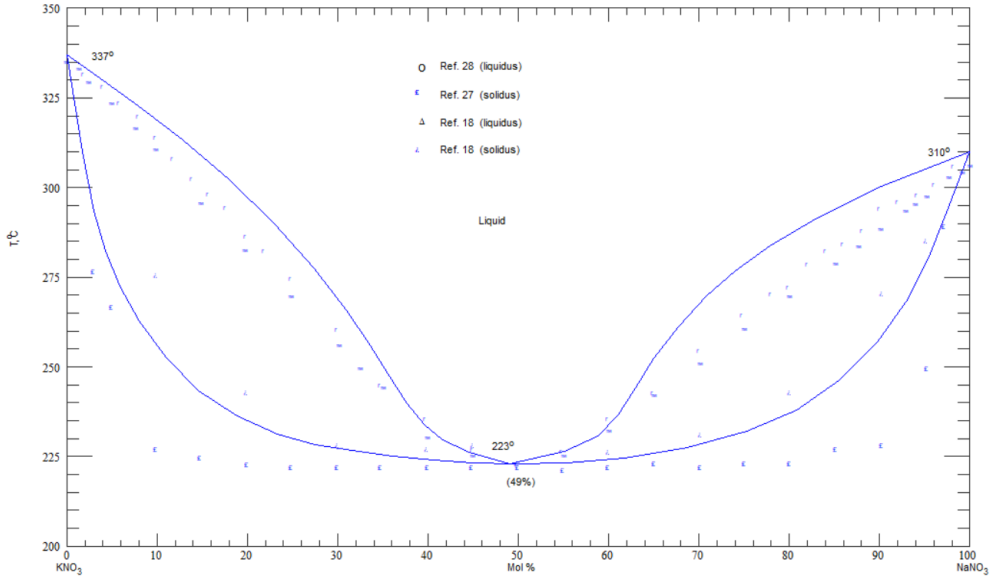

Figure 4.2: A phase diagram of the binary salt mixture $NaNO_3$-KNO_3. The y-axis represents the temperature in (°C), while the x-axis represents the molar ratio (mol%) between $NaNO_3$ and KNO_3. The phase diagram is sourced from the ACerS-NIST *Phase Equilibria Diagram Database* 3.1.0[63].

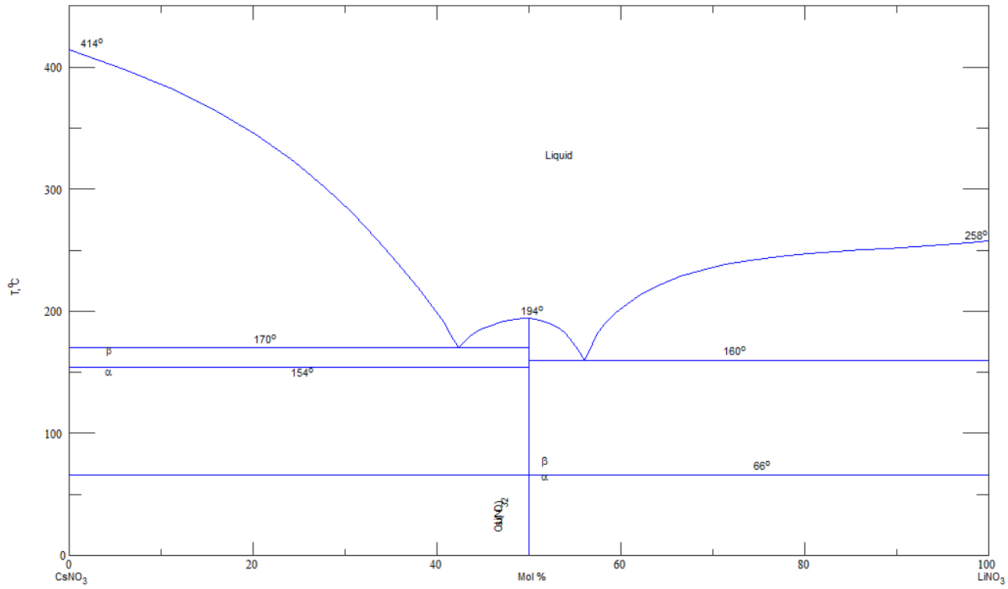

Figure 4.3: A phase diagram of the binary salt mixture $LiNO_3$-$CsNO_3$. The y-axis represents the temperature in °C, while the x-axis represents the molar ratio (mol%) between $LiNO_3$ and $CsNO_3$. The phase diagram is sourced from the ACerS-NIST *Phase Equilibria Diagram Database* 3.1.0[63].

When simulating Reaction (2.7) and (2.8), the simulations show that none of the salt mixtures in Table 4.1 have a negative Gibbs free energy within the operating temperature range. This means that none of the molten alkali metal salt mixtures has a component that reacts with MgO and CO_2, or $MgCO_3$[1]. When Reaction (2.7) and (2.8) do not occur in the molten salt, the CO_2 capture by the MgO sorbent could be less efficient, see Figure 4.4 and 4.5.

Since MgO will stay inert in a nitrate salt melt, it is pointless to discuss the reaction enthalpy of Reaction (2.7) and (2.8), since the reactions do not occur during the specified operating temperature of CCMS with MgO as sorbent, see Table 4.2.

[1]This is not entirely accurate, there will always be a reaction in either directions for Reaction (2.7) and (2.8). Since these reactions are in this case insignificant, we consider them as not occurring.

Table 4.2: The table show the equilibrium temperature ($T_{\Delta G = 0}$) and the reaction enthalpy of the carbonation reaction between MgO, CO_2, and an alkali metal nitrate salt (ANO_3), $MgO + CO_2 + 2ANO_3 \rightleftharpoons Mg(NO_3)_2 + A_2CO_3$ (Total reaction), along with the reaction $MgCO_3 + 2ANO_3 \rightleftharpoons Mg(NO_3)_2 + A_2CO_3$ (Exchange reaction). The data is gathered from HSC Chemistry 6.12[45].

	Total reaction		Exchange reaction	
Salt (AH)	$T_{\Delta G = 0}$	ΔH	$T_{\Delta G = 0}$	ΔH
$LiNO_3$	3771	1588	2804	809
$NaNO_3$	3371	1382	2457	679
KNO_3	3478	1506	2635	862

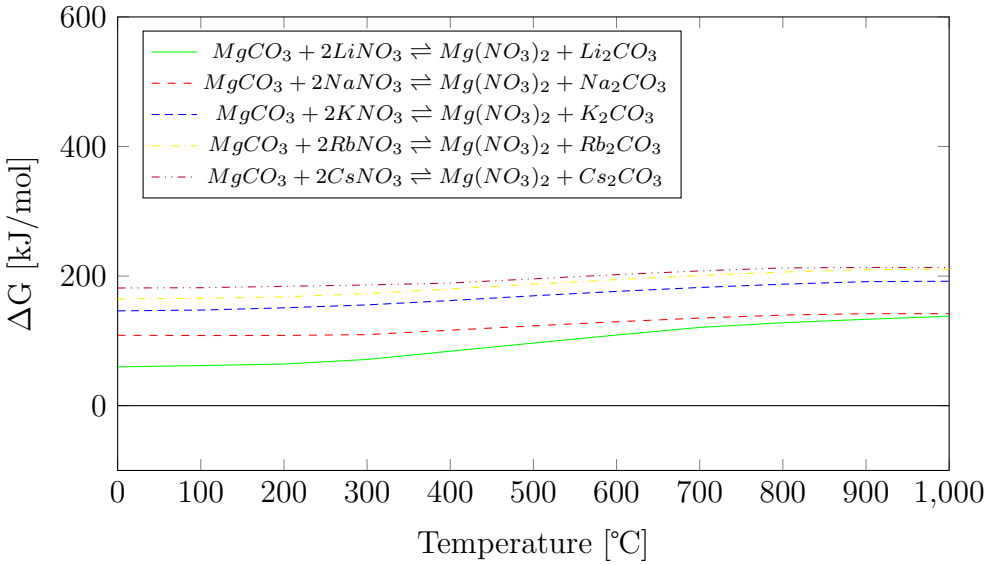

Figure 4.4: The figure illustrates the Gibbs free energy (ΔG) of the Reaction $MCO_3 + 2AH \rightleftharpoons MH_2 + A_2CO_3$ or Reaction (2.7) against temperature (°C). NO_3 is represented by H in this case, not a halide as it is explained in earlier sections. The ΔG value does not become negative through the temperature range, meaning that Reaction (2.7) will not occur, or go rightwards. The figure is made from simulations from HSC Chemistry 6.12[45].

None of the alkali metal nitrate mixtures showed any apparent hydrolysis reaction that happened under the specified operating temperature. When simulating the Reaction (2.16), all of the alkali metal salt mixtures had positive Gibbs free energy, see Figure 4.6

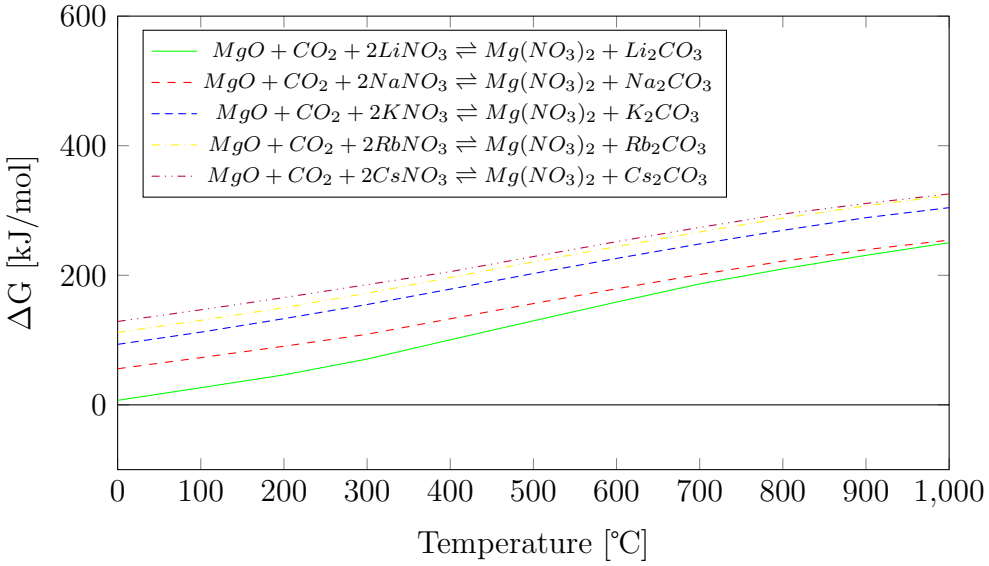

Figure 4.5: The figure illustrates the Gibbs free energy (ΔG) of the Reaction $MO+CO_2+2AH \rightleftharpoons MH_2 + A_2CO_3$ or Reaction (2.8) against temperature (°C). NO_3 is represented by H in this case, not a halide as it is explained in earlier sections. The ΔG value does not become negative through the temperature range, meaning that Reaction (2.8) does not occur. The figure is made from simulations from HSC Chemistry 6.12[45].

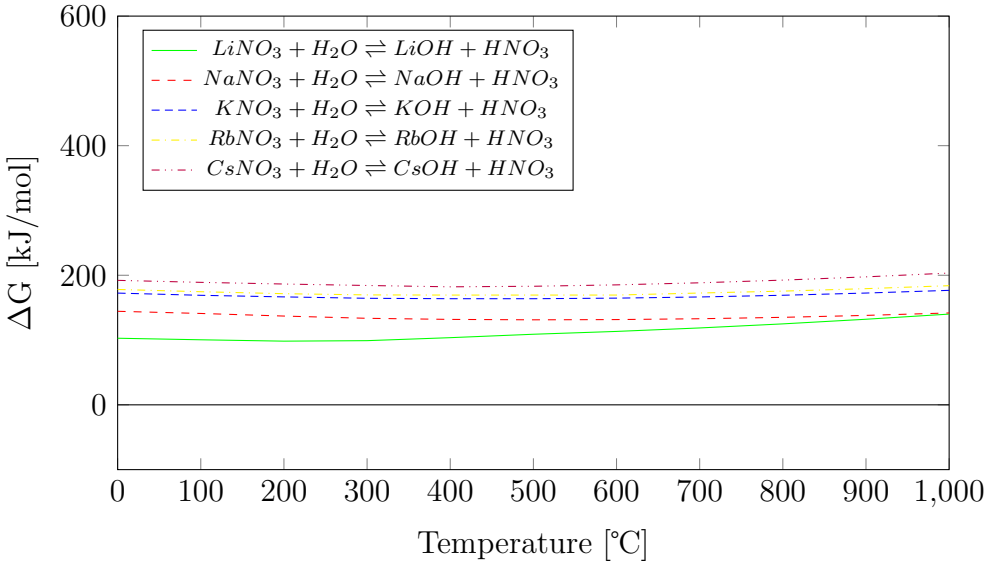

Figure 4.6: The figure illustrates the Gibbs free energy (ΔG) of the Reaction $MN+H_2O \rightleftharpoons MOH+HN$ or Reaction (2.16) against temperature (°C). NO_3 is represented by N in this case. The ΔG value does not become negative through the temperature range, meaning that no hydrolysis apparent in a CCMS process with the nitrate salts listed in Table 4.1. The figure is made from simulations from HSC Chemistry 6.12[45].

As the description in Subsection 2.3.6 explains, a molten salt mixture that is a Lewis base possesses an abundance of anions that can donate electrons. If the NO_3^- ion is considered as an uncomplexed anion, it can potentially fulfill this role. The pure alkali metal nitrate salts should then be categorized as a Lewis base since the melt also contains an abundance of alkali metal ions. As per today, there is no literature found that supports that NO_3^- ion can act as the electron-donating anion, so this claim should be considered as speculation. Since the assumption here is that the pure alkali metal nitrates are Lewis bases, the MgO probably will not be able to dissolve sufficiently in molten alkali metal nitrate melts.

In economic terms, if any salt mixtures in Table 4.1 are to be used in a CCMS process, it is unlikely that $RbNO_3$ and $CsNO_3$ will be used. Mainly due to that they are rare in nature, and thus expensive[71][72].

4.2.2 Alkali and Alkaline Earth Metal Nitrates

In this subsection, the focus of the discussion will be about the salt mixtures containing a combination of alkali metal nitrates and alkaline earth metals nitrates. The salt mixtures in focus contain the alkaline earth metal nitrates: magnesium nitrate ($Mg(NO_3)_2$) and calcium nitrate ($Ca(NO_3)_2$), mixed with either $LiNO_3$, $NaNO_3$, and KNO_3.

The nitrate salt mixtures with $Mg(NO_3)_2$ screened in this thesis are listed on Table 4.3.

Table 4.3: List of the alkali and alkaline earth metal nitrate salt mixtures, where $Mg(NO_3)_2$ is the alkaline earth metal nitrate. The eutectic compositions and melting points of the salt mixtures are listed.

Salt mixture	Eutectic composition (mol%)	Eutectic (°C)
$LiNO_3$ - $Mg(NO_3)_2$	70.53 - 29.47	200
$NaNO_3$ - $Mg(NO_3)_2$	61.72 - 38.28	135
KNO_3 - $Mg(NO_3)_2$	51.17 - 48.83	178

The salt mixtures listed on Table 4.3, do not have any unifying characteristics concerning the curve of the phase diagrams of these salt mixtures. Figure 4.7 displays the phase diagram of $LiNO_3$-$Mg(NO_3)_2$. The curve of phase diagram is characterised by its wide "valley." The stippled line at the upper right hand corner is the projected melting point of the corresponding wt% ratio.

The phase diagram of $NaNO_3$-$Mg(NO_3)_2$ is illustrated in Figure 4.8. The curve of this phase diagram is much steeper than the curve of the $LiNO_3$-$Mg(NO_3)_2$. This makes slight mixing errors with $NaNO_3$-$Mg(NO_3)_2$ more consequential compared to $LiNO_3$-$Mg(NO_3)_2$.

Illustrated in Figure 4.9 the phase diagram of KNO_3-$Mg(NO3)_2$ has two eutectic melting points similar to $LiNO_3$-$CsNO_3$. Both eutectic melting points have steep "valleys", making the KNO_3-$Mg(NO_3)_2$ salt mixture less practical in use for CCMS.

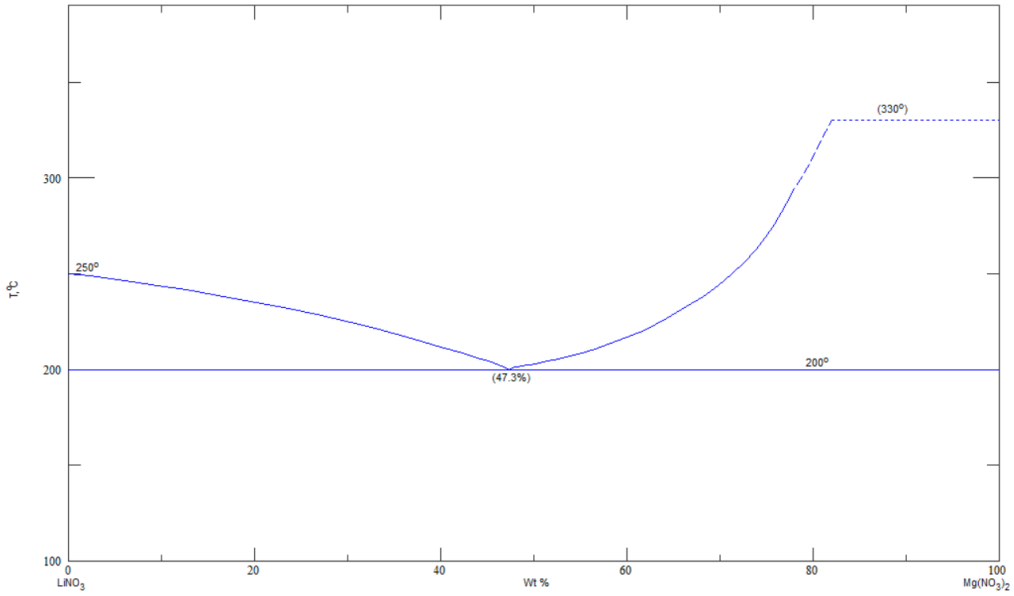

Figure 4.7: A phase diagram of the binary salt mixture $LiNO_3$-$Mg(NO_3)_2$. The y-axis represents the temperature in (°C), while the x-axis represents the weight ratio (wt%), not the molar ratio (mol%) between $LiNO_3$ and $Mg(NO_3)_2$. The phase diagram is sourced from the ACerS-NIST *Phase Equilibria Diagram Database* 3.1.0[63].

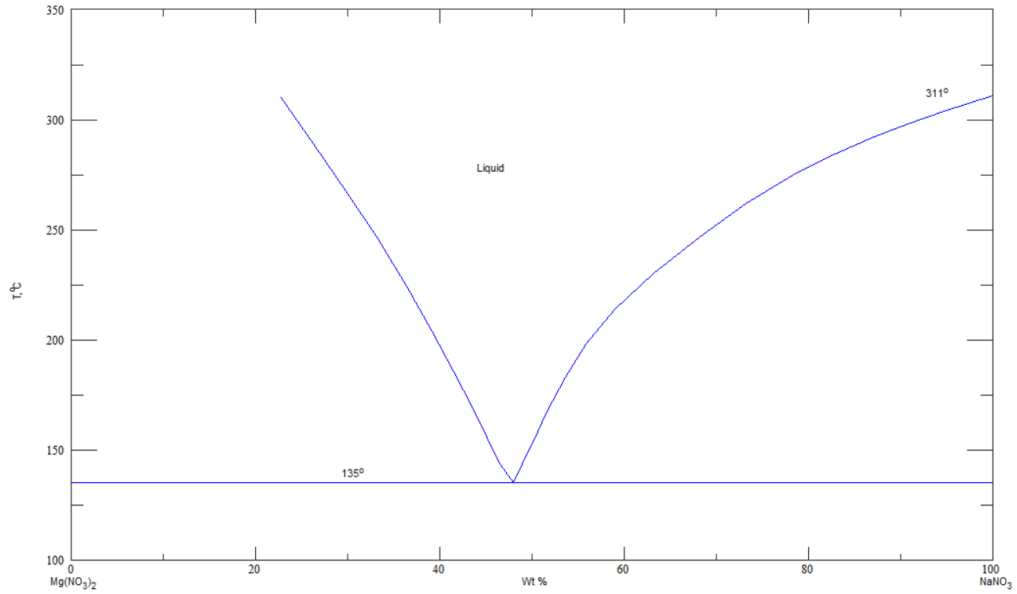

Figure 4.8: A phase diagram of the binary salt mixture $NaNO_3$-$Mg(NO_3)_2$. The y-axis represents the temperature in (°C), while the x-axis represents the weight ratio (wt%), not the molar ratio (mol%) between $NaNO_3$ and $Mg(NO_3)_2$. The phase diagram is sourced from the ACerS-NIST *Phase Equilibria Diagram Database* 3.1.0[63].

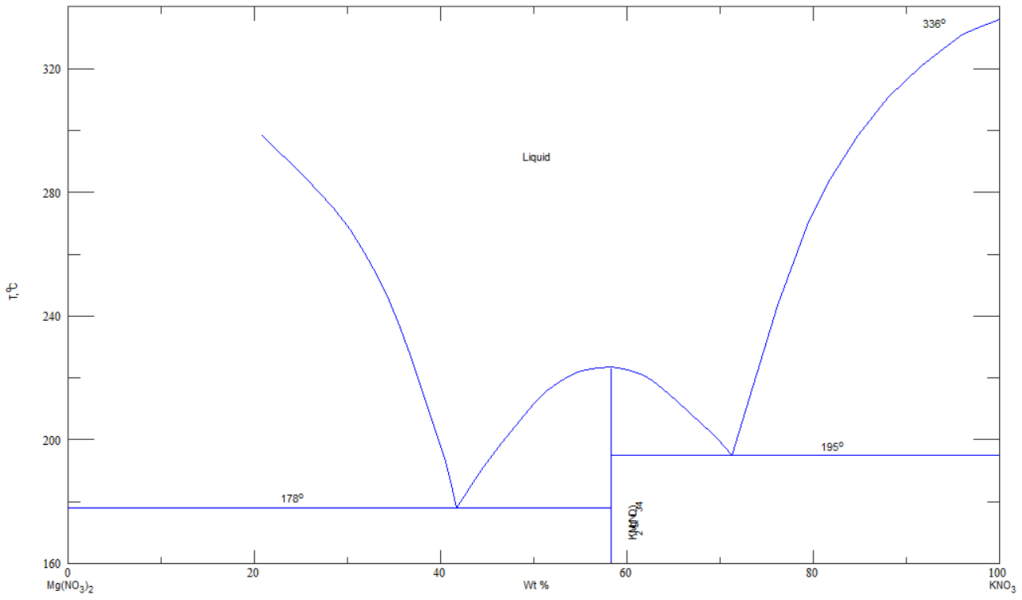

Figure 4.9: A phase diagram of the binary salt mixture KNO_3-$Mg(NO_3)_2$. The y-axis represents the temperature in °C, while the x-axis represents the weight ratio (wt%), not the molar ratio (mol%) between KNO_3 and $Mg(NO_3)_2$. The phase diagram is sourced from the ACerS-NIST *Phase Equilibria Diagram Database* 3.1.0[63].

As explained in the previous subsection, $LiNO_3$, $NaNO_3$, and KNO_3 do not react with $MgCO_3$, and the three nitrate salts are thermally stable within the operating temperature range. The salt mixtures listed in Table 4.3 do not have similar eutectic molar composition, and all three salt mixtures have eutectic melting points at 200 °C or lower. Unfortunately, the thermal stability of $Mg(NO_3)_2$ does not meet the requirements needed for the carbon capture process. The $Mg(NO_3)_2$ molecule starts decomposing in temperatures higher than 300 °C, see Reaction (4.1), and Figure 4.10, making any salt mixture with $Mg(NO_3)_2$ not suitable candidate for CCMS.

$$2Mg(NO_3)_2 \rightleftharpoons 2MgO + 4NO_2 + O_2 \tag{4.1}$$

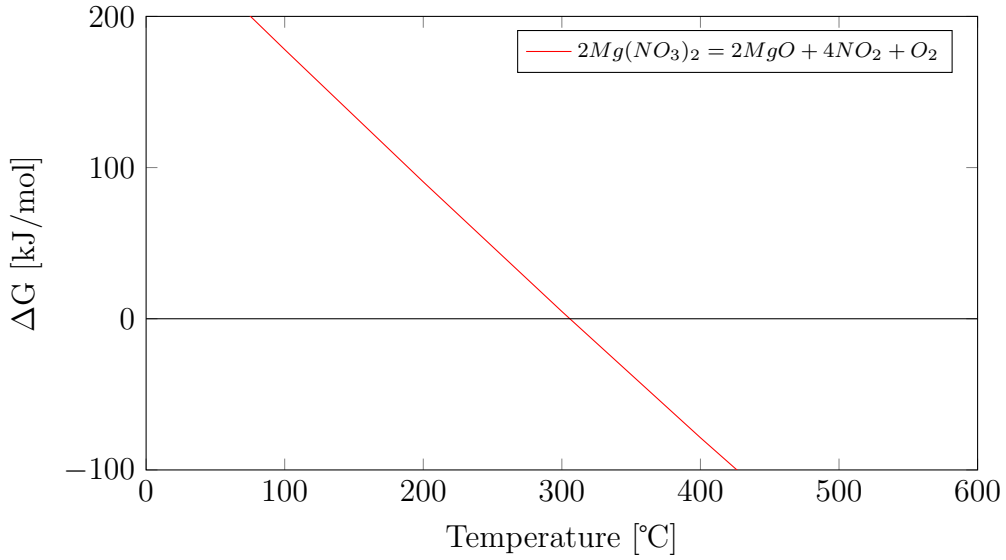

Figure 4.10: The figure depicts the Gibbs free energy (ΔG) vs. temperature (°C) for the reaction $2Mg(NO_3)_2 \rightleftharpoons 2MgO + 4NO_2 + O_2$, or Reaction (4.1). The graph shows when $Mg(NO_3)_2$ starts disintegrating into MgO, NO_2, and O_2, at 300°C. The figure is made from simulations from HSC Chemistry 6.12[45].

None of the three nitrate salt mixtures showed any apparent hydrolysis effect either.

In Subsection 2.3.6, it is explained that if a molten salt mixture is a Lewis acid, most of its "free" anions are localized in coordinate complexes present in

the melt. In this case, the coordinate complexes are the $Mg(NO_3)_2$ molecules. The $Mg(NO_3)_2$ molecule has a central metal atom surrounded by nonmetal compounds[73]. Molten $Mg(NO_3)_2$ salt by itself by this definition should be a Lewis acid. However, all of the salt mixtures screened containing $Mg(NO_3)_2$ also contain alkali metal nitrates. The eutectic molar composition between $Mg(NO_3)_2$ and the alkali metal nitrate is higher for the alkali metal nitrate, see Table 4.3. As explained in the previous subsection, the molten alkali metal nitrate salts are Lewis bases. Thus, the screened molten salt mixtures containing both $Mg(NO_3)_2$ and an alkali metal nitrate would probably be more similar to a Lewis base due to the higher molar amount of alkali metal nitrates. Although KNO_3-$Mg(NO_3)_2$ has a molar eutectic ratio of 50% for both salts, such a molten salt mixture might act as a Lewis acid to the MgO sorbent, could potentially dissolve the sorbent.

The mixtures of nitrate salts containing $Ca(NO_3)_2$ and alkali metal nitrates show somewhat same behavior as the pure alkali metal nitrate mixtures. One notable exception is that when $Ca(NO_3)_2$ is involved in Reaction (2.8), the Gibbs free energy had a negative value in the temperature range from absolute zero to 93.6 °C. This temperature range is below the eutectic melting points of all the nitrate salt mixtures containing $Ca(NO_3)_2$ screened in this thesis, see Table 4.4.

Table 4.4: List of the alkali and alkaline earth metal nitrate salt mixtures, where $Ca(NO_3)_2$ is the alkaline earth metal nitrate. The eutectic composition and melting point of the salt mixtures are listed.

Salt mixture	Eutectic composition (mol%)	Eutectic (°C)
$LiNO_3$ - $Ca(NO_3)_2$	84.0 - 16.0	237
$NaNO_3$ - $Ca(NO_3)_2$	70.38 - 29.62	230
KNO_3 - $Ca(NO_3)_2$	49.50 - 50.50	146
$LiNO_3$ - $NaNO_3$ - $Ca(NO_3)_2$	40.30 - 30.60 - 40.30	170
$LiNO_3$ - KNO_3 - $Ca(NO_3)_2$	32.14 - 58.71 - 9.15	117
$NaNO_3$ - KNO_3 - $Ca(NO_3)_2$	53.8 - 12.41 - 39.23	133

The salts on Table 4.4 consist of either $LiNO_3$, $NaNO_3$, and KNO_3 with $Ca(NO_3)_2$. Explained in the previous section, neither $LiNO_3$, $NaNO_3$, and KNO_3 reacts with MgO, CO_2, or $MgCO_3$, making MgO inert in all of the salt mixtures on Table 4.4. Since MgO is inert in the salt mixtures on Table 4.4, the reaction enthalpy of the interaction between the nitrate salt and the sorbent will not be discussed, see Table 4.5.

Table 4.5: The table show the equilibrium temperature ($T_{\Delta G = 0}$) and the reaction enthalpy of the carbonation reaction between MgO, CO_2, and an alkali/alkaline earth metal nitrate salt (ANO_3), $MgO + CO_2 + 2ANO_3 \rightleftharpoons Mg(NO_3)_2 + A_2CO_3$ (Total reaction), along with the reaction $MgCO_3 + 2ANO_3 \rightleftharpoons Mg(NO_3)_2 + A_2CO_3$ (Exchange reaction). The data is gathered from HSC Chemistry 6.12[45].

	Total reaction		Exchange reaction	
Salt (AH)	$T_{\Delta G = 0}$	ΔH	$T_{\Delta G = 0}$	ΔH
$LiNO_3$	3771	1588	2804	809
$NaNO_3$	3371	1382	2457	679
KNO_3	3478	1506	2635	862
$Ca(NO_3)_2$	3563	773	1754	169

Unlike the earlier examples, the binary salt mixtures listed on Table 4.4 do have resembling phase diagram curves. Where they are characterized by having a wide "valley" at the eutectic melting point. Figure 4.11 illustrates the phase diagrams of both KNO_3-$Ca(NO_3)_2$ and $NaNO_3$-$Ca(NO_3)_2$, where they are numbered (I) and (II), respectively. Both salt mixtures possess a wide "valley," making mixing errors less consequential.

The tertiary salt mixtures listed in Table 4.4, do not seem to have phase diagrams that have characteristics that are unusual for tertiary salt mixtures.

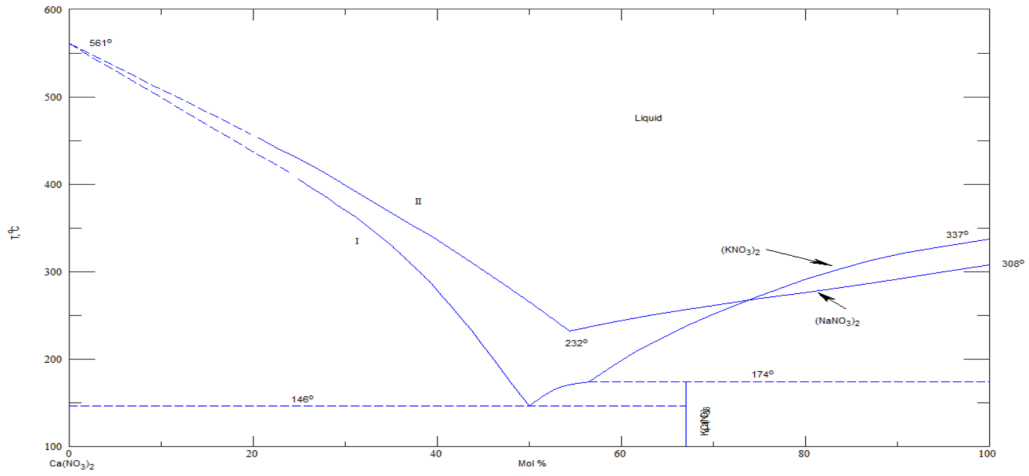

Figure 4.11: A phase diagram of the binary salt mixtures $NaNO_3$-$Ca(NO_3)_2$ and KNO_3-$Ca(NO_3)_2$. The y-axis represents the temperature in (°C), while the x-axis represents the molar ratio (mol%) between $NaNO_3$ or KNO_3, and $Mg(NO_3)_2$. The phase diagram is sourced from the ACerS-NIST *Phase Equilibria Diagram Database* 3.1.0[63].

Like the $Mg(NO_3)_2$ is $Ca(NO_3)_2$, also a coordinate complex. The "free" anions are localized in the $Ca(NO_3)_2$ molecule, which means that molten $Ca(NO_3)_2$ salt by itself is a Lewis acid. However, the screened salt mixtures on Table 4.4 show that all of them contain alkali metal nitrate salt. All of the screened salts on Table 4.4 possess a higher molar ratio for the alkali metal nitrates, except for KNO_3-$Ca(NO_3)_2$, which means that the most of salt mixtures on Table 4.4 will probably act as a Lewis base to MgO. The KNO_3-$Ca(NO_3)_2$ possesses a 49.5-50.5 eutectic molar ratio, respectively. This molar composition might cause the molten KNO_3-$Ca(NO_3)_2$ to act as a Lewis acid to the MgO. Lastly, no hydrolysis is apparent in any of the molten salt mixtures on Table 4.4.

The discussion thus far points to the nitrate salt mixtures screened would probably not be suitable CCMS with MgO as sorbent. Mainly due to the Lewis base characteristics of the nitrate salt mixture listed in this thesis. However, the nitrate salts might have properties that enhance the MgO sorbent's ability to react with CO_2.

Several studies have been conducted where a solid-state MgO sorbent is enhanced with molten alkali metal nitrate salt to increase the sorbent's ability to capture CO_2. Although these studies use a different method of capturing CO_2 compared to CCMS, it should be noted that the findings of these studies might find a place for nitrate salt in CCMS.

Hwang *et al.* (2018) tested the CO_2-sorption capabilities of solid-state MgO in a melt of KNO_3, $NaNO_3$, and KCO_3 salt. They were able to achieve a 76% carbonation of the sorbent during the first cycle of CO_2 capture. The study argues that the nitrates are not directly involved in the reaction between the CO_2 and the sorbent. However, the nitrates do increase the MgO sorbents CO_2-carrying capacity[74].

Yu *et al.* (2019) conducted a study where molten nitrate salts promoted the MgO sorbent. The study tested MgO sorbent doped with molten ($LiNO_3$-$NaNO_3$-KNO_3) and ($NaNO_3$-KNO_3-$NaNO_2$). The results showed that the doped MgO had a much higher sorption of CO_2 than plain MgO. The CO_2 uptake by the doped MgO was 13.52 mmol and 10.53 mmol per g of doped MgO, respectively. The CO_2 uptake by the doped MgO sorbents is much higher than plain solid-state MgO, which only adsorbs <1 mmol per g MgO[75].

The studies mentioned above show that the presence of alkali metal nitrate salt increases the CO_2 carrying capacity of MgO. Adding alkali metal nitrate into different types of melts, such as FLiNaK melt, for example, might increase the CO_2 capture efficiency of MgO sorbent in the melt.

Another interesting proposal for the usage of nitrates in CCMS is to dope the MgO sorbent with alkali metal nitrates, such as in the studies of Yu *et al.* (2019)[75], and then add it to the salt mixture in the molten salts reactor. By using a doped MgO sorbent, it could potentially raise the efficiency of the CO_2 capture in a CCMS process.

4.3 Halides

This section focuses on salt mixtures that only contain halide salts. The halide salt mixtures screened are salts that contain fluoride (F), and chloride (Cl), meaning no salts containing bromine (Br) and iodine (I) are present in the screening. No salt mixtures with Br and I salt were found that fitted the necessary criteria of the screening.

Fluoride and chloride salts have similar qualities, such as high thermal stability, stable >700 °C, and >800 °C for fluoride and chloride salts, respectively, low viscosity, high electrical conductivity, and excellent heat transfer capabilities[76]. Both salts possess highly corrosive qualities in high-temperature settings, more than the nitrate salts discussed earlier[77][78].

There are differences between the two halide salts. Molten fluoride salts possess higher heat capacity than molten chloride salt, while fluoride salts are toxic while chloride salts are not. Chloride salts are cheap since they are abundant, especially NaCl and KCl, while fluoride salts are not as abundant and thus more expensive. Molten fluoride salt tends to be more volatile[76][78].

Molten chloride salts are widely used in several industrial applications, for example electrolysis in high-temperature electrochemical plating and extraction of metals[76]. Molten fluoride salt is used in aluminum production, where molten fluoride salt is cryolite (Na_3AlF_6)[79]. The use of molten fluoride salt as a coolant for reactors has been proposed, a transfer medium for high-temperature process heat from nuclear reactors has been proposed as well[77]. Molten chloride salts have been proposed for *thermal energy storage* (TES) and *heat transfer fluid* (HTF) in concentrated solar power[76].

The following discussion will consist of two parts, where the salts NaF-$CdCl_2$, LiCl-$BeCl_2$, NaCl-$BeCl_2$, and KCl-$BeCl_2$ will be discussed first; FLi-NaK and CuCl-KCl salt mixtures with MgO was tested in the molten salt reactor, thus will be discussed last, see Table 4.6.

Table 4.6: List of the pure halide salt mixtures, the eutectic compositions and melting points of the salt mixtures are listed. The table is divided in two, the upper salt mixtures are the halide mixtures that are screened, the lower salt mixtures were experimentally tested in the molten salt reactor.

Salt mixture	Eutectic composition (mol%)	Eutectic (°C)
NaF - $CdCl_2$	43.4 - 56.6	298
LiCl - $BeCl_2$	42.7 - 57.3	301
NaCl - $BeCl_2$	49.7 - 50.3	217
KCl - $BeCl_2$	52.1 - 47.9	300
LiF - NaF - KF	46.5 - 11.5 - 42.0	454
CuCl - KCl	35.0 - 65.0	150

The salt mixtures NaF-$CdCl_2$, LiCl-$BeCl_2$, NaCl-$BeCl_2$, and KCl-$BeCl_2$, have similar characteristics; all of the salts have a relative high eutectic melting points, around 300 °C except for NaCl-$BeCl_2$ which has 217 °C as the eutectic melting point. The eutectic melting point of 300 °C is very close to the temperature limit 305 °C. All of the salt mixtures have similar eutectic molar ratios.

The phase diagram graphs of the salt mixtures have similar curves, except for KCl-$BeCl_2$. The curves corresponding to NaF-$CdCl_2$, LiCl-$BeCl_2$, and NaCl-$BeCl_2$ have wide a "valley" at the eutectic point, see Figure 4.12. This makes small mixing errors less problematic for the CCMS process. KCl-$BeCl_2$, however, has three eutectic points, two local eutectic points, and one global eutectic point. The global eutectic point has a steep "valley", see Figure 4.13, making any small mixing errors much more consequential, and thus less practical for CCMS.

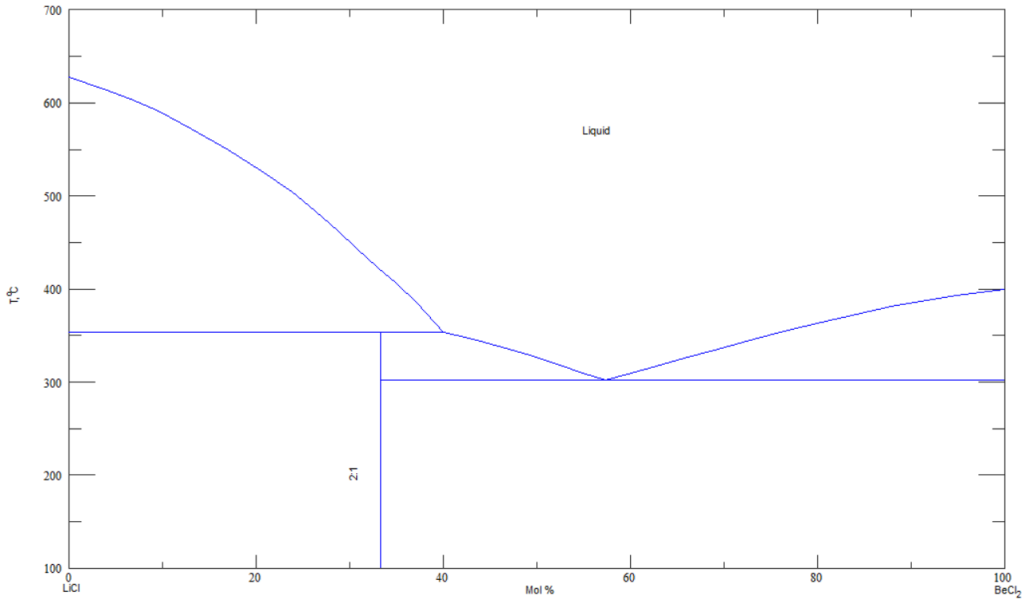

Figure 4.12: A phase diagram of the binary salt mixture LiCl-$BeCl_2$. The y-axis represents the temperature in (°C), while the x-axis represents the molar ratio (mol%) between LiCl, and $BeCl_2$. The salt mixtures NaF-$CdCl_2$ and NaCl-$BeCl_2$ possess very similar phase diagram curves as well. The phase diagram is sourced from the ACerS-NIST *Phase Equilibria Diagram Database* 3.1.0[63].

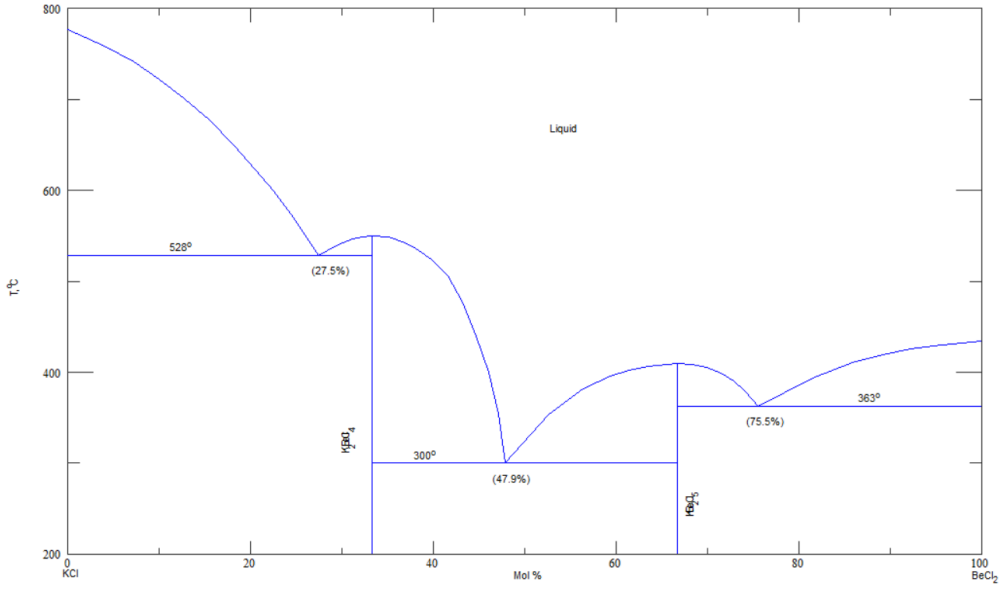

Figure 4.13: A phase diagram of the binary salt mixture KCl-$BeCl_2$. The y-axis represents the temperature in (°C), while the x-axis represents the molar ratio (mol%) between KCl, and $BeCl_2$. As described above the phase diagram has three eutectic points. The phase diagram is sourced from the ACerS-NIST *Phase Equilibria Diagram Database* 3.1.0[63].

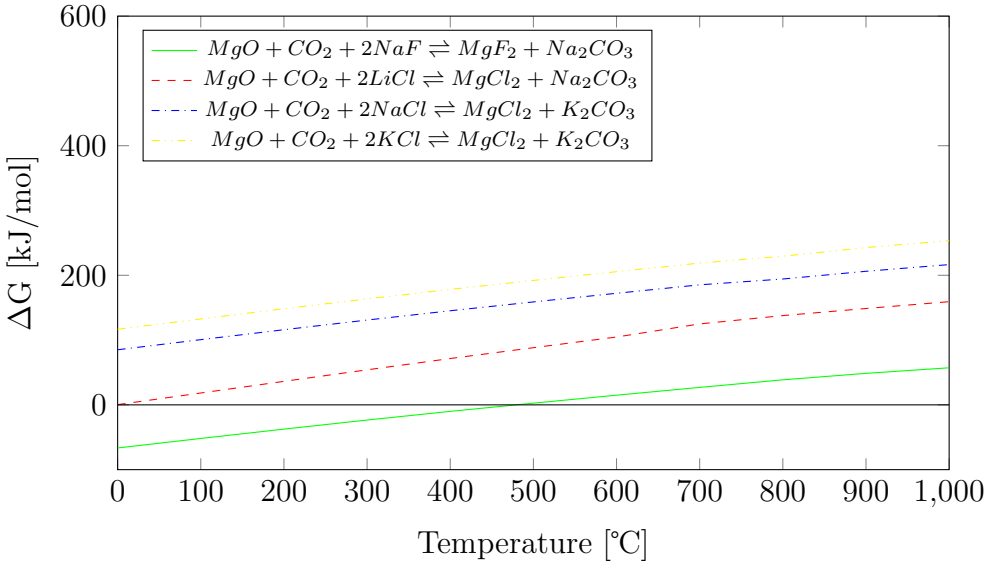

Figure 4.14: The figure illustrates the Gibbs free energy (ΔG) of the Reaction $MgO + CO_2 + 2AH \rightleftharpoons MH_2 + A_2CO_3$ or Reaction (2.8) against temperature (°C). The ΔG value for the Reaction $MgO + CO_2 + NaF \rightleftharpoons MgF_2 + Na_2CO_3$ is negative below 478 °C, meaning that MgO and CO_2 do have an exchange reaction with NaF. The figure is made from simulations from HSC Chemistry 6.12[45].

When simulating the Reaction (2.8) for the four salt mixtures, all four had a component that reacted with MgO and CO_2. For NaF-$CdCl_2$, it was NaF that reacted with the MgO and CO_2. For mixtures LiCl-$BeCl_2$, NaCl-$BeCl_2$, and KCl-$BeCl_2$, it was $BeCl_2$ that reacted with MgO and CO_2. HSC chemistry simulated that the turning point of Reaction (2.8) with NaF as 479 °C, while the turning point of $BeCl_2$ was at 849 °C, see Figure 4.14 for NaF and Figure 4.15.

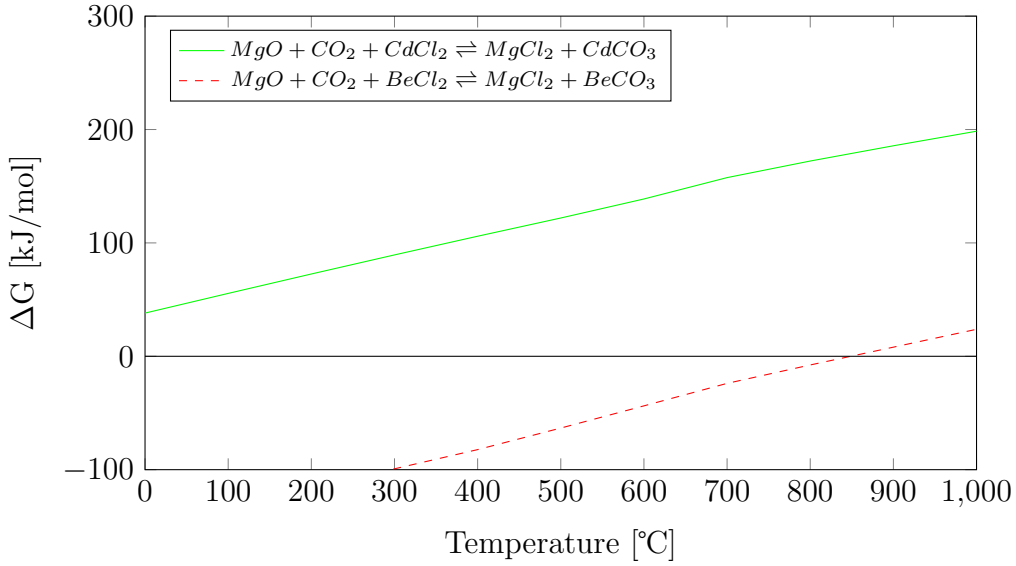

Figure 4.15: The figure illustrates the Gibbs free energy (ΔG) of the Reaction $MgO + CO_2 + AH_2 \rightleftharpoons MH_2 + ACO_3$ or a variation of Reaction (2.8) against temperature (°C). The ΔG value for the reaction $MgO + CO_2 + BeCl_2 \rightleftharpoons MgCl_2 + BeCO_3$ is negative below 849 °C, meaning that MgO and CO_2 do have an exchange reaction with NaF. The figure is made from simulations from HSC Chemistry 6.12[45].

Since NaF and $BeCl_2$ react with MgO and CO_2, or $MgCO_3$ through Reaction (2.7) and (2.8) the enthalpy of the reactions must be considered. Shown in Table 4.7, Reaction (2.8) with NaF has a ΔH of -93 kJ/mol which is relatively low. The relatively low ΔH means that the decarbonation process of $MgCO_3$ in molten NaF-$CdCl_2$ could require less energy compared to other chemical systems. $BeCl_2$ however, has a reaction enthalpy of -176 kJ/mol for the Reaction (2.8) which is relatively high, thus making the decarbonation process of $MgCO_3$ more energy intensive in a LiCl-$BeCl_2$, NaCl-$BeCl_2$, or KCl-$BeCl_2$ melt.

Table 4.7: The table show the equilibrium temperature ($T_{\Delta G = 0}$) and the reaction enthalpy of the carbonation reaction between MgO, CO_2, and a halide salt (AH), $MgO + CO_2 + 2AH \rightleftharpoons MgH_2 + A_2CO_3$ (Total reaction), along with the reaction $MgCO_3 + 2AH \rightleftharpoons MgH_2 + A_2CO_3$ (Exchange reaction). The data is gathered from HSC Chemistry 6.12[45].

	Total reaction		Exchange reaction	
Salt (AH)	$T_{\Delta G = 0}$	ΔH	$T_{\Delta G = 0}$	ΔH
LiF	410	-103	$\Delta G < 0$	
NaF	475	-93	$\Delta G < 0$	
KF	675	-125	$\Delta G < 0$	
LiCl	-2	-49	4168	149
NaCl	$\Delta G > 0$		$\Delta G > 0$	
KCl	$\Delta G > 0$		$\Delta G > 0$	
$CdCl_2$	5309	1334	3047	406
$BeCl_2$	849	-176	2360	-182

Explained in the Subsection 2.3.6, a molten salt mixture that is a Lewis base, possesses an abundance of "free" anions, and the presence of alkali metal ions in the melt, salts such as NaF, LiCl, NaCl, and KCl fit this description. While the molten salts that are Lewis acids have an abundance of coordinate complexes, the "free" anions are stored in these coordinate complexes. As well as being rich in cations that belong to the transition metals, thus $CdCl_2$ and $BeCl_2$ salts should fit this description. The salt mixtures on Table 4.6, except FLiNaK and CuCl-KCl, have components that fit both descriptions. The molar composition of these salt mixtures does have a slightly higher composition for the acidic salts, except KCl-$BeCl_2$. Thus it is reasonable to expect that NaF-$CdCl_2$, LiCl-$BeCl_2$, and NaCl-$BeCl_2$ melts would act like Lewis acids, while KCl-$BeCl_2$ be more akin to a Lewis base. By this logic, the assumption here is the NaF-$CdCl_2$, LiCl-$BeCl_2$, and NaCl-$BeCl_2$ melts could have a higher chance of dissolving the MgO sorbent sufficiently, than KCl-$BeCl_2$.

When simulating the Reaction (2.14), HSC chemistry showed that there was no apparent hydrolysis of the salt mixture NaF-$CdCl_2$, while the three other salt mixtures start hydrolyzing at 650 °C.

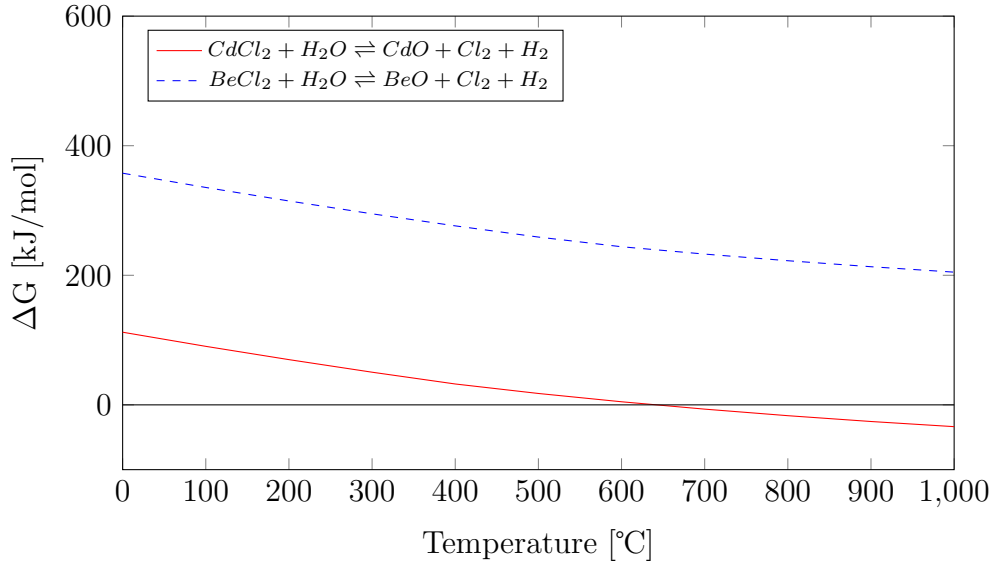

Figure 4.16: The figure illustrates the Gibbs free energy (ΔG) of the Reaction $MX_2 + H_2O \rightleftharpoons MO + X_2 + H_2$ or Reaction (2.15) against temperature (°C). Where X is represented by a halide in this case. The ΔG value does become negative for the reaction $BeCl_2 + H_2O \rightleftharpoons BeO + Cl_2 + H_2$ for temperatures over 650 °C, the salt mixtures containing $BeCl_2$ on Table 4.6 do hydrolyze at temperatures over 650 °C. The figure is made from simulations from HSC Chemistry 6.12[45].

Concerning safety, $CdCl_2$ is a compound that, when heated, forms toxic fumes, in the form of cadmium oxide (CdO). Exposure to $CdCl_2$ can cause several adverse health effects. $CdCl_2$ is also a known carcinogen, where it is associated with an elevated risk of developing lung cancer[80].

Like $CdCl_2$, $BeCl_2$ is a highly toxic compound that can have several adverse health effects if exposed to it. There is evidence that beryllium and its compounds are carcinogenic for humans, where it is associated with lung cancer[81].

With the health risks associated with the four halide salt mixtures, it is unlikely that these salts will be suitable for CCMS with MgO as sorbent, in the practical sense.

4.3.1 Experimental Results and Discussion of FLiNaK and CuCl-KCl in CCMS

FLiNaK

Further testing of CO_2 absorption by MgO in FLiNaK salt was suggested by former NMBU master student Åshild Grøtan in the conclusion chapter of her master thesis. She tested the CO_2 capture abilities of 15 g MgO in 150 g of a eutectic mixture of FLiNaK at 600 °C. In the first 200 minutes of the experiment the CO_2-absorption rate by MgO was maintained at 20% of the total amount of CO_2 entering the reactor. The experiment lasted over 400 minutes, where the total absorbed CO_2 was 12 g. 73% of the 15 g of MgO had reacted with the CO_2. The results of this experiment show that MgO has a slow reaction rate with CO_2.

She concludes that the height of the molten salt column were to shallow, thus, not allowing the CO_2 to stay long enough in the melt to properly react with the sorbent. She suggests that further investigation should be conducted with a taller melt column of FLiNaK salt. Meaning more salt and sorbent in the molten salt reactor.[59].

Molten FLiNaK has properties that make it well suited for the CCMS process. Molten FLiNaK has a low eutectic melting point, high boiling point, and low viscosity, and excellent heat transfer properties[82][83].

The eutectic molar ratio of FLiNaK is 46.5-11.5-42 mol% for LiF, NaF, and KF in the corresponding order. The melting point of FLiNaK is 454 °C, which is higher than 305 °C, the temperature where $MgCO_3$ start decarbonating into MgO and CO_2. However, due to Reaction (4.2),

$$\begin{aligned} &MgO + CO_2 + 2KF \rightleftharpoons K_2CO_3 + MgF_2 \\ &T_{\Delta G=0} = 675°C \end{aligned} \tag{4.2}$$

, the operating temperature CCMS with FLiNaK salt can be higher than 305 °C since the Reaction (4.2) does not reverse unless the temperature reaches over 675 °C. When MgO and CO_2 react with one of the components shown in Reaction (4.3), KF in this case, it allows for higher operating temperatures since the decarbonization process starts at higher temperatures.

KF is the compound in the FLiNaK melt that will interact the most with the MgO or $MgCO_3$. The Reaction (4.3) with LiF or NaF instead of KF has a positive Gibbs free energy value for temperatures over 480 °C, meaning

little carbonation of Li and Na will happen under temperatures higher than 480 °C.

As explained in the introduction chapter, this thesis was initially an experimental oriented thesis before the SARS-CoV-2 virus outbreak. Two experiments with FliNaK were conducted. The first test was 450 g FLiNaK salt with 45 g of MgO at 500 °C, and the second test had the same amount of salt and sorbent at 650 °C. The absorption of CO_2 for the experiments at 500 °C and 650 °C is shown in Figure 4.17 and 4.18, respectively.

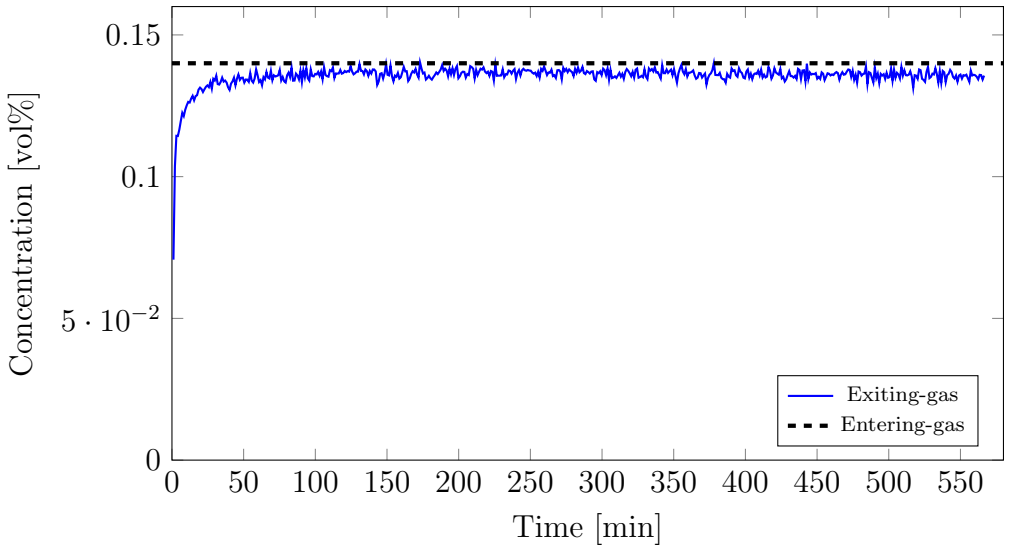

Figure 4.17: T = 500 °C experiment with MgO-FLiNaK, The blue line represents the CO_2 concentration exiting the molten salt reactor, the dashed black line represents the CO_2 concentration (14 vol%) entering the molten salt reactor.

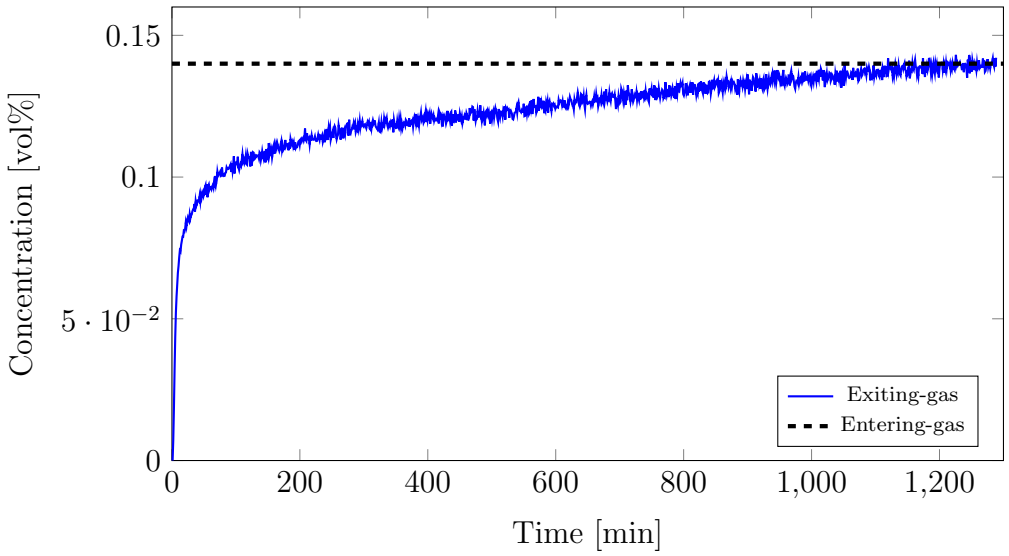

Figure 4.18: T = 650 °C experiment with MgO-FLiNaK, The blue line represents the CO_2 concentration exiting the molten salt reactor, the dashed black line represents the CO_2 concentration (14 vol%) entering the molten salt reactor.

The absorption curve of Figure 4.17 shows that the initial concentration CO_2 exiting the reactor was around 12 vol%, rapidly rising to just under 14 vol% where the concentration plateaus. It shows that most of the CO_2 entering the reactor are also exiting, meaning the CO_2 absorption rate of the MgO sorbent was slow.

After 550 minutes, the experiment was over, and according to the calculations, the total amount of CO_2 captured was 16.6 g. This amount was probably too high because the calibration constant was probably not accurate. The process of gathering the data needed to make the calibration constant was stopped prematurely because the MFC started logging numbers that were too high. Due to time constraints, it was decided to proceed with the experiment.

Using the calibration constant for the 650 °C experiment, the total amount of CO_2 absorbed by MgO under 500 °C was around 3.8 g. This amount is probably closer to the correct amount of absorbed CO_2 during the experiment.

The second experiment showed a different result; Figure 4.18 shows that the initial CO_2 concentration exiting the reactor was 8.0 vol%, where the exiting concentration rises relatively quickly in 100 minutes. After 100 minutes,

the concentration of CO_2 had reached 10 vol%, and the rise of CO_2 exiting the reactor slows down. As Figure 4.18 shows, for the next 1100 minutes, the concentration of CO_2 exiting the reactor was slowly increasing until it reached 14 vol% CO_2.

The total amount of CO_2 captured during this experiment was around 44.5 g. This amount is credible since the MgO can theoretically absorb 1.10 g of CO_2 per 1 g of MgO. Meaning almost all of the 45 g of MgO present in the reactor reacted with CO_2. However, it did take 1200 minutes to saturate almost all of the MgO, showing that the reaction rate between CO_2 and MgO in this experiment was very slow.

It is clear from the two experiments conducted in this thesis with molten FLiNaK salt that the temperature affects the reaction kinetics between MgO sorbent and CO_2. The reason for this might be because of the Reaction (4.3) has a decreasing Gibbs free energy as the temperature is increasing.

$$MgCO_3 + 2KF \rightleftharpoons MgF_2 + K_2CO_2 \tag{4.3}$$

This means the Reaction (4.3) will have faster rightward reaction rate as the temperature rises, see Figure 4.19.

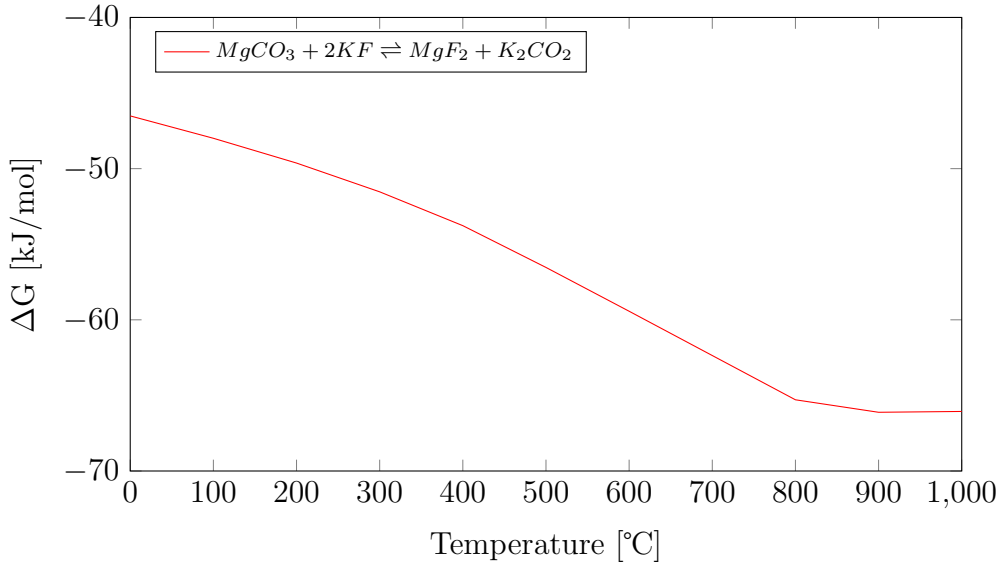

Figure 4.19: The Gibbs free energy (ΔG) of the Reaction 4.3, the ΔG value is decreasing as the temperature is rising, this might explain why the CO_2 capture rate was higher for the experiment with 650 °C than 500 °C. The figure is made from simulations from HSC Chemistry 6.12[45].

The hypothesis laid out by Åshild Grøtan in her master thesis is the slow reaction rate between CO_2 and MgO, were due to the height of the melt column were to shallow, making the CO_2 gas' residence time in the molten salt too short so that the CO_2 does not have time to react with the MgO. By having more salt and sorbent in the reactor, thus making the melt column taller, the CO_2 might be present in the salt long enough to react properly with the MgO[59]. Unfortunately, the two experiments conducted in this thesis show that is hypothesis probably not correct; both experiments conducted in this thesis use over double the amount of salt and sorbent and still having a less efficient absorption rate of CO_2 than her experiment. Figure 4.20 shows the CO_2 concentration exiting the reactor.

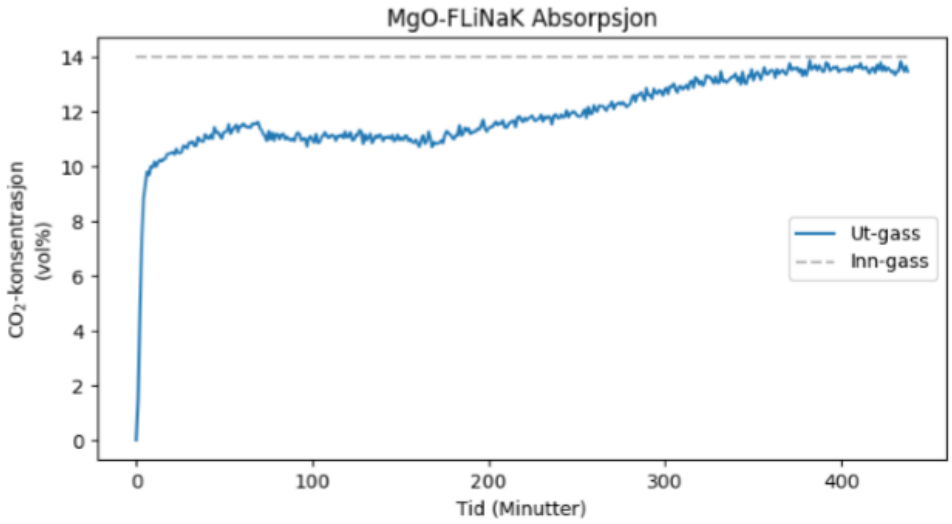

Figure 4.20: The figure is displaying Åshild Grøtan's experiment of CO_2 capture with MgO and molten FLiNaK salt. The figures labeling is written in Norwegian. "MgO-FLiNaK Absorpsjon" - MgO-FLiNaK Absorption. "CO_2-konsentrasjon (vol%)" - CO_2-concentration (vol%). "Ut-gass" - Exiting-gas. "Inn-gass" - Entering-gas. "Tid (Minutter)" - Time (Minutes). This figure orinates from Åshild Grøtan's master thesis[59].

The CO_2 concentration curve shows that the CO_2 concentration exiting the reactor is stable at around 10 vol% for around 200 minutes. This result shows a better reaction rate between MgO and CO_2 in the original experiment of Åshild Grøtan than the two experiments done with more salt and sorbent done in this thesis.

According to the discussion chapter in Åshids Grøtan's master thesis, one possible reason why the absorption rate of CO_2 by MgO is relatively poor is the wide temperature difference between Reaction (4.4), and Reaction (4.2) start decarbonizing.

$$\begin{aligned} &MgO + CO2 \rightleftharpoons MgCO_3 \\ &T_{\Delta G=0} = 305°C \end{aligned} \tag{4.4}$$

Reaction (4.4) start decarbonizing at 305 °C, while Reaction (4.2) decarbonizes at 675 °C, a temperature difference of 370 °C. It is explained in Åshild Grøtan's thesis that it is unclear how much the temperature difference affects the reaction kinetics between the MgO and CO_2 since it is impossible

to test CCMS with FLiNaK at under 305 °C empirically because eutectic FLiNaK salt melts at 454 °C[59].

Another reason why the slow reaction kinetics between the CO_2 and MgO sorbent is MgO not sufficiently dissolving in the FLiNaK melt. Figure 4.21 shows the nickel crucible used in the molten salt reactor. The figure shows the remains of the FLiNaK salt and undissolved MgO after the crucible was emptied of molten FLiNaK salt.

Figure 4.21: The figure shows a nickel crucible after being emptied of FLiNaK salt. There is solid MgO attached to the insides of the crucible, showing that much of the MgO has not been dissolved in the molten FLiNaK salt.

It is clear from this picture that much of the MgO did not dissolve in the melt. Thus probably contributed to the slow reaction kinetics between the CO_2 and MgO. The probable reason why MgO did not properly dissolve in the FLiNaK melt is that both FLiNaK and MgO are Lewis bases; see the example at the end of Subsection 2.3.6 for further explanation.

CuCl-KCl

Copper(I)chloride-sodium chloride (CuCl-KCl) salt was chosen because of the salt mixture's low eutectic melting point, around 150 °C. It is cheap, low toxicity, thermally stable up to 800 °C, and is readily available[84]. The

eutectic of this salt mixture is well below the temperature where the $MgCO_3$ starts decarbonate, which is at 305 °C. The eutectic molar composition of the two CuCl and KCl is 66.6-33.4 mol%, respectively, according to the phase diagram of CuCl-KCl, see Figure 4.22.

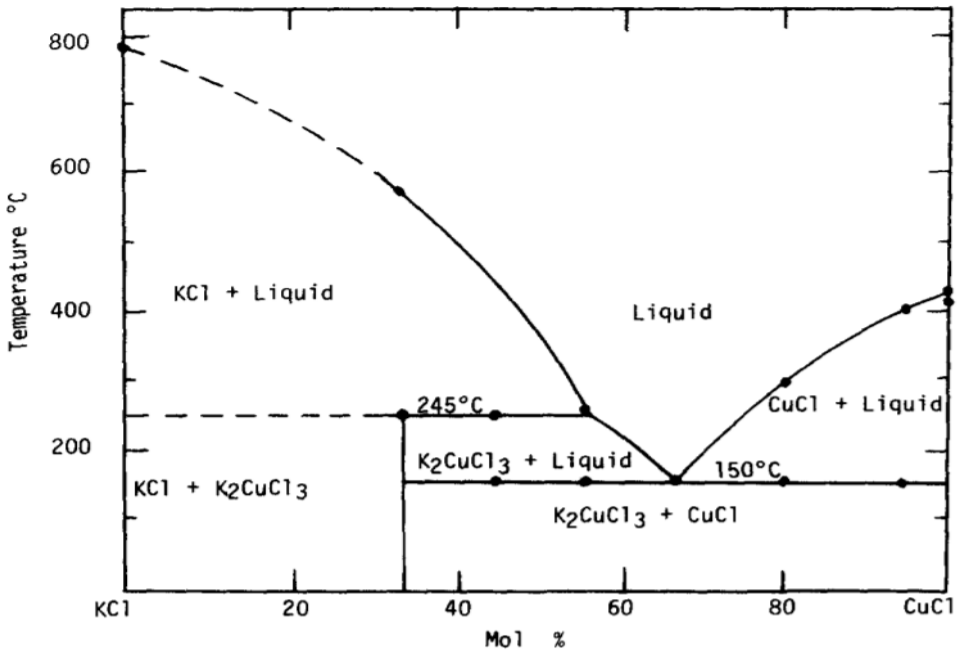

Figure 4.22: The phase diagram of the binary salt mixture CuCl-KCl, the y-axis is representing the temperature and the x-axis is representing the molar ratio between CuCl and KCl. This figure is reproduced by permission of D.E. Etter *et al.* [84].

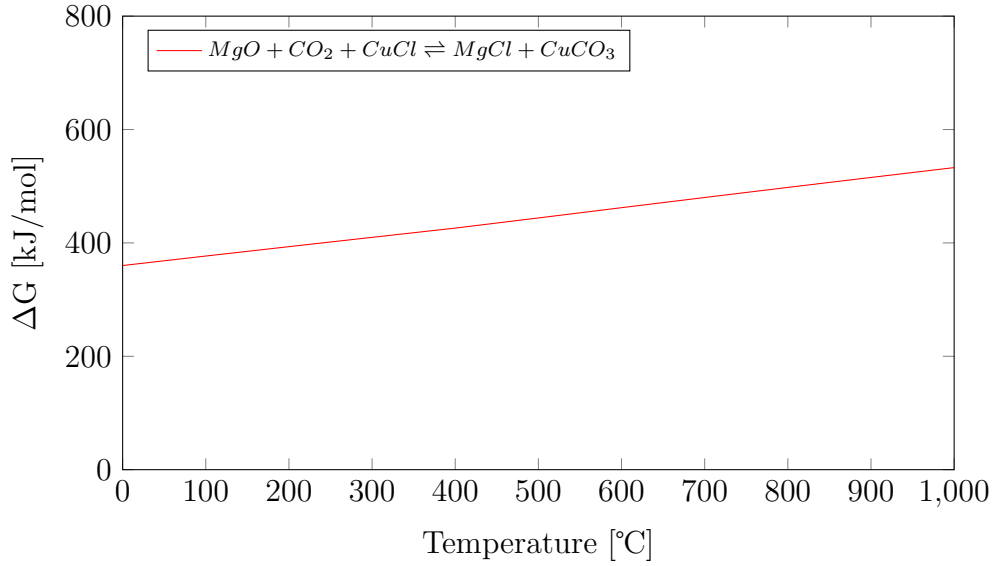

Figure 4.23: The figure shows the Gibbs free energy of the reaction $MgO + CO_2 + CuCl \rightleftharpoons MgCl + CuCO_3$, the y-axis is representing the Gibbs free energy ΔG and the x-axis is representing the temperature. The value of ΔG is positive as the temperature is rising, meaning the MgO and CO_2 will not react with CuCl. The figure is made from simulations from HSC Chemistry 6.12[45].

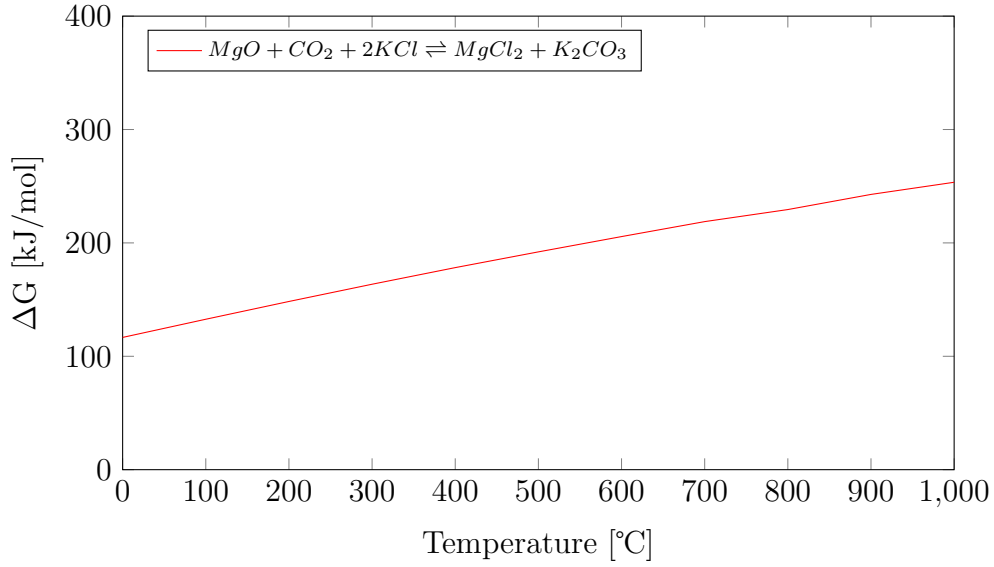

Figure 4.24: The figure shows the Gibbs free energy of the reaction $MgO + CO_2 + 2KF \rightleftharpoons MgCl_2 + K_2CO_3$, the y-axis is representing the Gibbs free energy ΔG and the x-axis is representing the temperature. The value of ΔG is positive as the temperature is rising, meaning the MgO and CO_2 will not react with KCl. The figure is made from simulations from HSC Chemistry 6.12[45].

None of the two salts reacts with the MgO, the MgO sorbent will thus stay inert in a CuCl-KCl melt, see Figure 4.23 and 4.24. Figure 4.23 displays the Gibbs free energy against the temperature of the reaction $MgO + CO_2 + CuCl \rightleftharpoons MgCl + CuCO_3$. Whereas Figure 4.24 illustrates the Gibbs free energy against the temperature of the reaction $MgO + CO_2 + 2KF \rightleftharpoons MgCl_2 + K_2CO_3$. The figures show that the ΔG is more than 0 for both reactions.

One failed experiment was conducted before the societal shutdown caused by the SARS-CoV-2 outbreak. The experiment was initially successful; however, after 10 minutes, the MFC, started logging much higher values for the concentration of CO_2 entering the reactor since the FTIR did not register any increased amounts of CO_2 exiting the reactor.

Since the data from the MFC was useless, the entire experiment had to be stopped. The MFC error could be caused by molten salt that had entered one of the pipes leading to the MFC or the FTIR, and then solidified, causing a partial blockage in the pipe. By partially blocking the pipe, the solidified salt creates backpressure. Since the MFC are dependent on being supplied gas at a certain pressure from the gas tanks, the backpressure changes that pressure. Thus, the computer program logging the CO_2 concentration flowing through the MFC will "think" that a much higher concentration of CO_2 is flowing through the MFC.

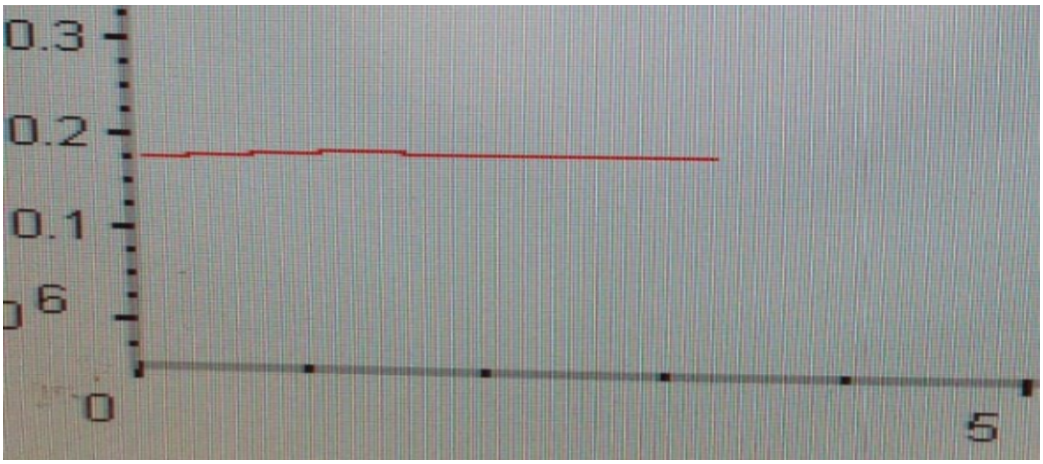

Figure 4.25: The figure is a picture taken from the display showing the CO_2 concentration measured by the FTIR during the CO_2 capture experiment with MgO and molten CuCl-KCl salt. The line represents the CO_2 concentration exiting the reactor. The concentration is almost 200 ppm_m (0.2), meaning almost no CO_2 is being absorbed.

The first successful minutes of this experiment showed that almost no CO_2 had been absorbed, see Figure 4.25. The red line shows that the CO_2 concentration exiting the reactor is right below the 0.2 mark, meaning almost 200 ppm CO_2 by mass was exiting the reactor. This concentration shows that almost all the CO_2 entering the reactor was exiting the reactor, and the MgO sorbent has very ineffective reaction kinetics with the CO_2.

The ineffective CO_2 absorption rate might be caused by the MgO sinking to the bottom of the nickel crucible. When cleaning out the nickle crucible for CuCl-KCl salt and MgO, a slab of solidified MgO was stuck at the bottom of the crucible unlike the MgO after the FLiNaK experiments where the MgO were stuck to the sides of the crucible. This means that the MgO probably sunk to the bottom and thus did not come in sufficient contact with the CO_2.

Since both CuCl and KCl are not coordination complexes, they cannot act as electron-accepting cations when melted. Both compounds contain a halide, Cl^-, that can act as an electron-donating anion, which means that molten CuCl-KCl probably is a Lewis base. Since MgO also is a Lewis base, the MgO probably was not be able to be sufficiently dissolved in the CuCl-KCl melt. See Subsection 2.3.6 for further description of Lewis acids and bases.

4.4 Halides-Nitrates

In this section, the discussion will proceed with the salt mixtures of halide and nitrate salts. In this group, four salt mixtures will be discussed.

Table 4.8: List of the halide-nitrate salt mixtures, the eutectic compositions and melting points of the salt mixtures are listed.

Salt mixture	Eutectic composition (mol%)	Eutectic (℃)
LiF - $LiNO_3$	5.0 - 95.0	251
NaF - $NaNO_3$	3.5 - 96.5	303
LiCl - $LiNO_3$	12.3 - 87.7	244
NaCl - $NaNO_3$	6.7 - 93.3	298

The salts LiF-$LiNO_3$, NaF-$NaNO_3$, LiCl-$LiNO_3$, and NaC-$NaNO_3$, possess similar characteristics. The eutectic melting points of all the halide-nitrate salt mixtures are heavily skewed towards the nitrates, see Figure 4.26,

all of the screened halide-nitrate salt mixtures have >87 mol% of nitrates in their eutectic mix ratio.

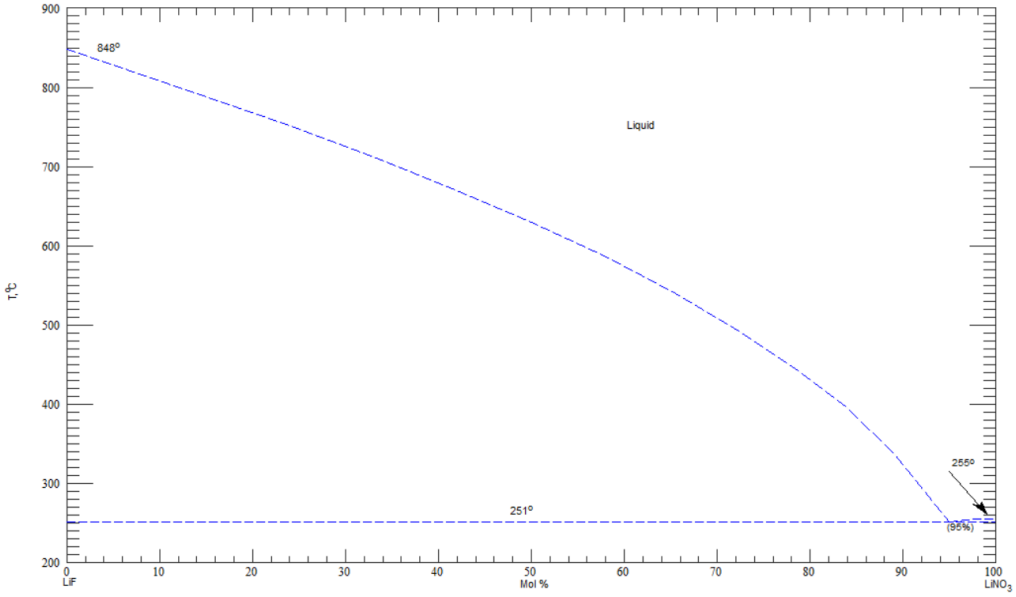

Figure 4.26: A phase diagram of the binary salt mixture LiF-$LiNO_3$. The y-axis represents the temperature in (°C), while the x-axis represents the molar ratio (mol%) between LiF and $LiNO_3$. As described above the molar ratio between LiF and $LiNO_3$ is heavily skewed towards the $LiNO_3$. This is also true for the salt mixtures NaF-$NaNO_3$, LiCl-$LiNO_3$, and NaCl-$NaNO_3$, which also have very similar phase diagram curves as displayed in this figure. The phase diagram is sourced from the ACerS-NIST *Phase Equilibria Diagram Database* 3.1.0[63].

The mixtures containing Li-salt, LiF-$LiNO_3$, and LiCl-$LiNO_3$, have similar eutectic melting points, around 250 °C. The Na-containing salt mixtures, NaF-$NaNO_3$, and NaCl-$NaNO_3$, also have similar eutectic melting points, around 300 °C.

When simulating Reaction (2.8) with HSC Chemistry, the salt mixtures containing fluoride salt were found to react with MgO and CO_2 within the operating temperature range. In contrast, the salt mixtures containing Cl-salt did not react with the MgO sorbent and CO_2 within the temperature range, see Figure 4.14. None of the salt mixtures showed any apparent hydrolysis when simulating Reaction (2.14), under the operating temperature range, see Figure 4.27.

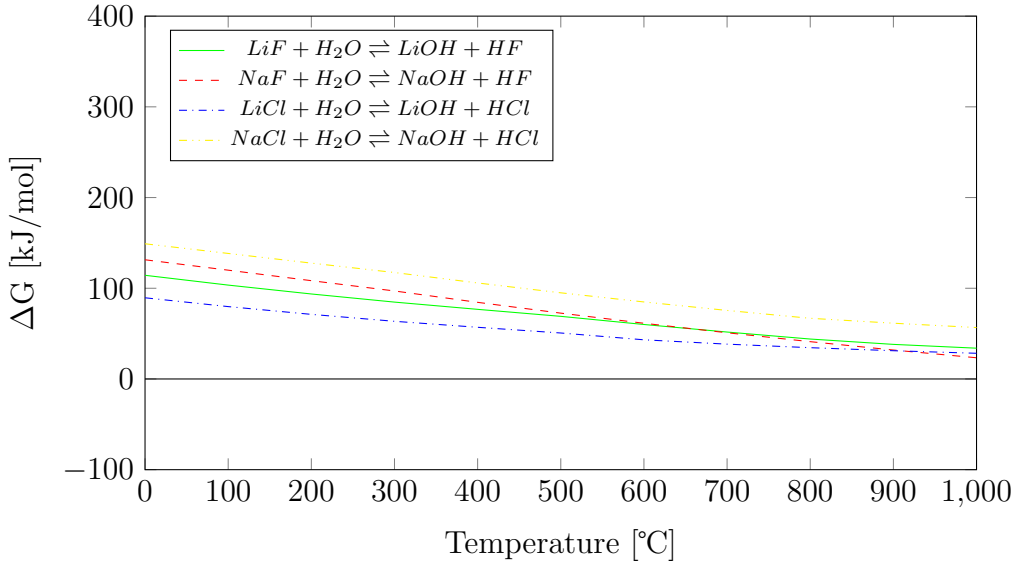

Figure 4.27: The figure illustrates the Gibbs free energy (ΔG) of the Reaction $MX + H_2O \rightleftharpoons MOH + HX$ or a variatoin of Reaction (2.14) against temperature (°C). The ΔG value does not become negative through the temperature range, meaning that no hydrolysis is apparent in a CCMS process with the salt mixtures listed in Table 4.8. The figure is made from simulations from HSC Chemistry 6.12[45].

As explained in the Subsection 2.3.6, the salt mixtures in Table 4.8 fit the Lewis base description. Thus all of the salt mixtures listed in Table 4.8 will act as a Lewis base and probably will not be able to dissolve MgO sufficiently. See the earlier sections in this chapter for further discussion in this matter.

Using any of these four salt mixtures in a CCMS process would probably be impractical. The salt mixtures containing Na possess relatively high eutectic melting points. NaF-$NaNO_3$ and NaCl-$NaNO_3$ possess the eutectic melting points of 303 °C and 298 °C, respectively. Both of these eutectic melting points are very close to the 305 °C limit, and thus using NaF-$NaNO_3$ and NaCl-$NaNO_3$ for a CCMS process would be impractical. The Li-containing salt mixtures do fare better when concerning the eutectic melting point temperature. LiF-$LiNO_3$ and LiCl-$LiNO_3$ possess the eutectic melting points of 251 °C and 244 °C, respectively.

Using the Li-containing salts would undoubtedly be an easier task in a CCMS process, mainly due to the significant temperature differences between the temperature limit of 305 °C and the eutectic melting points of the Li-containing salts. However, as explained in the Section 4.3, fluorides are

relatively expensive, especially LiF, mainly due to the relative scarcity of Li[85]. Of the two Li-containing salt mixtures, only LiF-$LiNO_3$ do react with MgO and CO_2, within the specified temperature range. The eutectic molar ratio between LiF and $LiNO_3$ is 5-95 mol%; this means very little LiF can react with MgO, thus making the CO_2 capturing process inefficient.

Chapter 5

Conclusion

This thesis summarizes the literature research of eutectic salt mixtures potentially suitable for CCMS with MgO as sorbent. The thesis also summarizes the experiments conducted before the societal shut down by SARS-CoV-2.

The salt mixtures screened must possess a sufficiently low eutectic melting point, unless if the salt mixture's components have an exchange reaction with $MgCO_3$, which allows for higher eutectic melting points and operating temperatures. The salt mixtures screened should not ideally have components that hydrolyzes with water with in the operating temperature range. If hydrolysis occurs measures have to be taken. The salt mixtures should act as Lewis acids towards MgO, if a molten salt mixture has Lewis acid characteristics, the melt could dissolve the MgO sorbent sufficiently. The components of the salt mixtures should be safe to handle, cheap, and readily available. The curve representing the eutectic melting point of a salt mixture should preferably have a wide "valley," thus, making the mixing of the salts easier.

By analyzing the published literature of molten salts and phase diagrams of salt mixtures, the salt mixtures potentially suitable for CCMS with MgO has been categorized by the components of the salt mixtures. The salt mixtures have been categorized into the nitrate salts, halides salts, and salt mixtures consisting of both nitrate and halide salts.

The salt mixtures consisting of purely nitrate salts are the most numerous group, this is due to their relatively low eutectic melting points, usually between 120 °C to 250 °C. The benefits of the nitrates are that they are cheap, readily available, less corrosive than other salts, possess relatively high thermal stability. However, the pure nitrate salt mixtures do not react

with $MgCO_3$, thus no exchange reaction, which means that higher operating temperatures cannot be achieved, and the CCMS process could be less efficient. Most of the screened nitrate salt mixtures will probably act as a Lewis base to MgO, making it unlikely that MgO will be sufficiently dissolved in any of the screened nitrate salt mixtures. The characteristics of the nitrate salts explained above indicate that the nitrate salt mixtures can be used in a CCMS process. However, due to the Lewis basicity of the salt mixtures, the CO_2 capture rate of MgO in a nitrate melt will probably be poor.

The group consisting purely of halide salts are considerably smaller than the nitrates group. Mainly due the selection of halide salt mixtures was based on the salt mixtures reactivity with $MgCO_3$. The pure halide salt group is divided into two sections; the first one consists of screened salt mixtures for CCMS with MgO, and the second part consists of the salt mixtures used in the experiments. The beneficial characteristics of halide salts are high thermal stability, high electrical, low viscosity, and excellent heat transfer properties. A negative side effect is the high corrosivity of molten halide salts and the following increased upkeep cost of CCMS equipment. The first section of the halide group is the screened salt mixtures. The salt mixtures listed in the first section all have a similar molar ratio between the different salt mixtures' components. The salt mixtures' eutectic melting points are relatively high, around 300 °C, except for NaCl-$BeCl_2$, who has a eutectic melting point of 217 °C. The high eutectic melting points of the salt mixtures makes the CCMS process difficult since it is necessary to have an operating temperature higher than the eutectic melting point. All of the salt mixtures in the section have a component of either $BeCl_2$ or $CdCl_2$. Both $BeCl_2$ and $CdCl_2$ are potentially hazardous for humans, making any of the salt mixtures in the section not suitable for CCMS.

FLiNaK salt was tested with MgO as sorbent. Two experiments with temperatures of 500 °C and 650 °C. The 650 °C had a higher CO_2 capture rate than the 500 °C experiment. The amount of FLiNaK salt was 450 g and MgO of 50 g. Both experiments were to test Åshild Gøtan's hypothesis. The hypothesis states that a higher CO_2 rate could be achieved by having a higher molten salt column in the reactor, meaning a larger amount of salt and sorbent in the reactor during a CCMS process. Unfortunately, the experiments yielded worse CO_2 capture rate than Åshild Grøtan's experiment with FLiNaK. The low CO_2 capture rate could be caused by the large amount undissolved MgO in the FLiNaK melt.

The CuCl-KCl experiment, unfortunately, failed. However, some informa-

tion on CuCl-KCl was noted. The initial 10 minutes of the experiment with CuCl-KCl showed that the CO_2 capture rate was very low. This information tells us that CuCl-KCl is probably not suited for CCMS.

The last group is the halides-nitrate salt mixtures. The group consists of four salt mixtures; all of them have the characteristic that the molar ratio is heavily skewed to the nitrate salt, which means that most of the MgO in a halide-nitrate melt would stay inert. The four salt mixtures' eutectic melting points are relatively high, between 244 °C to 303 °C, which means that these salt mixtures are not practical in a CCMS process. These salt mixtures will probably act like pure nitrate salt mixtures, due to the skewed molar ratio towards the nitrate salt component. As concluded above, the salt mixtures in this group could be used in a CCMS process; however, probably with a low CO_2 capture rate.

An interesting proposal for further research in this field is the use of enhanced MgO with alkali metal nitrates. The efficiency of CO_2 capture might increase if the MgO is enhanced with a nitrate. Studies conducted where MgO and CO_2 have a solid-gas reaction with each other, the CO_2 capture rate of MgO was increased when doped or enhanced with an alkali metal nitrate. In the same studies, alkali metal carbonates have been used as well. Even if these studies uses a solid CO_2-sorbent, it would be interesting to test enhanced MgO in molten salts. Another proposal is to blend alkali metal nitrate salt or carbonates with FLiNaK. Blending specific alkali metal nitrates or carbonates in a FLiNaK melt could increase the CO_2 capture rate of MgO.

Bibliography

[1] V. Masson-Delmotte mfl. *IPPC, 2018: Global warming of 1.5°C. An IPCC Special Report on the impacts of global warming of 1.5°C above pre-industrial levels and related global greenhouse gas emission pathways, in the context of strengthening the global response to the threat of climate change, sustainable development, and efforts to eradicate poverty.*

[2] Charles D Keeling et al. "Atmospheric carbon dioxide variations at Mauna Loa observatory, Hawaii". In: *Tellus* 28.6 (1976), pp. 538–551.

[3] Jack C Pales and Charles D Keeling. "The concentration of atmospheric carbon dioxide in Hawaii". In: *Journal of Geophysical Research* 70.24 (1965), pp. 6053–6076.

[4] R.K. Pachauri and L.A. Meyer (eds.) *Climate Change 2014: Synthesis Report. Contribution of Working Groups I, II and III to the Fifth Assessment Report of the Intergovernmental Panel on Climate Change.*

[5] Steffen. Jakobsen Ingvild Ulrikke & Kallbekken. *Parisavtalen. I Store norske leksikon.* URL: `https://snl.no/Parisavtalen`. (accessed: 03.04.2020).

[6] Espen Olsen and Viktorija Tomkute. "Carbon capture in molten salts". In: *Energy Science & Engineering* 1.3 (2013), pp. 144–150.

[7] Viktorija Tomkute, Asbjørn Solheim, and Espen Olsen. "Investigation of high-temperature CO2 capture by CaO in CaCl2 molten salt". In: *Energy & fuels* 27.9 (2013), pp. 5373–5379.

[8] Jostein Mamen and Rasmus Benestad. *Drivhuseffekten. I Store norske leksikon.* URL: `https://snl.no/drivhuseffekten`. (accessed: 13.03.2020).

[9] Stephen T. Jackson. *Climate change. Encyclopædia Britannica*. URL: https://www.britannica.com/science/climate-change. (accessed: 23.03.2020).

[10] Inge Bryhni, Kåre Olerud, and Jostein Mamen. *Klimagasser. I Store norske leksikon*. URL: https://snl.no/klimagasser. (accessed: 16.03.2020).

[11] *Phase Diagrams*. URL: https://chem.libretexts.org/Bookshelves/General_Chemistry/Map%5C%3A_General_Chemistry_(Petrucci_et_al.)/12%5C%3A_Intermolecular_Forces%5C%3A_Liquids_And_Solids/12.4%5C%3A_Phase_Diagrams#title. Accessed: 29.07.2020.

[12] Haakon Haraldsen and Bjørn Pedersen. *Karbondioksid. I Store norske leksikon*. URL: https://snl.no/karbondioksid. (accessed: 15.03.2020).

[13] National Oceanic & Atmospheric Administration (NOAA): Earth System Research Laboratory (ESRL). *Trends in Atmospheric Carbon Dioxide*. URL: https://www.esrl.noaa.gov/gmd/ccgg/trends/. (accessed: 29.07.2020).

[14] B. Metz mfl. "IPCC special report on Carbon Dioxide Capture and Storage (SR CCS)". In: *Cambridge University Press, UK*. (2005).

[15] IEA (2019). *CO2 Emissions from Fuel Combustion 2019*. URL: https://www.iea.org/reports/co2-emissions-from-fuel-combustion-2019.

[16] Roger G. Barry and Richard J. Chorley. *Atmosphere, Weather and Climate*. Ninth Edition. 2 Park Square, Milton Park, Abington, Oxon, OX14 4RN, UK: Routledge, 2010.

[17] Rasmus Benestad et al. *Klimaendringer. I Store norske leksikon*. URL: https://snl.no/klimaendringer. (accessed: 15.03.2020).

[18] Knut Hofstad. *Karbonfangs og -lagring. I Store norske leksikon*. URL: https://snl.no/karbonfangst_og_-lagring. (accessed: 24.03.2020).

[19] Daniel Jansen et al. "Pre-combustion CO2 capture". In: *International Journal of Greenhouse Gas Control* 40 (2015), pp. 167–187.

[20] Calin-Cristian Cormos. "Evaluation of power generation schemes based on hydrogen-fuelled combined cycle with carbon capture and storage (CCS)". In: *International Journal of Hydrogen Energy* 36.5 (2011), pp. 3726–3738.

[21] Min Chul Lee et al. "Gas turbine combustion performance test of hydrogen and carbon monoxide synthetic gas". In: *Fuel* 89.7 (2010), pp. 1485–1491.

[22] Bryce Dutcher, Maohong Fan, and Armistead G Russell. "Amine-based CO2 capture technology development from the beginning of 2013 · A Review". In: *ACS applied materials & interfaces* 7.4 (2015), pp. 2137–2148.

[23] Deanna M D'Alessandro, Berend Smit, and Jeffrey R Long. "Carbon dioxide capture: prospects for new materials". In: *Angewandte Chemie International Edition* 49.35 (2010), pp. 6058–6082.

[24] Dennis YC Leung, Giorgio Caramanna, and M Mercedes Maroto-Valer. "An overview of current status of carbon dioxide capture and storage technologies". In: *Renewable and Sustainable Energy Reviews* 39 (2014), pp. 426–443.

[25] Matthew E Boot-Handford et al. "Carbon capture and storage update". In: *Energy & Environmental Science* 7.1 (2014), pp. 130–189.

[26] TA Smith. "Amines in food". In: *Food Chemistry* 6.3 (1981), pp. 169–200.

[27] Niall MacDowell et al. "An overview of CO 2 capture technologies". In: *Energy & Environmental Science* 3.11 (2010), pp. 1645–1669.

[28] J Blamey et al. "The calcium looping cycle for large-scale CO2 capture". In: *Progress in Energy and Combustion Science* 36.2 (2010), pp. 260–279.

[29] Charles C Dean et al. "The calcium looping cycle for CO2 capture from power generation, cement manufacture and hydrogen production". In: *Chemical Engineering Research and Design* 89.6 (2011), pp. 836–855.

[30] Dawid P Hanak, Edward J Anthony, and Vasilije Manovic. "A review of developments in pilot-plant testing and modelling of calcium looping process for CO 2 capture from power generation systems". In: *Energy & Environmental Science* 8.8 (2015), pp. 2199–2249.

[31] Mai Bui et al. "Carbon capture and storage (CCS): the way forward". In: *Energy & Environmental Science* 11.5 (2018), pp. 1062–1176.

[32] Rajab Khalilpour et al. "Membrane-based carbon capture from flue gas: a review". In: *Journal of Cleaner Production* 103 (2015), pp. 286–300.

[33] Shuaifei Zhao et al. "Status and progress of membrane contactors in post-combustion carbon capture: A state-of-the-art review of new developments". In: *Journal of membrane science* 511 (2016), pp. 180–206.

[34] Ofélia de Queiroz Fernandes Araújo and Jose Luiz de Medeiros. "Carbon capture and storage technologies: present scenario and drivers of innovation". In: *Current Opinion in Chemical Engineering* 17 (2017), pp. 22–34.

[35] Michele Aresta, Angela Dibenedetto, and Antonella Angelini. "The changing paradigm in CO2 utilization". In: *Journal of CO2 Utilization* 3 (2013), pp. 65–73.

[36] Javier A Lara-Gil, Carolina Senés-Guerrero, and Adriana Pacheco. "Cement flue gas as a potential source of nutrients during CO2 mitigation by microalgae". In: *Algal research* 17 (2016), pp. 285–292.

[37] Valentin Gutknecht et al. "Creating a carbon dioxide removal solution by combining rapid mineralization of CO2 with direct air capture". In: *Energy Procedia* 146 (2018), pp. 129–134.

[38] Australia: Global CCS Institute. 2019. *The Global Status of CCS: 2019*.

[39] D. G. Lovering. *Molten Salt Technology*. 1982. ISBN: 978-1-4757-1724-2.

[40] Andrew L. Dicks and David A. J. Rand. *Fuel Cell Systems Explained*. Third Edition. The Atrium, Southern Gate, Chichester, West Sussex, PO19 8SQ, UK: John Wiley & Sons Ltd., 2018.

[41] Angel G Fernández et al. "Mainstreaming commercial CSP systems: A technology review". In: *Renewable energy* (2019).

[42] A Maccari et al. "Archimede Solar Energy molten salt parabolic trough demo plant: a step ahead towards the new frontiers of CSP". In: *Energy Procedia* 69 (2015), pp. 1643–1651.

[43] David LeBlanc. "Molten salt reactors: a new beginning for an old idea". In: *Nuclear Engineering and design* 240.6 (2010), pp. 1644–1656.

[44] Heidi S Nygård, Viktorija Tomkute, and Espen Olsen. "Kinetics of CO2 absorption by calcium looping in molten halide salts". In: *Energy Procedia* 114 (2017), pp. 250–258.

[45] Outotec Research Oy. *HSC Chemistry*. Versjon 6.12.

[46] Raymond Chang and Ken Goldsby. *General Chemistry: The Essential Concepts*. Seventh Edition. 1221 Avenue of the Americas, New York, NY 10020, US: McGraw-Hill, 2014.

[47] H. Scott Folger. *Elements of Chemical Reaction Engineering*. Fifth Edition. Prentice Hall, 2016. ISBN: 978-0-13-388751-8.

[48] The Editors of Encyclopaedia Britannica. *Heat of reaction. Encyclopædia Britannica*. URL: `https://www.britannica.com/science/heat-of-reaction`. (accessed: 28.07.2020).

[49] Helmer Fjellvåg. *Hydrolyse. I Store norske leksikon*. URL: `https://snl.no/hydrolyse`. (accessed: 22.06.2020).

[50] Maria Hansen. "Karbonfangst i saltsmelter: effekten av hydrolyse". MA thesis. Norwegian University of Life Sciences, Ås, 2017.

[51] David F Williams et al. "The influence of Lewis acid/base chemistry on the removal of gallium by volatility from weapons-grade plutonium dissolved in molten chlorides". In: *Nuclear Technology* 136.3 (2001), pp. 367–370.

[52] Bjørn Kofstad Per K. & Pedersen. *Magnesium. I Store norske leksikon*. URL: `https://snl.no/magnesium`. (accessed: 29.03.2020).

[53] Steve Gagnon. *The Element Magnesium*. URL: `https://education.jlab.org/itselemental/ele012.html`. (accessed: 25.03.2020).

[54] Ping Li et al. "Synthetic architecture of MgO/C nanocomposite from hierarchical-structured coordination polymer toward enhanced CO2 capture". In: *ACS applied materials & interfaces* 9.11 (2017), pp. 9592–9602.

[55] Xinfang Yang et al. "Magnesium Oxide-Based Absorbents for CO 2 Capture at Medium Temperature". In: *Current Pollution Reports* 4.1 (2018), pp. 13–22.

[56] Viktorija Tomkute, Asbjørn Solheim, and Espen Olsen. "CO2 capture by CaO in molten CaF2–CaCl2: optimization of the process and cyclability of CO2 capture". In: *Energy & Fuels* 28.8 (2014), pp. 5345–5353.

[57] Espen Olsen, Maria Hansen, and Heidi Nygård. "Hydrolysis of molten CaCl2-CaF2 with additions of CaO". In: (2017).

[58] Nils Amund Rusås Ruud. "Karbonfangst i saltsmelter: effekten av sulfatering". MA thesis. Norwegian University of Life Sciences, Ås, 2018.

[59] Åshild Grøtan. "Karbonfangst med metalloksider i saltsmelter: MgO, SrO og CaO som sorbenter". MA thesis. Norwegian University of Life Sciences, Ås, 2019.

[60] Grethe Wibetoe. *IR-spektroskopi. I Store norske leksikon.* URL: `https://snl.no/IR-spektroskopi`. (accessed: 08.03.2020).

[61] Thermo Fisher Scientific. *Advantages of a Fourier Transform Infrared Spectrometer*. 2015.

[62] Wikimedia Commons the free media repository. *File:FTIR Interferometer.png. 2017.* URL: `https://commons.wikimedia.org/wiki/File:FTIR_Interferometer`. (accessed: 31.03.2020).

[63] ACerS-NIST. *Phase equilibria diagrams database*. Version 3.1.0. CD-ROM Database. 2005.

[64] Masaaki Ito and Kazuki Morita. "The solubility of MgO in molten MgCl2-CaCl2 salt". In: *Materials transactions* 45.8 (2004), pp. 2712–2718.

[65] Kevin Coscia et al. "Thermophysical properties of LiNO3–NaNO3–KNO3 mixtures for use in concentrated solar power". In: *Journal of solar energy engineering* 135.3 (2013).

[66] Keling Zhang et al. "Molten salt promoting effect in double salt CO2 absorbents". In: *The Journal of Physical Chemistry C* 120.2 (2016), pp. 1089–1096.

[67] Soo Chool Lee et al. "Effects of alkali-metal carbonates and nitrates on the CO 2 sorption and regeneration of MgO-based sorbents at intermediate temperatures". In: *Korean Journal of Chemical Engineering* 33.12 (2016), pp. 3448–3455.

[68] Robert W Bradshaw and Nathan P Siegel. "Molten nitrate salt development for thermal energy storage in parabolic trough solar power systems". In: *ASME 2008 2nd International Conference on Energy Sustainability collocated with the Heat Transfer, Fluids Engineering, and 3rd Energy Nanotechnology Conferences*. American Society of Mechanical Engineers Digital Collection. 2008, pp. 631–637.

[69] K Federsel, J Wortmann, and M Ladenberger. "High-temperature and corrosion behavior of nitrate nitrite molten salt mixtures regarding their application in concentrating solar power plants". In: *Energy Procedia* 69 (2015), pp. 618–625.

[70] Tao Wang, Divakar Mantha, and Ramana G Reddy. "Thermal stability of the eutectic composition in LiNO3–NaNO3–KNO3 ternary system used for thermal energy storage". In: *Solar Energy Materials and Solar Cells* 100 (2012), pp. 162–168.

[71] Bjørn Pedersen. *Rubidium. I Store norske leksikon*. URL: `https://snl.no/rubidium`. (accessed: 22.06.2020).

[72] Bjørn Pedersen. *Alkalimetallene. I Store norske leksikon*. URL: `https://snl.no/alkalimetallene`. (accessed: 22.06.2020).

[73] Jack Kauffman George B. & Halpern. *Coordination compound. Encyclopædia Britannica*. URL: `https://www.britannica.com/science/coordination-compound`. (accessed: 22.06.2020).

[74] Byung Wook Hwang et al. "CO2 capture and regeneration properties of MgO-based sorbents promoted with alkali metal nitrates at high pressure for the sorption enhanced water gas shift process". In: *Process Safety and Environmental Protection* 116 (2018), pp. 219–227.

[75] Chao Yu et al. "Characteristics of Alkali Nitrates Molten Salt-Promoted MgO as a Moderate-Temperature CO2 Absorbent". In: *Energy Procedia* 158 (2019), pp. 5776–5781.

[76] Wenjin Ding, Alexander Bonk, and Thomas Bauer. "Corrosion behavior of metallic alloys in molten chloride salts for thermal energy storage in concentrated solar power plants: a review". In: *Frontiers of Chemical Science and Engineering* 12.3 (2018), pp. 564–576.

[77] Luke Olson et al. "Nickel-plating for active metal dissolution resistance in molten fluoride salts". In: *Journal of nuclear materials* 411.1-3 (2011), pp. 51–59.

[78] Wenjin Ding et al. "Molten chloride salts for next generation concentrated solar power plants: Mitigation strategies against corrosion of structural materials". In: *Solar Energy Materials and Solar Cells* 193 (2019), pp. 298–313.

[79] H Kvande. "Production of primary aluminium". In: *Fundamentals of Aluminium Metallurgy*. Elsevier, 2011, pp. 49–69.

[80] National Center for Biotechnology Information. *Cadmium chloride*. URL: `https://pubchem.ncbi.nlm.nih.gov/compound/Cadmium-chloride`. (accessed: 19.06.2020).

[81] National Center for Biotechnology Information. *Cadmium chloride*. URL: `https://pubchem.ncbi.nlm.nih.gov/compound/Beryllium-chloride`. (accessed: 19.06.2020).

[82] Luke C Olson et al. "Materials corrosion in molten LiF–NaF–KF salt". In: *Journal of Fluorine Chemistry* 130.1 (2009), pp. 67–73.

[83] DF Williams. *Assessment of candidate molten salt coolants for the NGNP/NHI heat-transfer loop*. Tech. rep. Oak Ridge National Lab.(ORNL), Oak Ridge, TN (United States), 2006.

[84] DE Etter and CJ Wiedenheft. "The study of KCl-CuCl eutectic fused salt as a potential intermediate temperature heat transfer and storage medium". In: *Solar Energy Materials* 2.4 (1980), pp. 423–431.

[85] H Aral and A Vecchio-Sadus. "Lithium: environmental pollution and health effects". In: (2011).

[86] Ana Korvald. "CO2-fangst i saltsmelter: absorpsjon og desorpsjon av CO2 i smeltet NaF/CaF2 med CaO-sorbent". MA thesis. University of Life Sciences, Ås, 2013.

[87] Yasen Alhaj-Saleh. "Karbonfangst i saltsmelter: absorpsjon og desorpsjon av CO2 med CaO-sorbent i eutektisk CaF2/CaCl2-smelte". MA thesis. Norwegian University of Life Sciences, Ås, 2014.

Appendix A

Appendix

A.1 Phase Diagrams

All of the screened salt mixtures are displayed in the Figures A.1-A.26. The phase diagrams is taken from the ACerS-NIST *Phase Equilibria Diagram Database* 3.1.0[63].

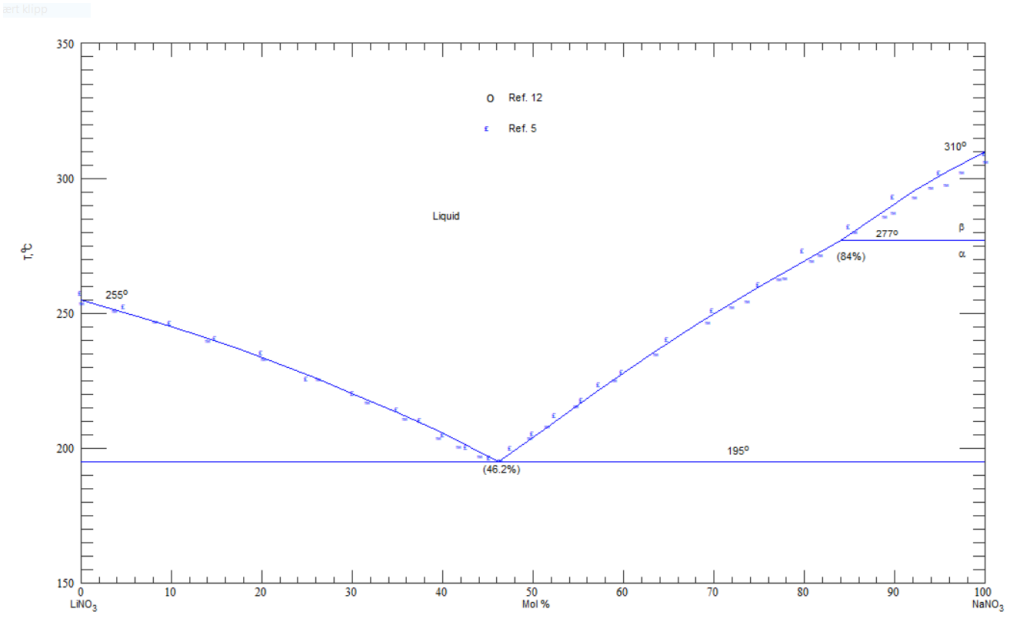

Figure A.1: The phase diagram of $LiNO_3$-$NaNO_3$.

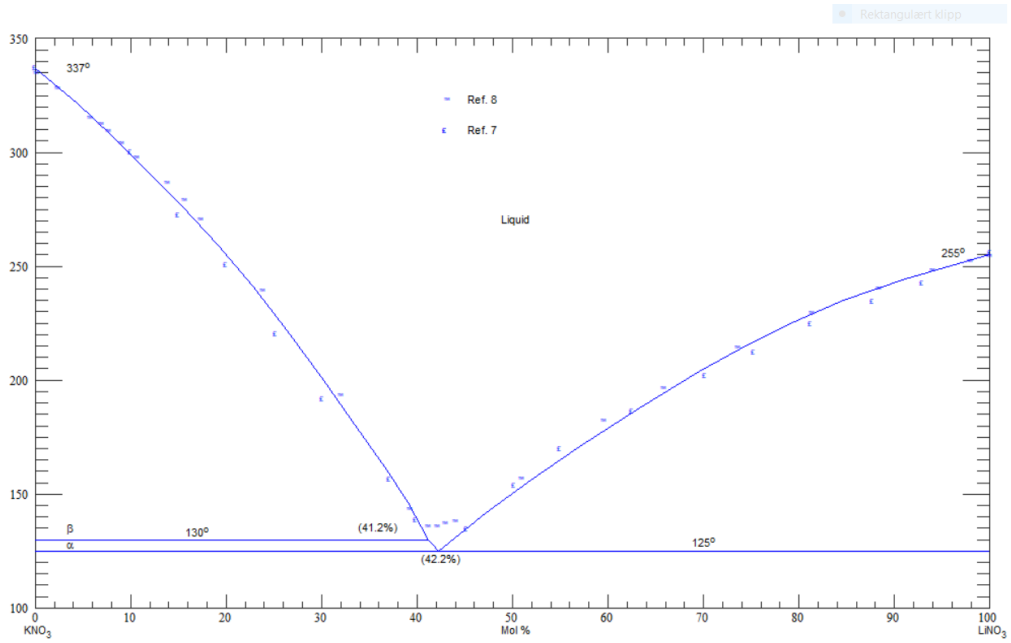

Figure A.2: The phase diagram of $LiNO_3$-KNO_3.

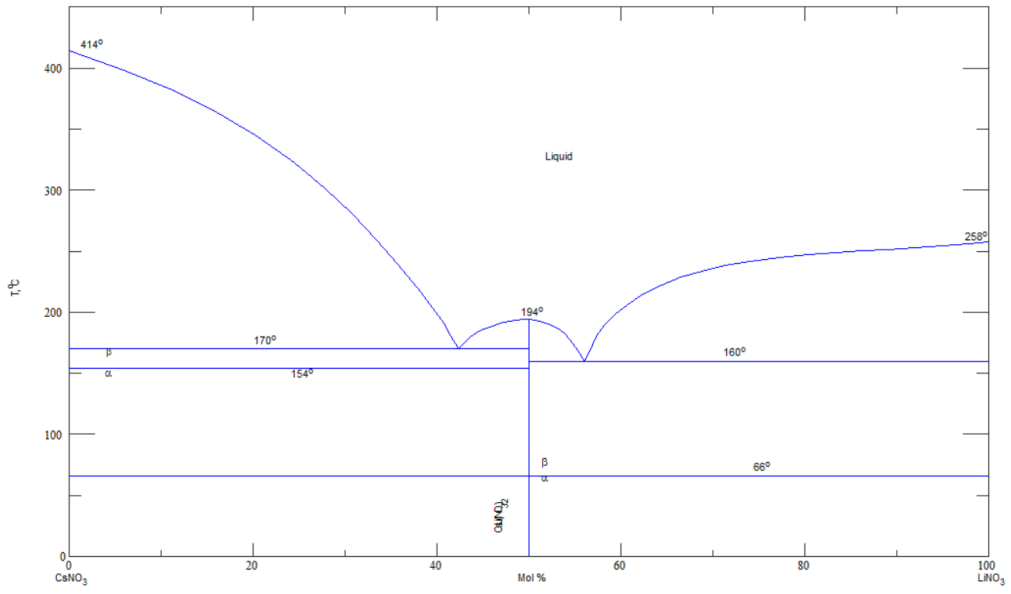

Figure A.3: The phase diagram of $LiNO_3$-$CsNO_3$.

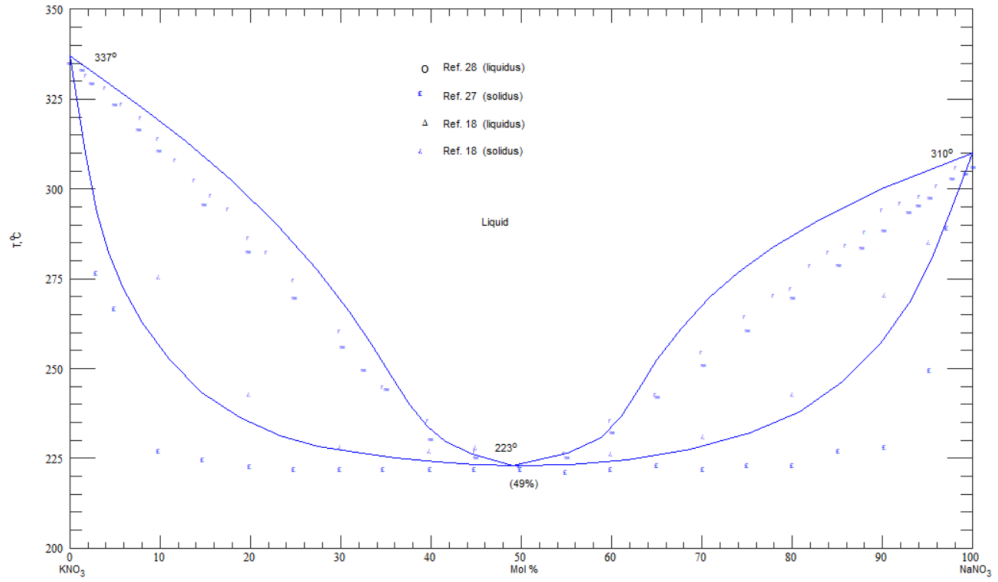

Figure A.4: The phase diagram of $NaNO_3$-KNO_3.

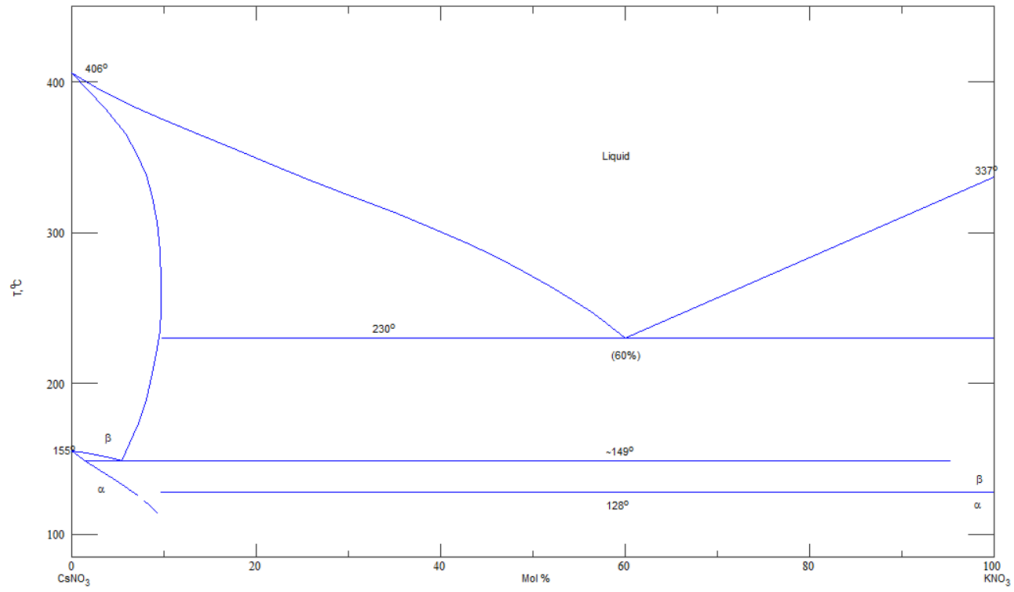

Figure A.5: The phase diagram of KNO_3-$CsNO_3$.

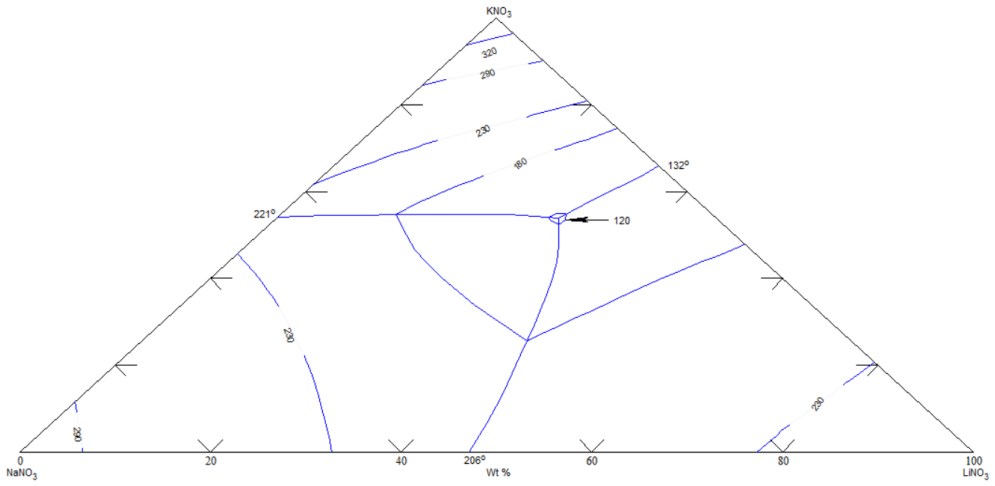

Figure A.6: The phase diagram of $LiNO_3$-$NaNO_3$-KNO_3.

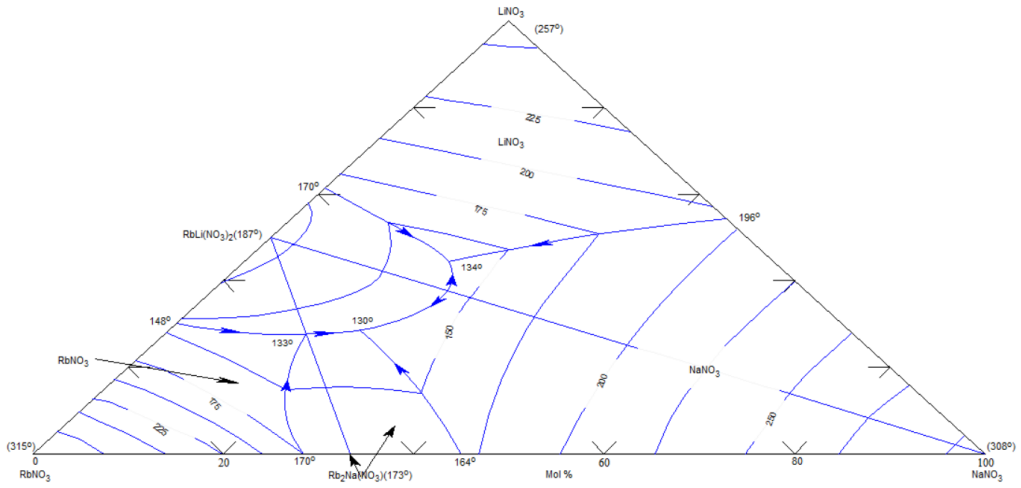

Figure A.7: The phase diagram of $LiNO_3$-$NaNO_3$-$RbNO_3$.

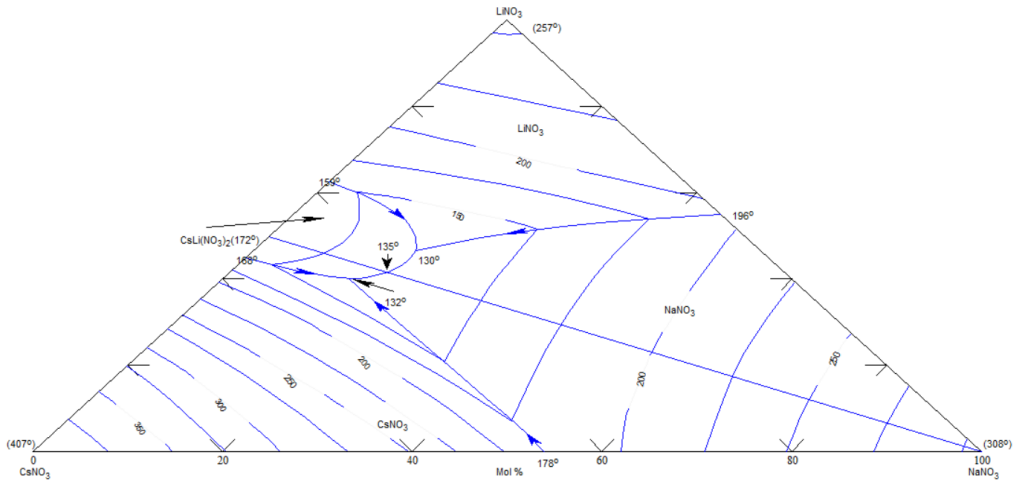

Figure A.8: The phase diagram of $LiNO_3$-$NaNO_3$-$CsNO_3$.

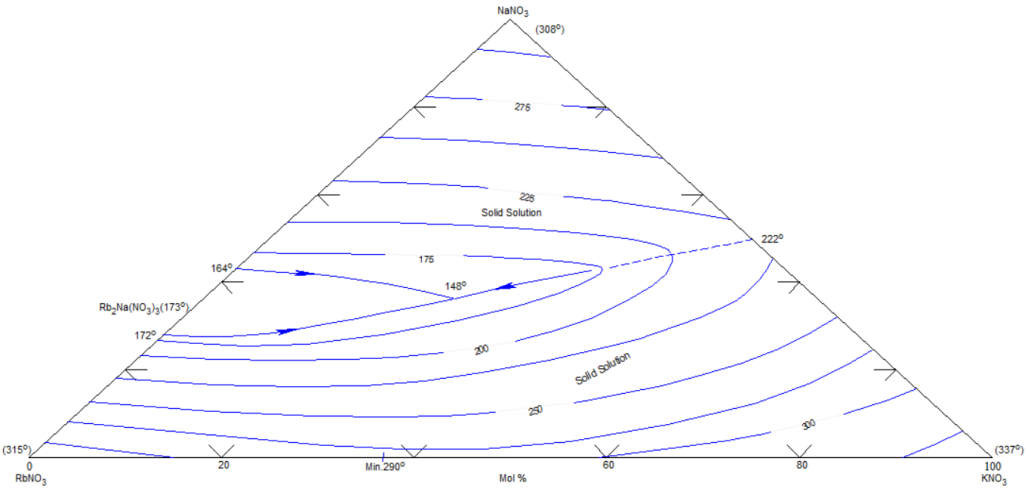

Figure A.9: The phase diagram of $NaNO_3$-KNO_3-$RbNO_3$.

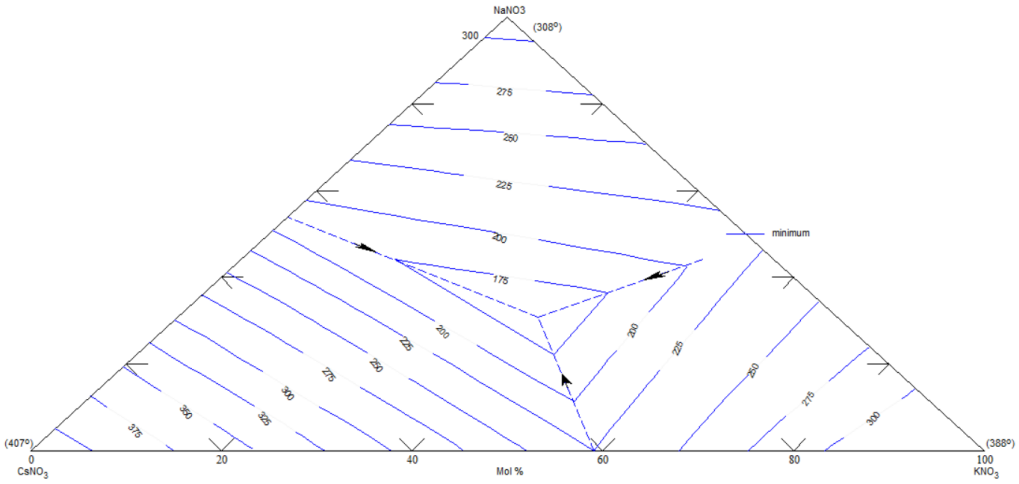

Figure A.10: The phase diagram of $NaNO_3$-KNO_3-$CsNO_3$.

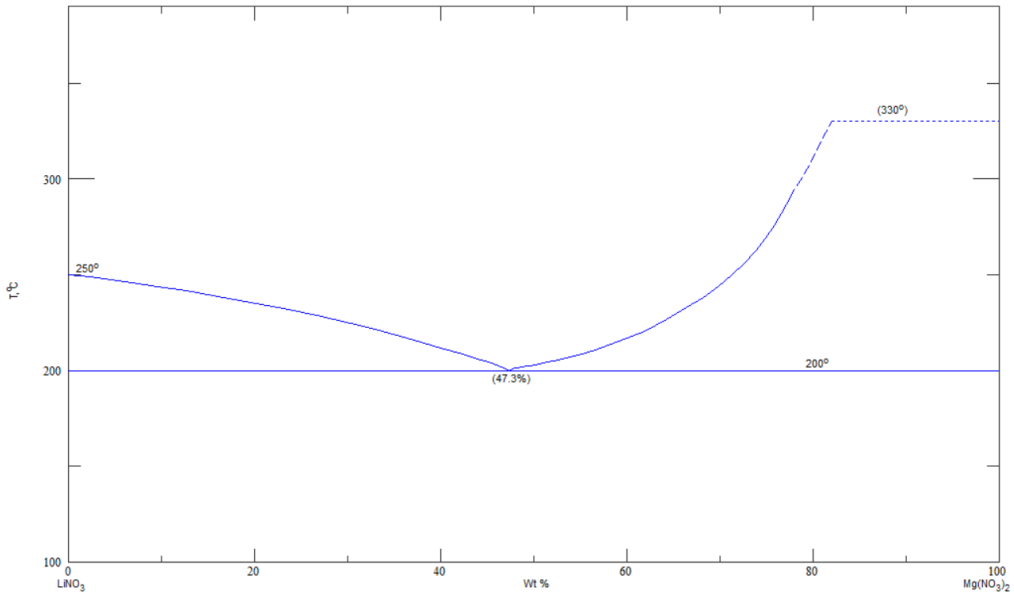

Figure A.11: The phase diagram of $LiNO_3$-$Mg(NO_3)_2$.

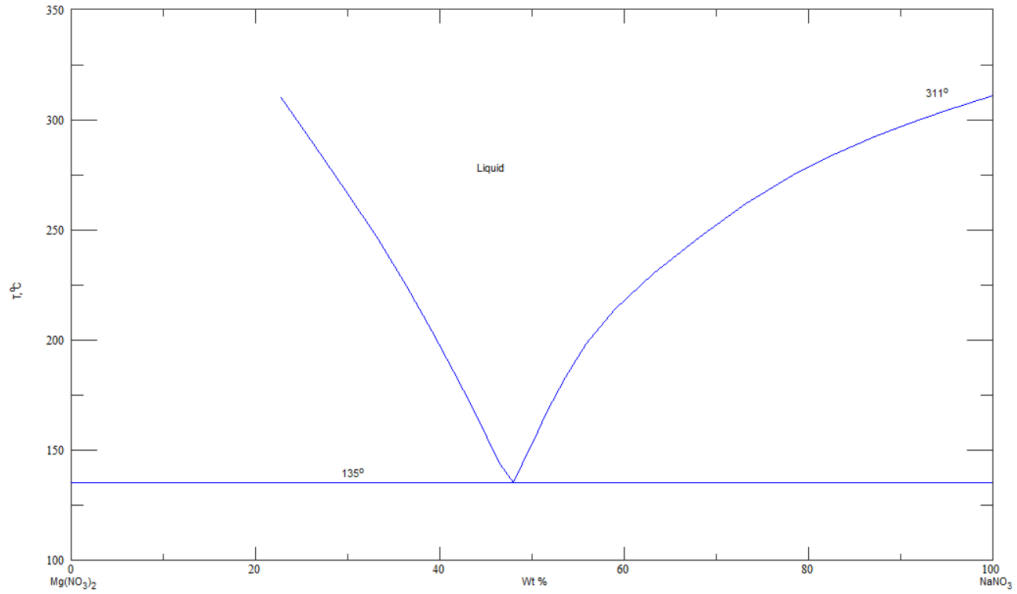

Figure A.12: The phase diagram of $NaNO_3$-$Mg(NO_3)_2$.

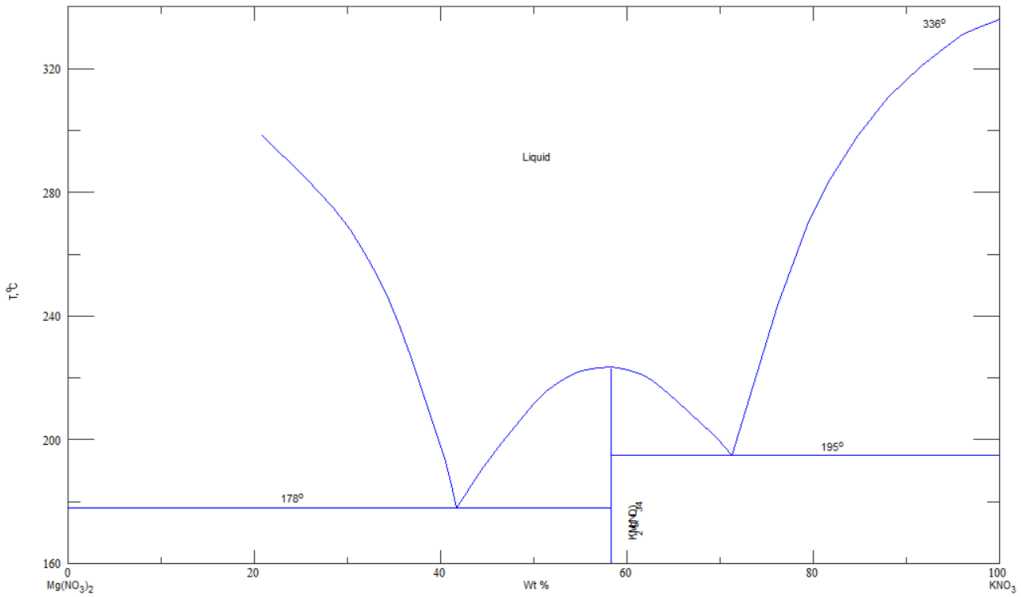

Figure A.13: The phase diagram of KNO_3-$Mg(NO_3)_2$.

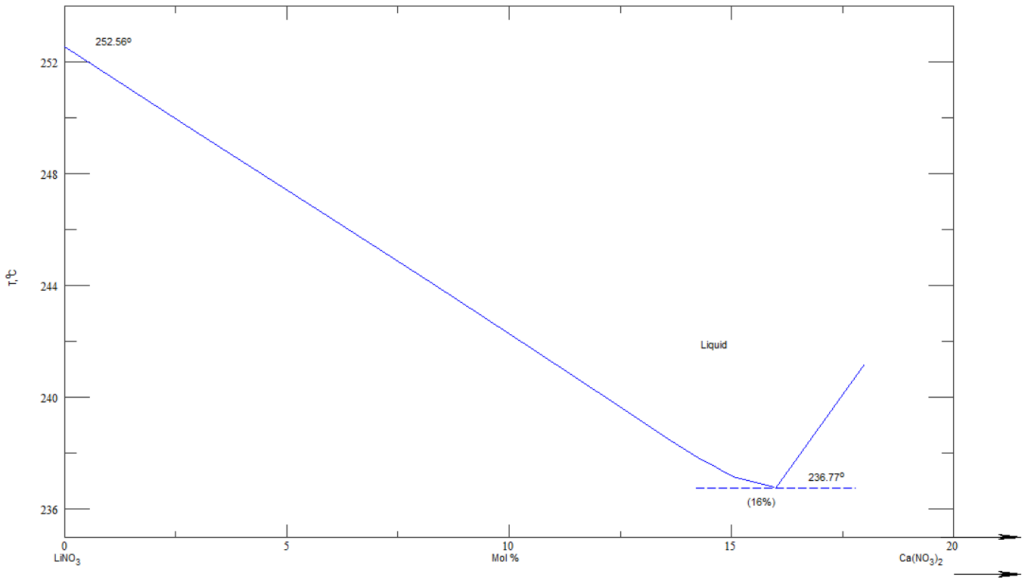

Figure A.14: The phase diagram of $LiNO_3$-$Ca(NO_3)_2$.

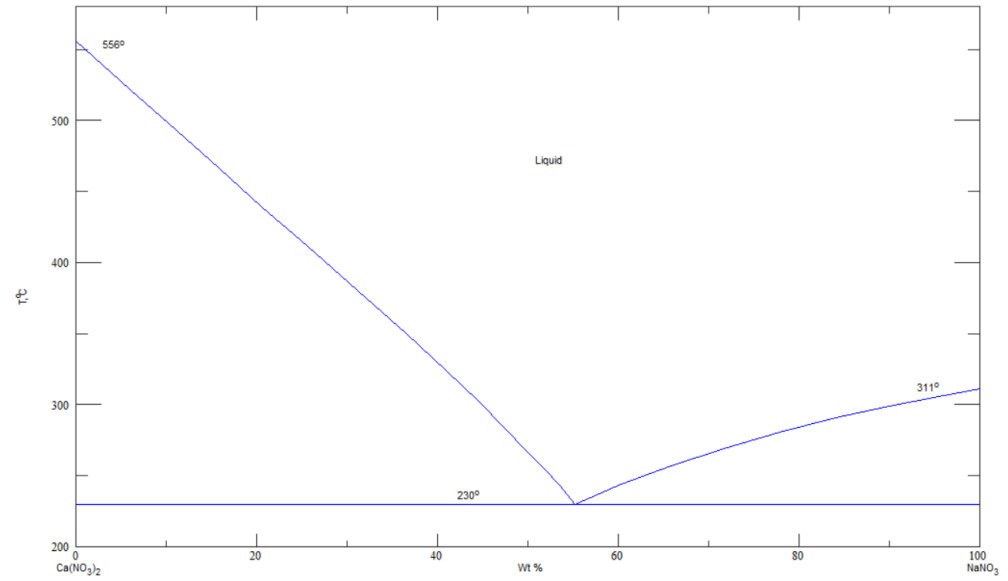

Figure A.15: The phase diagram of $NaNO_3$-$Ca(NO_3)_2$.

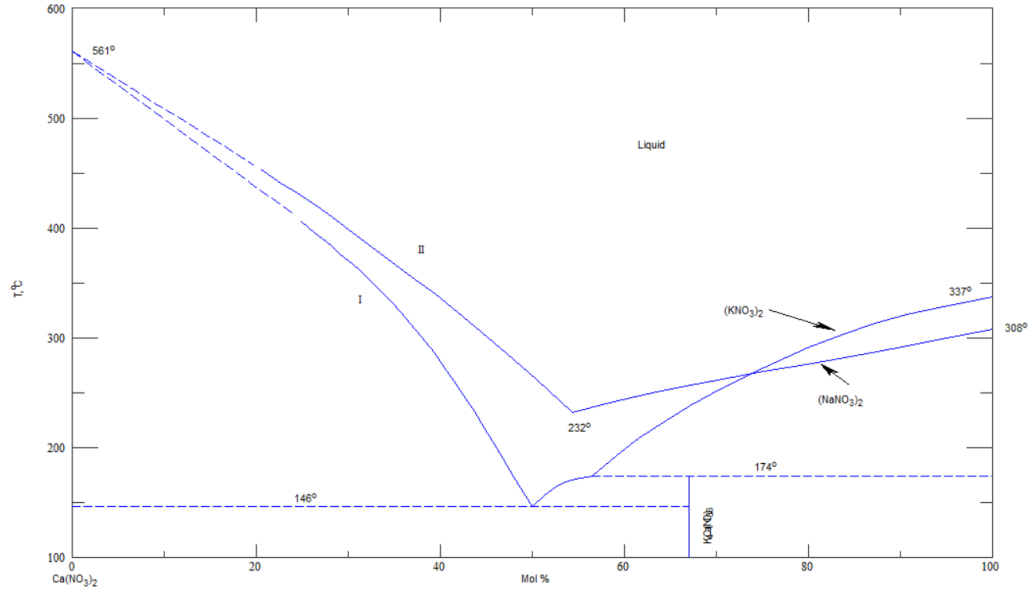

Figure A.16: The phase diagram of $NaNO_3$-$Ca(NO_3)_2$ and KNO_3-$Ca(NO_3)_2$.

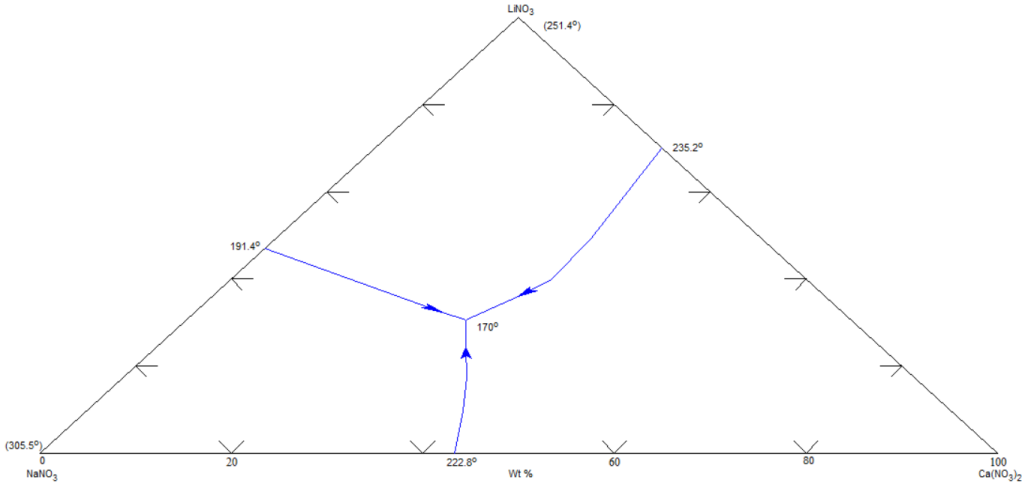

Figure A.17: The phase diagram of $LiNO_3$-$NaNO_3$-$Ca(NO_3)_2$.

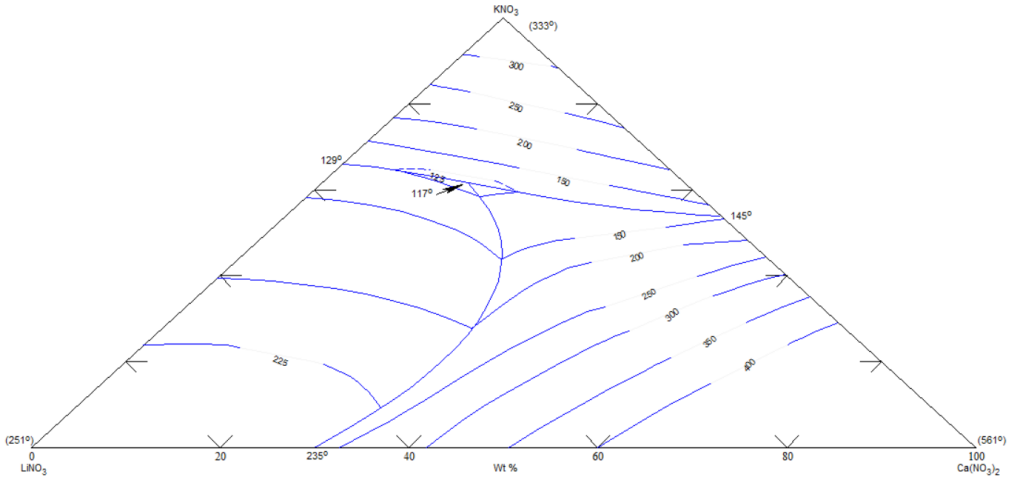

Figure A.18: The phase diagram of $LiNO_3$-KNO_3-$Ca(NO_3)_2$.

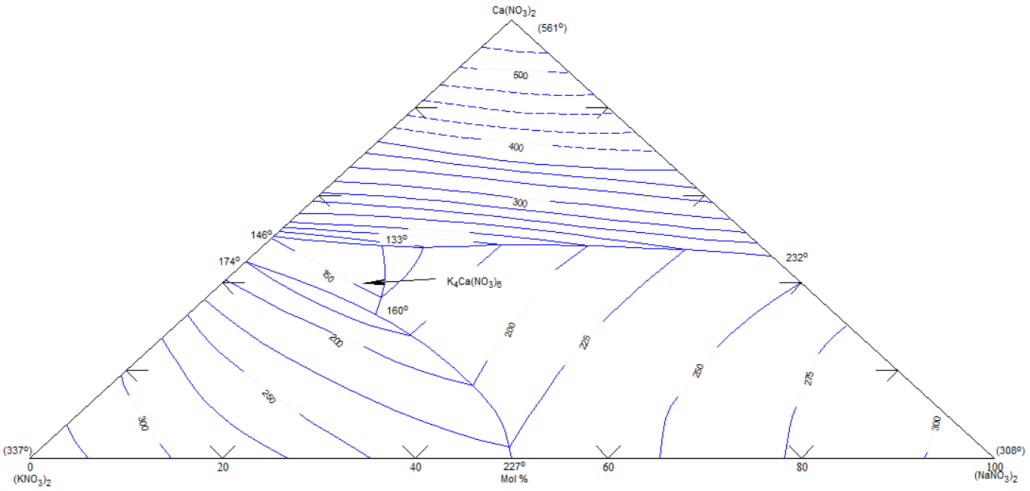

Figure A.19: The phase diagram of $NaNO_3$-KNO_3-$Ca(NO_3)_2$.

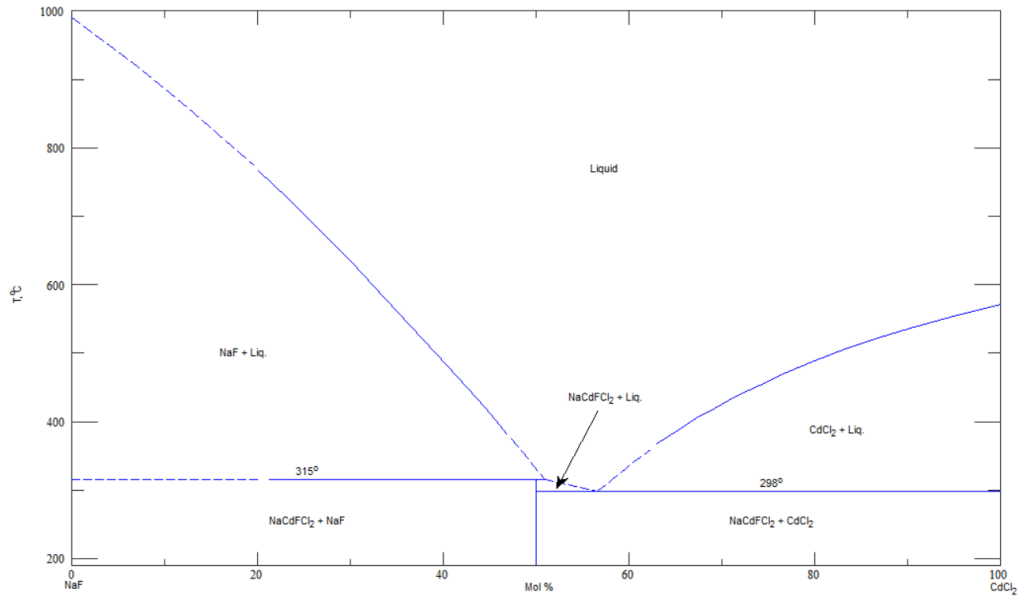

Figure A.20: The phase diagram of NaF-Cd_2.

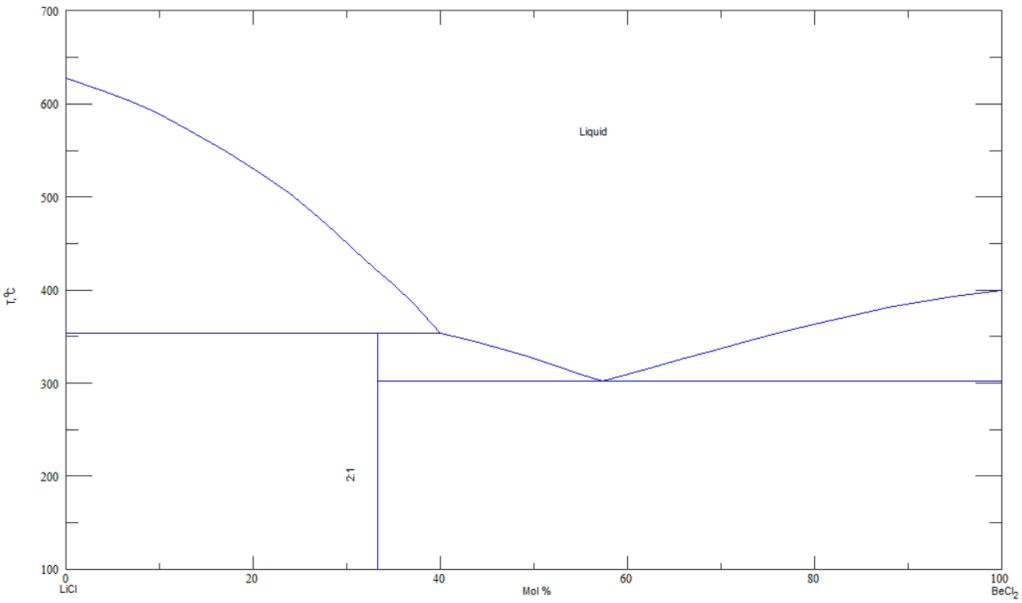

Figure A.21: The phase diagram of LiCl-$BeCl_2$.

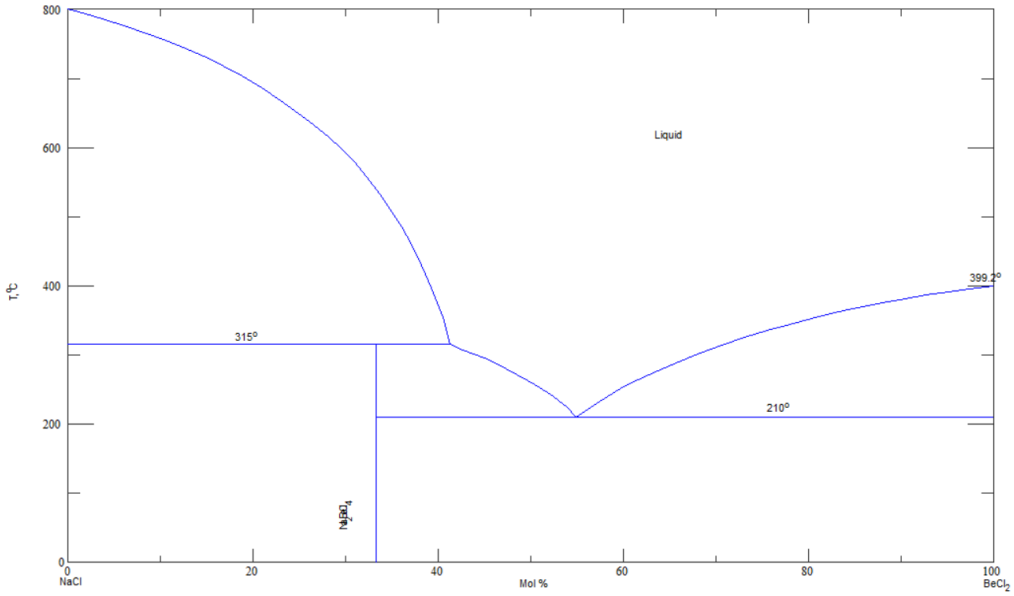

Figure A.22: The phase diagram of NaCl-$BeCl_2$.

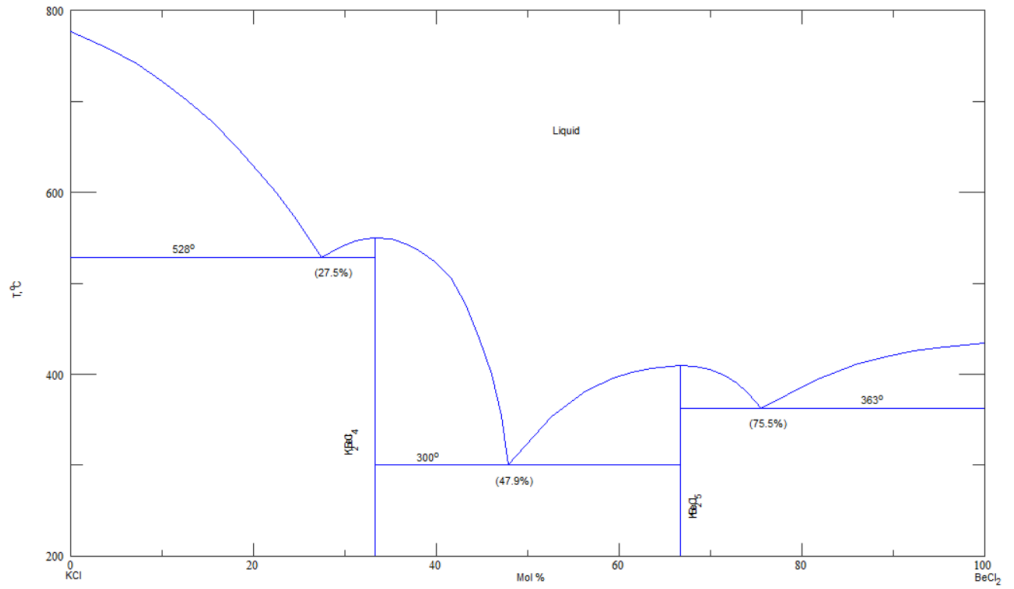

Figure A.23: The phase diagram of KCl-$BeCl_2$

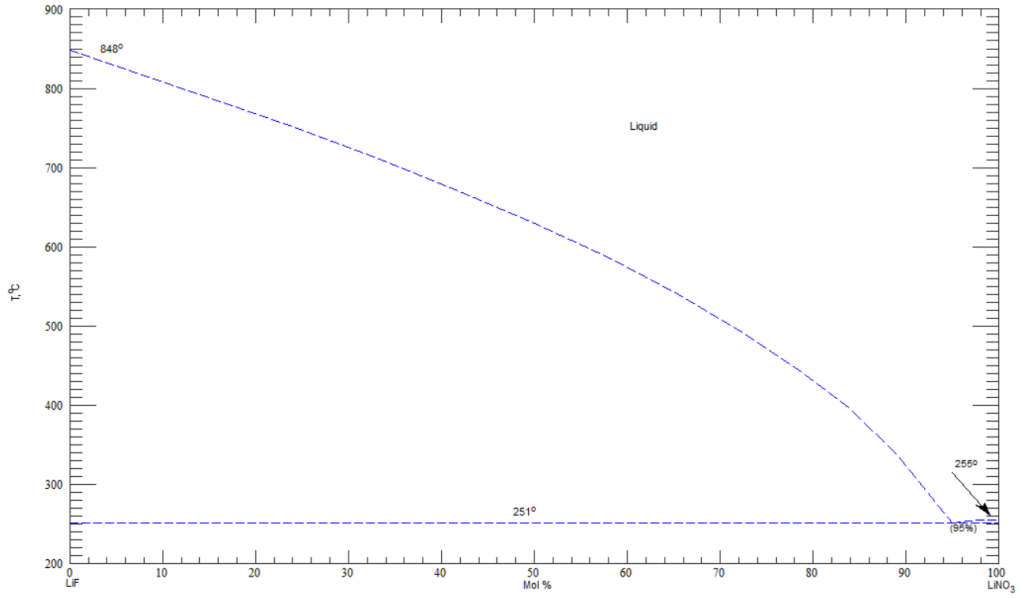

Figure A.24: The phase diagram of LiF-$LiNO_3$.

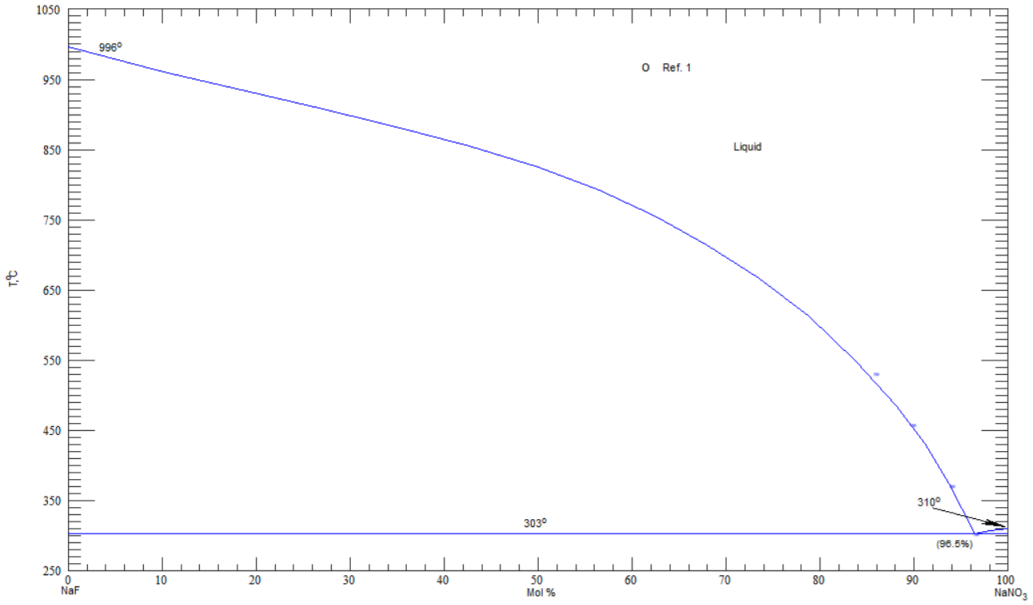

Figure A.25: The phase diagram of NaF-$NaNO_3$.

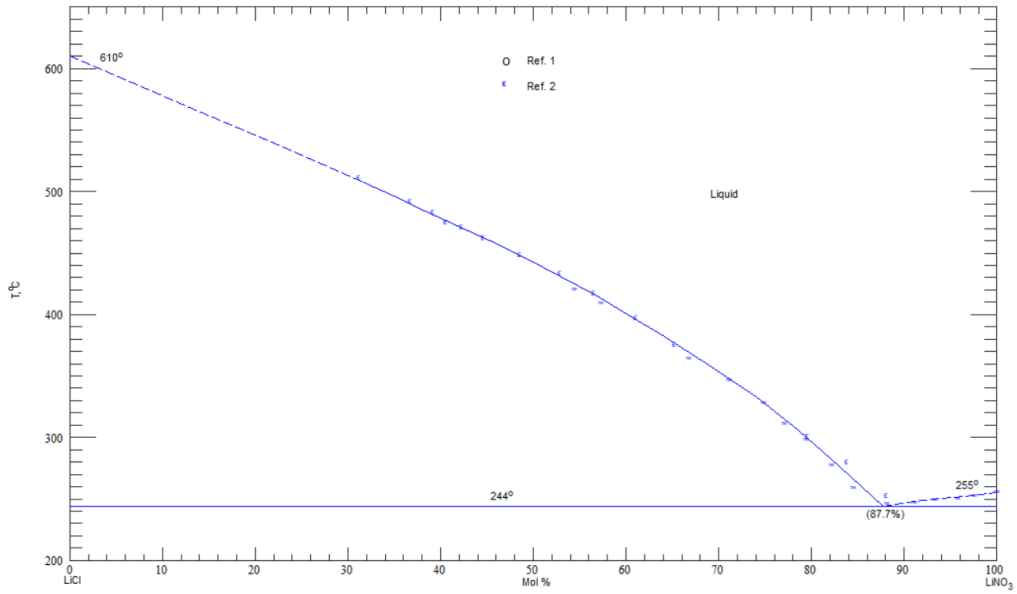

Figure A.26: The phase diagram of LiCl-$LiNO_3$.

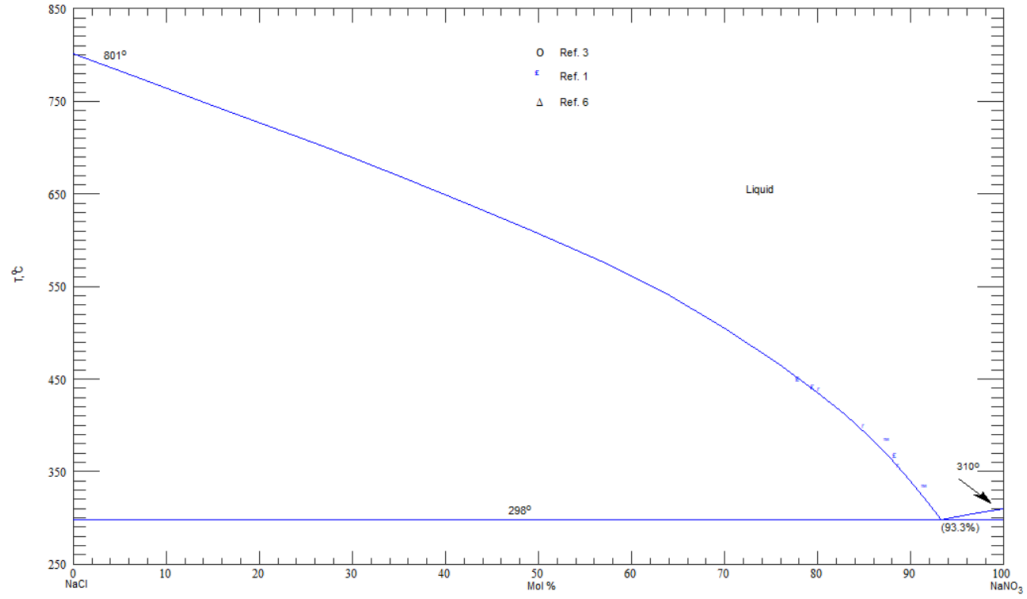

Figure A.27: The phase diagram of NaCl-$NaNO_3$.

A.2 Timeline of CCMS

A simplified timeline of CCMS is presented below[44][50][56, 58, 59][86, 87].

TABLE A.1 Timeline

2001	Espen Olsen discovers that CaO reacts with CO_2 in molten salts
2009	Application for patent of the CCMS process is submitted to the patent office
2010	Doctorate student Viktorija Tomkute conducts her first CCMS experiments
2012	Ana Korvald's master thesis, it was found that Na_2CO_3 is formed when NaF is in the melt, which gives a very effective CO_2 capture rate, but less efficient regeneration of the sorbent
2013	The first research articles on CCMS is published, by E. Olsen and V. Tomkute
2014	Viktorija Tomkute finishes her doctorates degree, her doctorates thesis contains large amounts of research which gives the grounds further research into CCMS
2014	Yasrn Alhaj-Saleh's master thesis, discovers that the carrying capacity of CaO is the highest when CaO is 30% of the melt
2017	Heidi S. Nygård, V. Tomkute, and E.Olsen published an article about kinetics in CCMS, $CaF_2/CaCl_2$ is shown give a faster reaction kinetics between sorbent and CO_2 compared to $CaCl_2$. The CO_2 capture cycling did not affect the kinetics. The capture rate was around 90% and carrying capacity of CO_2 by CaO at around 85%

TABLE A.2 Timeline

2017	Maria Hansen's master thesis, hydrolysis occurs when water vapour are present the simulated flue gas. The hydrolysis effect is reduced by the higher CaO concentrations and lower temperatures. The findings in the thesis were published in an article
2018	Nils Rurås Ruud's master thesis, tested the effects sulfation the sorbent by having SO_2 in the simulated flue gas, and to see the effects SO_2 has on CCMS
2019	Åshild Grøtan's master thesis, tested alternative chemical systems for CaO, as well as testing chemical systems with MgO and SrO as CO_2 sorbents
2020	Petter Nygård Lerøen's master thesis, conducted en extensive screening of chemical systems for CCMS where MgO is the CO_2 sorbent

Norges miljø- og biovitenskapelige universitet
Noregs miljø- og biovitskapelege universitet
Norwegian University of Life Sciences

Postboks 5003
NO-1432 Ås
Norway